Gas Antisolvent Micronization of Pharmaceutical Powders

(Spine title: Gas Antisolvent Micronization of Pharmaceutical Powders)

(Thesis format: Monograph)

by

Shawn <u>Dodds</u>

Graduate Program in Engineering
Department of Chemical and Biochemical Engineering

A thesis submitted in partial fulfillment
of the requirements for the degree of
Master of Engineering Science

Faculty of Graduate Studies
The University of Western Ontario
London, Ontario, Canada

THE UNIVERSITY OF WESTERN ONTARIO
FACULTY OF GRADUATE STUDIES

Certificate of Examination

Supervisor

_____
Dr. Paul Charpentier

Supervisory Committee

_____
Dr. Sohrab Rohani

Examiners

_____
Dr. Amin Rizkalla

_____
Dr. Kibret Mequanint

_____
Dr. Lars Konermann

The thesis by

Shawn Dodds

entitled:

Gas Antisolvent Micronization of Pharmaceutical Powders

is accepted in partial fulfilment of the
requirements for the degree of
Master of Engineering Science

Date August 10th, 2006   _____
                                        Chair of the Thesis Examination Board

Abstract

The purpose of this work was to study the effect of process conditions on the crystallization of beclomethasone-17,21-dipropionate (BDP), an anti-inflammatory steroid commonly used to treat asthma, using the gas antisolvent (GAS) technique. A better understanding of how GAS process conditions affect the particle size distribution (PSD) of BDP through experimental and modelling work is desirable to optimize GAS operating conditions for the production of inhalable powders. The GAS technique was chosen for its ability to produce micron sized particles, while reducing the residual organic solvent content to the ppm level.

The effects of temperature, agitation rate, and antisolvent addition rate on the PSD were studied. An increase in the agitation rate led to a decrease in particle size at 20^oC, but affected only the level of aggregation at 25^oC. Therefore, it was concluded that at 20^oC mass transfer was limiting, while at 25^oC it was not. It was also found that an increase in the CO_2 addition rate led to a decrease in the size of both aggregates and particles. However, the particle sizes were identical at both 20 and 25^oC, though the aggregate sizes were lower at 20^oC. Therefore an increase in flowrate acts by decreasing the precipitation time scale, but has little effect on mass transfer.

A phase equilibrium study was performed using two different models: an expanded liquid phase model (ELPM), and a relative partial molar volume fraction (RPMVF) model. While both models were satisfactory for model compounds such as naphthalene, only the RPMVF model could describe the more complicated cholesterol-acetone-CO_2 system.

A population balance was used to model the PSDs of GAS processed powders. Secondary nucleation was implemented to account for the bimodal nature of the PSD. While a good representation of the primary mode was achieved, secondary nucleation could not account for the second mode. Therefore, an effect other than secondary nucleation, such as agglomeration, was responsible for producing the bimodal PSDs observed experimentally in the BDP/acetone/CO_2 system. However, the model still achieved a good fit of the $d_p(50\%)$ and $d_p(90\%)$ experimental results, and so is useful for approximating particle sizes, and could be used to estimate the inhalable fraction of a powder.

Keywords: *Beclomethasone-17,21-dipropionate,   gas   antisolvent   process, supercritical fluids, phase modelling, population balance*

Acknowledgements

No project is ever the work of an individual, and as such there are many people to thank. First of all, I would like to thank my advisor, Dr. Paul Charpentier, for his support and friendship throughout this project. Dr. Jolyon Mitchell's expertise in particle sizing and the pharmaceutical industry in general was invaluable, and this project certainly would have stalled very early without his help. Also, I would like to thank Mr. Jeff Wood for providing a critical eye when things were going well, and excellent ideas when they were not.

The help of Todd Simpson and Mohamad Rahbari running the SEM was greatly appreciated, as was the help of Tim Stephens with the Mastersizer and Touraj Manifar with the HPLC. Also, Mehdi Sheikhzadeh, Mike Gaylard and Souheil Afara provided technical assistance on numerous occasions.

I would like to thank all of my colleagues in the Laboratory for Environmentally Friendly Solvents, my friends and my family for their support. Finally, I would like to thank Kathy for her constant moral support, and for not getting angry after a few too many late nights in the lab.

Table of Contents

List of Figures

List of Tables

Nomenclature

List of Symbols for Sections 5 and 6

A Dimensionless parameter in PR-EOS

a Parameter in the PR-EOS, $J \cdot m^3 / mol^2$

a_v Specific surface area of the particles, m^2 / m^3

B Dimensionless parameter in PR-EOS

b Parameter in the PR-EOS, m^3 / mol

B Nucleation rate, $\#/\left(m^3 \cdot s\right)$

c_p Concentration of solute in liquid phase, mol / m^3

D_{AB} Diffusion coefficient for solute in liquid phase, m^2 / s

d_M Molecular diameter, m

$\hat{f}_i^\alpha$ Fugacity of component i in phase α, Pa

G Growth rate, m / s

g Growth rate exponent

H_{fusion} Heat of fusion for the solute, J / g

k Boltzmann's constant, J / K

k_a Surface shape factor

k_g Growth rate constant, m / s

k_{ij} Interaction parameter in the PR-EOS

k_s Secondary nucleation rate constant

l_{ij} Interaction parameter in the PR-EOS

m_i i^{th} order moment of the particle size distribution, m^i / m^3

M_T Suspension density, kg / m^3

n Particle size distribution, $\#/ m^4$

N_A Avogadro's number, $\#/ mol$

N_i Molar holdup in phase i, $mole$

$\dot{Q}_a$ CO_2 flow rate, mol / s

R Ideal gas constant, $m^3 \cdot Pa /\left(mol \cdot K\right)$

S Supersaturation

T Temperature, K or ^oC

t Time, s

V Volume or precipitation vessel, m^3

$V_{crystal}$ Total volume of the crystal suspension, m^3

v_i Molar volume of phase i, mol / m^3

x_i Liquid phase mole fraction of component i

y_i Vapour phase mole fraction of component i

Z	Compressibility factor

Greek letters

α	Parameter in PR-EOS
α''	Secondary nucleation rate parameter
γ	Solid-liquid interfacial tension, N/m
γ_3^o	Activity coefficient for the solute at the initial conditions
η	Dynamic viscosity of the liquid phase, $Pa \cdot s$
ϕ_i^α	Fugacity coefficient of component i in phase α
ω	Acentric factor

Superscripts and subscripts

$'$	Primary nucleation
$''$	Secondary nucleation
o	Initial condition
A	Antisolvent
atm	Atmospheric pressure
c	Critical property
i	Dummy variable
i	Exponent on supersaturation in Eq. (6.11)
j	Exponent on suspension density in Eq. (6.11)
L	Liquid phase
P	Solute
S	Solvent
V	Vapour phase
α	Dummy variable

1. Introduction

The need to replace toxic solvents with more environmentally friendly ones has driven over a decade of research on supercritical and near critical fluids (CO_2 in particular) in areas such as extraction, fractionation, chromatography, and crystallization. Supercritical CO_2 is an effective solvent because its physical properties, such as density and viscosity, are highly tunable. This allows the properties to be easily adjusted with slight alterations in the process temperature or pressure. Therefore, good control of the solvent power can be achieved, leading to greater efficiency of the process in general. CO_2 is the most commonly used supercritical fluid because it is cheap, non-toxic, and has a low critical point (31°C and 74 bar) relative to other fluids (Foster et al. 2003).

Supercritical fluids have been exploited heavily as solvents and antisolvents in crystallization processes. As the precipitation time scale is normally on the order of a second or two, supercritical fluids have been able to create small particles with a (relatively) narrow size range compared to other techniques (Reverchon et al. 2003). Generally, the various crystallization techniques can be grouped into two systems: where CO_2 is used as a solvent to dissolve the solute (i.e. the RESS process, described in Section 2.1), and where CO_2 is used as an antisolvent to cause solute precipitation (i.e. the GAS process, see Section 2.2). Most pharmaceuticals of interest are not CO_2 soluble[1], so CO_2 is more often used as an antisolvent in drug crystallization studies. Therefore, this work will focus on the GAS technique for micronization of the drug beclomethasone-17,21-dipropionate (BDP). BDP is an anti-inflammatory corticosteroid

---

[1] The solubility of a compound in CO_2 can be increased with the use of a modifier, such as methanol (see Section 2.1). However, this does not always improve the solubility of the drug by enough to use CO_2 as a primary solvent.

commonly used in asthma treatments, and is normally delivered through the lungs as an aerosol (Lipworth 1993).

A great deal of experimental work has been done with the GAS process to determine how various operating conditions, such as temperature, pressurization rate, etc. affect the final particle size distribution (Foster et al. 2003). It has generally been determined that an increase in agitation, an increase in pressurization rate, a decrease in temperature or a decrease in solid loading will all cause smaller particles to form (Fusaro and Mazzotti 2004). Therefore, while each solid must be tested to determine its specific behaviour with respect to the operating conditions, the general trend that should be observed is already known.

Conversely, very little work has been performed on modelling the GAS process, which consists of a thermodynamic model for the phase equilibrium and a kinetic model for the crystallization. Any work which has been performed thus far has been restricted entirely to small, model compounds such as low molecular weight poly(L-lactide), phenanthrene and naphthalene (Dixon and Johnston 1991; Muhrer et al. 2002; Elvassore et al. 2003). Therefore, it would be desirable to study a more complex system to get a better understanding of the capabilities of the different modelling approaches (both thermodynamic and kinetic) in the literature.

A model of the crystallization procedure would also be useful from a process optimization point of view. By developing an accurate predictive model, it would be possible to optimize the GAS operating conditions to produce particles for a particular application (i.e. inhalation therapy) without performing a large number of experiments.

Given that the GAS process is often used on high value pharmaceuticals, such a model could save significant time and money.

The objectives of this thesis, then, were twofold. To study the effect of agitation rate, CO_2 addition rate, and temperature on the resulting particle size distributions for GAS processed BDP. Additionally, a model for the phase equilibrium and crystallization kinetics involved in the GAS process will be developed, and applied to the crystallization of BDP at various CO_2 addition rates.

2. Background and Literature Review

2.1. *Supercritical and near-critical fluids*

A supercritical fluid (SCF) is defined as a substance above its critical temperature and pressure, as shown in a typical phase diagram (Figure 2-1). The critical temperature (T_c) can be defined as the temperature above which a gas cannot be converted into a liquid regardless of the pressure (see Figure 2-1). Similarly, the critical pressure (P_c) can be defined as the pressure above which a liquid cannot be turned into a gas regardless of the temperature. Beyond the critical point, the gas and liquid phases become indistinguishable, and the fluid does not strictly exhibit the properties of either.
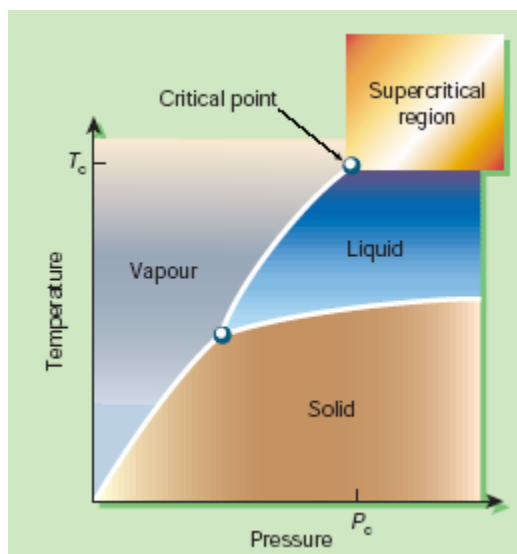
Figure 2-1 Phase diagram for a general substance (Poliakoff and King 2001)

Along the liquid-vapour equilibrium line both gas and liquid phases co-exist, each with distinct physical parameters (i.e. density, viscosity, etc.). As the system temperature and pressure are increased along the equilibrium line, the properties of the two phases will begin to blend together until eventually a single phase is present, termed the supercritical phase (see Figure 2-2). As this occurs, the physical properties of each phase

change and become similar, i.e. the liquid and gas properties converge to the same value as the two phases become one phase (Clifford 1999). The properties of the fluid tend to lie between the usual values for liquids and gases, which gives SCFs several interesting characteristics.
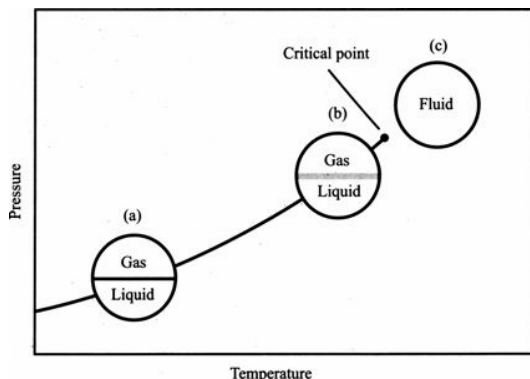
Figure 2-2: Phase blending along vapour liquid equilibrium line (Clifford 1999)

Three important examples of this property blending are density, viscosity and diffusivity, examples of which are listed in Table 2-1. It can be seen that the density of the SCF is similar to that of a liquid (see also Figure 2-3), whereas the viscosity and diffusivity are similar to that of a gas. It is this unique mixture of properties that makes SCFs excellent solvents. Density is related to the solvating power because a more dense fluid will form a more complete solvent shell around a solute molecule. This allows intermolecular attractive forces to be higher, increasing the fraction of solute dissolved. The high diffusivity/low viscosity are related to the mass transfer characteristics: high diffusivity increases the speed with which a molecule moves from one point to another (increasing the kinetics of dissolution), while the low viscosity allows the fluid to penetrate deep into a substance, including pores in a solid, without much resistance. A table of standard SCFs, along with their critical temperatures, pressures and densities are shown in Table 2-2. Carbon dioxide is the most commonly used SCF because it is

inexpensive, readily available, non-toxic, inert, and has a relatively low critical point (in both temperature and pressure) compared to other solvents (Foster et al. 2003).

Table 2-1: Order of magnitude comparison of gas, liquid, and supercritical fluid properties for CO_2 (Cansell et al. 1999)

	Density, kg/m^3	Viscosity, Pa-s	Diffusivity, m^2/s
Liquid	1000	10^{-3}	10^{-10}
Gas	1	10^{-5}	10^{-5}
Supercritical	100-800	$10^{-4} - 10^{-5}$	10^{-7}

Table 2-2: Critical properties of common fluids (Cansell et al. 1999)

Fluid	Critical Temperature (^{o}C)	Critical Pressure (bar)	Critical Density (kg/m^3)
Carbon Dioxide	31.2	73.8	468
Ammonia	132.4	112.9	235
Water	374.1	221	317
Ethylene	9.5	50.6	220
Ethane	32.5	49.1	212
Propane	96.8	42.6	225
n-Pentane	196.6	33.7	232
Cyclohexane	279.9	40.3	270
Methanol	240	79.5	275
Ethanol	243.1	63.9	280
Isopropanol	235.6	53.7	274
Acetone	235	47.6	273

It should be noted that fluids just below the critical point, called near-critical fluids or dense gases, exhibit similar properties to supercritical fluids. Most importantly, they exhibit large density fluctuations near the critical point (see Figure 2-3) causing a sharp increase in the fluid's solvent power. Therefore, while the term supercritical will be used in the bulk of this thesis, the discussion applies equally well to near critical fluids.
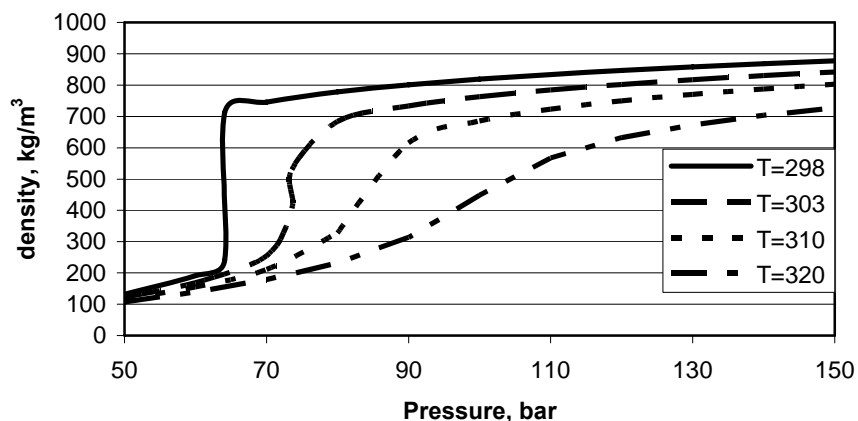
Figure 2-3: Density vs. pressure for CO_2, produced using data from NIST (NIST 2003)

Due to its non-toxic nature and low cost, CO_2 is the most popular supercritical solvent, especially in pharmaceutical research. CO_2 exists as a gas at ambient conditions, and can therefore be completely removed from the drug particles simply by lowering the pressure, reducing the number of downstream processing units. This prospect is especially attractive with pharmaceuticals, as it allows a more toxic organic solvent, which could potentially leave a residue, to be replaced. SCFs have been applied heavily to pharmaceutical crystallization processes (described shortly) for their ability to make small particles with a narrow size distribution. This allows better drug diffusion, and also means better control of the dosage given. A detailed survey of several drugs produced using supercritical fluids can be found in Section 2.6.

SCFs (and near-critical fluids) provide several major advantages over traditional particle formation techniques, such as jet milling, spray drying, etc. First, the process can occur at low temperatures (ambient or higher for CO_2), allowing processing of thermally sensitive compounds, such as proteins, without degradation. Second, because of the quick fluctuations in the fluid properties, the precipitation occurs rapidly and very small

particles can be formed. Also, the speed with which the particles form helps to prevent aggregation, allowing superior control of the particle size distribution (Reverchon et al. 2003).

In particle formation, SCFs are most often used as solvents in the rapid expansion of supercritical solutions (RESS) process, shown in Figure 2-4. In RESS, the solute in question is dissolved in the SCF. The solute-SCF mixture is then vented through an expansion nozzle into a low pressure vessel. The SCF will shift to the gas phase, accompanied by a rapid decrease in density and thus a large decrease in solvent strength, causing the solute to precipitate. The speed with which this process occurs is what allows the formation of very small particles (Foster et al. 2003).
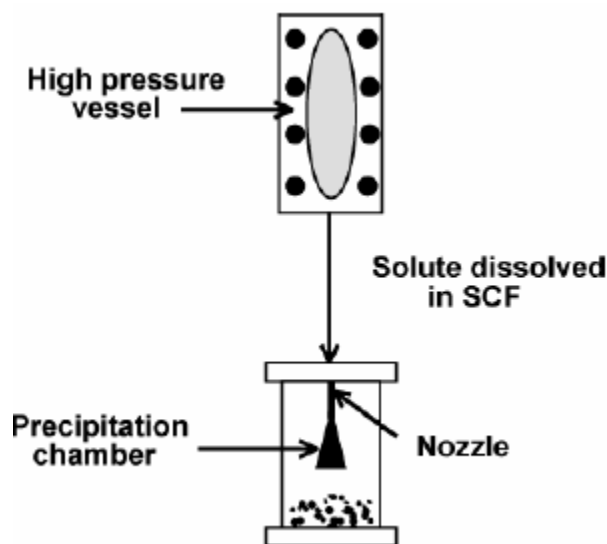
Figure 2-4: Standard RESS apparatus (Foster et al. 2003)

However, the RESS process is limited to compounds which exhibit reasonable solubility in the SCF, which is often not the case with pharmaceuticals due to the high molecular weight and polarity[2] of many drugs. Many researchers have used co-solvents such as methanol and ethanol to increase the solubility of the solute in the supercritical

---

[2] CO_2 is a non-polar molecule, and therefore would not be expected to dissolve polar compounds.

fluid. However, this can lead to solvent residues on the final product, and in many cases does not increase the solubility of the solute by enough to make RESS practical (Foster et al. 2003). In these cases RESS is not suitable, so an alternative approach must be considered.

2.2. *GAS process*

Originally developed as an alternative to RESS precipitation for compounds not soluble in SCFs, the gas antisolvent (GAS) process was first reported on the crystallization of nitroguanidine, an explosive, from the solvents N-methylpyrrolidone or N,N-dimethylformamide using chlorodifluoromethane as the antisolvent (Gallagher et al. 1989). That study found that the nitroguanidine could be precipitated in a variety of sizes and morphologies, depending on the experimental conditions used.

Unlike the RESS process, the GAS process utilizes the insolubility of the compound in a supercritical (or near critical) fluid to form the particles by using the fluid as an antisolvent instead of a solvent. GAS involves a minimum of three components: an organic solvent, a solid solute, and an antisolvent (the dense gas). The solvent must be able to dissolve the solid and the anti-solvent, whereas the solid must be soluble with the solvent but insoluble with the anti-solvent. As an example, consider the ternary system of insulin (the solute), dimethyl sulphoxide (DMSO, the solvent) and CO_2 (the anti-solvent). Insulin is soluble in DMSO, but has negligible solubility in CO_2. DMSO, however, can dissolve both insulin and CO_2 quite well. Therefore this system meets the solubility criteria for the GAS process (Winters et al. 1996).

In the GAS process (see Figure 2-5), CO_2 is pumped into a closed pressure vessel containing the solvent and the solute in a single phase. As the CO_2 is added, the pressure

rises and the CO_2 dissolves into the liquid phase due to the density change, and accompanied increase in solubility. This causes the liquid phase to expand as the CO_2 enters, and eventually only a single phase is present containing the solvent, solute, and CO_2. As CO_2 dissolves the liquid phase density decreases, forcing insulin to precipitate. Due to the excellent mass transfer properties of SCFs (i.e. high diffusivity and low viscosity) and the tunability of the density, which can cause the CO_2 to go from insoluble in the solvent to soluble with only slight adjustments in the pressure or temperature, the particles will precipitate from solution before they have time to grow (Foster et al. 2003). A thermodynamic model to describe this procedure will be developed in Section 5.
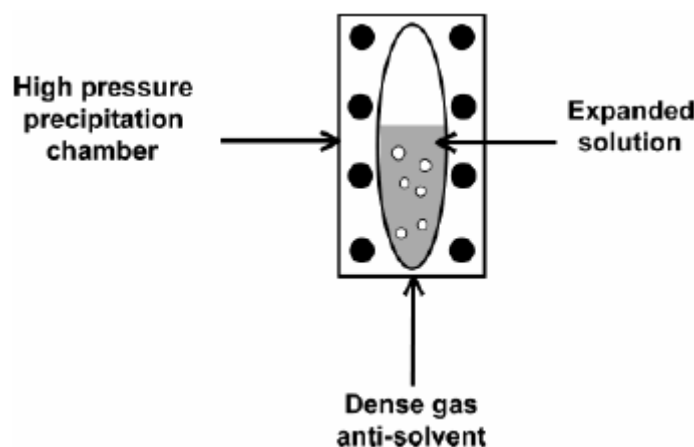
Figure 2-5: Standard apparatus for the GAS process (Foster et al. 2003)

Once the precipitation is complete, the remaining solvent must be rinsed away to ensure that little residue is left on the particles. This is where the majority of the time in the GAS process is spent, because if the pressure in the vessel is lowered before all the solvent is removed, the expanded phase will collapse as the solubility of the CO_2 in the solvent drops. Therefore, any solvent remaining will re-dissolve the particles which have been formed.

One interesting application of GAS is in fractional crystallization. The basic principle of fractional crystallization is to precipitate each solute out individually,

obtaining each compound as a pure powder. One of the first examples of this technique that involved SCFs was to separate phenanthrene and naphthalene from a toluene solution using CO_2 (Bertucco et al. 1998). In these experiments CO_2 was added to the vessel until the phenanthrene began to precipitate, and stopped immediately after; this way a maximum amount of naphthalene would remain in solution. The powder was then rinsed with more CO_2 through to a depressurization chamber, where the remaining solvent and solute were collected. Therefore, the phenanthrene powder was found in the initial crystallization vessel, and the naphthalene powder was found in the depressurization vessel. The phenanthrene powder produced was very pure (~97-98%) at the conditions studied. However, the naphthalene recovered was only around 87% pure because not all the phenanthrene would precipitate; only enough to create a stable solution. It should be noted that to fractionate a powder successfully, a detailed knowledge of the phase equilibrium for the system of interest should be known. Otherwise, it will not be possible to determine what pressure/temperature to use, etc.

2.3. *Crystallization*

The particle size distribution obtained in a crystallization process is generally determined by three different phenomena: nucleation, growth, and agglomeration/breakage. The nucleation phase occurs as the particles precipitate. As the solvent shell is removed, solute molecules diffuse together until they can no longer stay suspended. At this point the particles will begin to form nuclei. If the radius of the nuclei is larger than a critical radius, then the crystal will remain out of solution and can grow. If the nuclei radius is smaller than the critical radius, then the crystal will re-dissolve (Randolph and Larson 1988).

The critical radius is determined by the supersaturation in the system, which is loosely defined as the excess of solute with respect to the amount of solute present under the same conditions when the solution is saturated. Supersaturation can be described mathematically in several ways, as discussed in Section 6.1. The greater the level of supersaturation, the stronger the driving force for crystallization and the smaller the critical nuclei radius (Randolph and Larson 1988).

Nucleation can occur in two basic modes: primary and secondary. Primary nucleation is defined as nucleation without requiring the presence of solute crystals. It can occur either when the crystal forms freely in the liquid (homogeneous), or on the surface of an impurity in the liquid or on the vessel surfaces (heterogeneous). Secondary nucleation occurs when some crystal is already present in the solution. Two examples of the mechanisms of secondary nucleation are: particle breakage (i.e. attrition or fracture), and contact nucleation, where new particles grow off of other existing particles (Randolph and Larson 1988).

Once the crystals have formed, they are able to grow and aggregate/agglomerate and break. Growth is also driven by supersaturation, and it occurs when molecules diffuse to the surface of an existing crystal and attach, increasing the crystal volume without forming distinctly new particles (i.e. without secondary nucleation). Aggregation/agglomeration occurs when two or more crystals come into contact and adhere. Aggregation refers to weak adhesive forces, whereas agglomeration refers to very strong adhesive forces (Myerson 1993). Once again, the favourable mass transfer properties of supercritical CO_2, combined with the quick density fluctuations, means that the crystals have a very small time to diffuse, potentially minimizing the occurrence of

growth/aggregation/agglomeration. A mathematical description of the crystallization process is given is Section 6.1, where a crystal model is developed for the GAS process.

2.4. *Asthma*

Asthma is a respiratory illness which is generally characterized by "wide variations in resistance to airflow over short periods of time" in the lungs, though this does not describe all cases of asthma (Clark 1983). The narrowing of the airways in the lungs can result in wheezing, coughing, shortness of breath and, in extreme cases, an inability to breath. It is believed that asthma is caused by the interaction between three different factors: predisposition to the disease due to genetics, common airborne substances like cat hair or dust, and "unnatural" factors such as pollution, smoking, etc (Health Canada 2001).

It is believed that both the genetic and environmental effects play a strong role in the development of asthma, although neither effect can account for all cases. The genetic basis for asthma appears to be found in several genes, each having a moderate effect, instead of a small number of genes, each with a strong effect (Tattersfield et al. 2002). The genetic link to asthma can be seen in two examples. The first is with childhood asthma, where there has been little time to develop significant irritation due to environmental factors in most cases. The second example can be seen on the island of Tristan da Cunha, where a large proportion of the asthmatics can be traced back to three of the original settlers, each of whom had asthma (Rees and Price 1995). While neither of these examples provides irrefutable proof of a genetic link, they are certainly compelling.

The link between asthma and the environment is suggested because asthma is more prevalent in people growing up in industrialized nations. It is thought that this occurs due to the low level of infections in such societies, which causes T cells to shift from a T_h2 to a T_h1 phenotype (Tattersfield et al. 2002). The T_h2 phenotype produces immunoglobulin E, which attaches to mast cells[3] and causes the release of histamine (Campbell and Reece 2002). This hypothesis is also supported by a lower incidence of allergies in children brought up on farms, where there is presumably a higher level of airborne pollutants (i.e. dust, pollen, etc.). It should be noted, however, that the T_h1 phenotype can also contribute to asthma symptoms, though in a lesser manner than the T_h2 phenotype (Tattersfield et al. 2002).

Alternatively, asthma is commonly thought to be caused by particulate pollutants, which one would think explains the higher asthma rates in industrialised nations. However, in many industrial countries the level of airborne particulates has decreased, while asthma rates have increased. This can be explained by noting that pollutants seem to help prevent asthma (as discussed above), but can aggravate symptoms in cases of severe asthma (Tattersfield et al. 2002). Once again, the effect of the environment on asthma is complex, and is poorly understood at this point, making it difficult to form any definitive conclusions.

Asthma generally results in the narrowing of the airways in the lungs which can occur in many different ways, such as inflammation of the lung lining, mucus plugs, and

---

[3] Cells which produce inflammatory proteins, such as histamines, as an immunological response (Campbell and Reece, 2002)

airway remodelling[4]. The presence of mast cells in the smooth muscle lining in the lungs has been found to be a defining characteristic of asthma, and can cause the complete blockage of the airways in severe cases. The mast cells cause inflammation of the lungs either directly, by secreting inflammatory proteins, or indirectly by signalling for an immunological response which attracts other cells that will inflame the lungs. By producing Immunoglobulin E, helper T cells increase the allergic reaction which causes inflammation of the lungs, as discussed earlier. The third cell type which is commonly linked to asthma is eosinophils, which are white blood cells which protect against larger pollutants such as bacteria. However, studies have shown that when eosinophil levels were reduced, the lung lining did not lose its sensitivity to inflammation. Therefore, the role (if any) of eosinophils towards airway inflammation is questionable. Finally, these cells all produce cytokines, which cause inflammatory cells to collect nearby (Tattersfield et al. 2002).

A general overview of the various stages of asthma can be seen in Figure 2-6. On the left is a cross section of a normal bronchus. The initial reaction of the lungs is to swell slightly, restricting airflow, as seen in the figure. This reaction occurs soon after the irritant is introduced (~10 minutes), and is easily reversed. The second stage can occur up to six hours later, and shows significant airway restriction. This stage is characterized by the presence of mast cells, which are causing the inflammation. In severe asthma the airway can develop a mucus plug, which can lead to a complete blockage of the lung and in some cases cause death. However, this condition is extreme and can be prevented with early treatment (Clark 1983).

---

[4] Airway remodelling results from a poor repair system in the lungs, causing the epithelial to become distorted. This can cause the lungs to inflame, and can also lead to the growth of smooth muscles within the airway (Tattersfield et al. 2002).
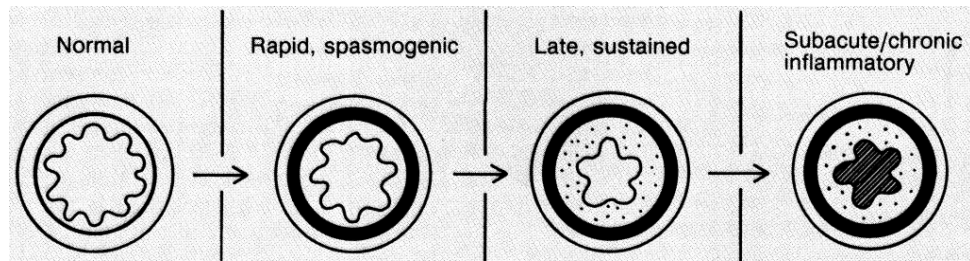
Figure 2-6: Lung cross-section in various stages of a mast cell induced asthma attack (Clark 1983)

Asthma rates have been increasing in Canada steadily over the last 10 years, going from 6.5% to 8.4% of Canadians diagnosed with asthma. The most affected age groups are 12-19, where approximately 13% (in 2001) of the population in either group was diagnosed (Statistics Canada 2005). Therefore, especially because of the high percentage of children afflicted, there is a need to develop better, easier, treatments for asthma. The most obvious treatment method is to target the lungs directly, since this is where the inflammation occurs, which is often done using corticosteroids, as discussed in the following section.

2.5. *Beclomethasone dipropionate*

Beclomethasone-17,21-dipropionate (BDP, see Figure 2-7) is a steroid used in the treatment of asthma. More specifically it is a glucocorticoid, meaning that it affects the body's metabolism (gluco-) and resembles the steroids output by the adrenal cortex (-corticoid). Glucocorticoids possess anti-inflammatory properties and therefore can be used to treat diseases such as asthma and eczema, and have been accepted as the most effective and widely used asthma medicines on the market (Bertoldo et al. 2005). BDP in particular has been used as a treatment for asthma since the 1970's (Lipworth 1993).
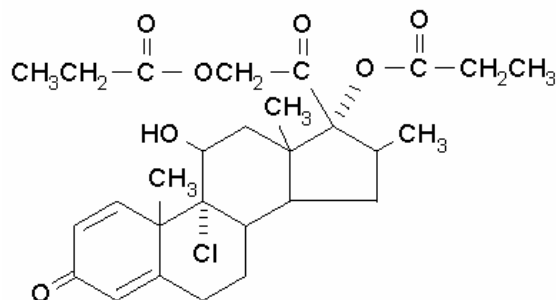
Figure 2-7: 2D Structure of beclomethasone-17,21-dipropionate (Sigma-Aldritch website)

Corticosteroids have been studied extensively and their medicinal properties are reasonably well understood, which has led to an increase in the number of patients that are prescribed corticosteroids, particularly children, as they have proven to be safe. The basic mechanism for corticosteroid action is shown in Figure 2-8. First, the glucocorticoid (GCS in the figure) diffuses across the cell membrane and binds to a glucocorticoid receptor (GR) protein in the cell cytosol. This complex is then able to do one of two things: either bind directly to the cell's DNA[5], preventing mRNA transcription directly, or by binding to transcription factors (written as AP-1 and NF-κB in Figure 2-8), preventing DNA transcription to mRNA which codes for inflammatory proteins (i.e. proteins which signal the cells to become inflamed) such as cytokines and inflammatory enzymes and receptors. Therefore, corticosteroids function by stopping the body's response at the top of the inflammatory cascade[6], making them very effective, especially because they do not target one specific cell type. Therefore, they have an effect on most of the immune responses in the lungs (see Figure 2-9). An additional mechanism of action may be to cause the cell to produce anti-inflammatory agents,

---

[5] Done using two "zinc fingers", which are zinc ions bound to two cysteine residues causing the protein to protrude in a loop which resembles a finger. These "fingers" bind in a major groove of the DNA.
[6] A discussion on cascading cellular responses is beyond the scope of this thesis, but can be found in any introductory cellular biology text book.

making the drug even more effective. All of these effects can be summarized by stating that corticosteroids inhibit the lung's immune response to an irritant (Barnes et al. 1998).
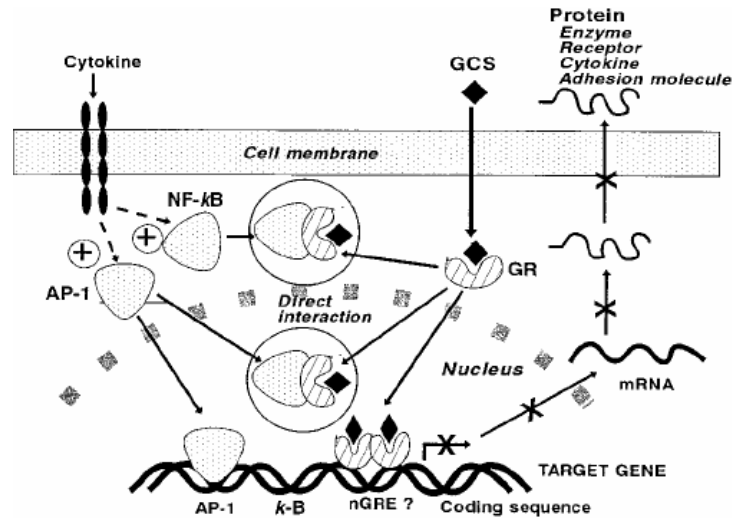
Figure 2-8: Mechanism of action of BMD (Barnes et al. 1998)
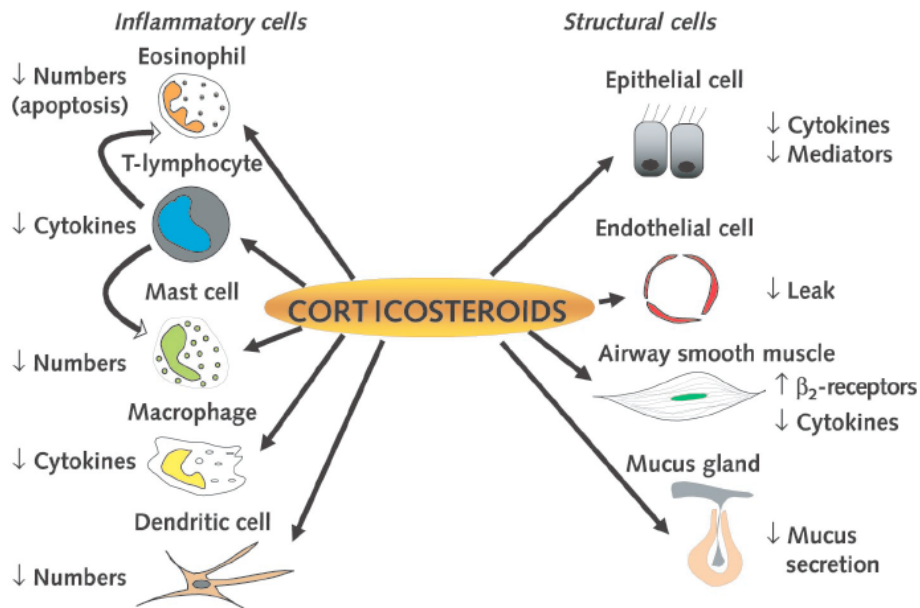
Figure 2-9: Schematic of glucocorticoids effect on immune response (Barnes and Adcock 2003)

In the body, BDP itself is not the active form which inhibits immune responses. First the steroid must be hydrolysed to beclomethasone-17-monopropionate (BMP), which occurs in either the intestines or the lungs, depending on where the drug travels

first, i.e. if it is inhaled or swallowed. BMP is the active form which produces the anti-inflammatory response described above. Any unused BMP is removed by the liver after travelling through the circulatory system (Lipworth 1993).

While they have proven useful in treatment, glucocorticoids are not without their side-effects. At low doses, there does not appear to be any significant side effects (Bertoldo et al. 2005). At higher doses, throat irritation, cough, dysphonia, fungal infections, cataracts and growth depression in children (Rees and Price 1995), as well as a decrease in mineral bone density, adrenal suppression, increased bruising and glaucoma have been observed (Mortimer et al. 2005). Glucocorticoids have even been linked to a decrease in tolerance of environmental allergens, confounding the symptoms of asthmatics and making them more prone to developing new allergies (Stock et al. 2005). However, given the large number of patients currently using corticosteroids, the incidence rate of these side effects is rather small. The end result, effective asthma symptom control, seems to outweigh the negatives (Kilpio and Hannuksela 2003).

A major problem with inhalation of corticosteroids is that usually only a small fraction of the drug is actually inhaled, around 20%, while the rest is deposited in the mouth and swallowed (Lipworth 1993). Therefore, high doses of the drug must be administered to get the appropriate amount to the lungs. Not only is this expensive, but it can be harmful to the patient. First, a higher dose is needed to achieve the desired effect because so much of the drug is swallowed instead of inhaled. Second, systemic side effects, such as those listed in the previous paragraph, can be caused from the excess drug as it passes through the circulatory system (see Figure 2-10).

There are two possible routes to minimize this problem: First, one could redesign the inhaler to increase the fraction of particles which reach their target in the lungs. Second, one could redesign the particles to give a higher fraction of particles within the size range of 1-3μm (Edwards and Dunbar 2002). This second method will be the approach taken in this thesis.
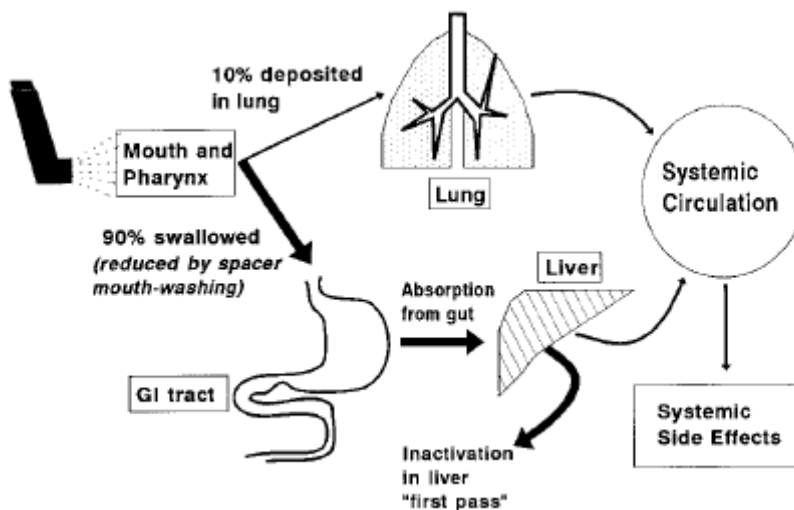
Figure 2-10: Schematic of the path followed by inhaled compounds within the body (Barnes et al. 1998)

2.6. *Literature Review: pharmaceutical micronization by supercritical fluids*

Traditionally, there are several problems in the pharmaceutical industry relating to particle formation. If the particles are formed through crystallization/precipitation then there is necessarily a solvent involved, which is often toxic to humans and the environment. To sell the drug, the solvent must be removed entirely and then be disposed of in an environmentally friendly way, or purified and reused. This is often quite difficult, especially considering pharmaceuticals cannot have total impurity levels that exceed a few ppm. It is also important to maintain good control of the particle size distribution (PSD) for the resulting crystals. Several methods can be used to tailor the PSD (see Table 2-3), but they all have disadvantages (Foster et al. 2003).

Table 2-3: Characteristics of traditional particle formation techniques (Foster et al. 2003)

method	size (μm)	disadvantage
fluid energy mill	1-5	high energy input, temperature increase, electrostatic charging
spray drying	~ 5	operation above ambient temperature
lyophilization	<1	poor control over size distribution, energy-intensive
Solution preparation	<1	poor control over size distribution, solvent recovery

SCFs can be used to overcome many of these disadvantages. The mild operating temperatures allow SCFs to be used with thermally sensitive compounds. Also, the tuneability of SCFs allows for good control of the PSD within the desired size range. One commonly mentioned disadvantage of SCFs is that the operating pressures are prohibitively high, leading to increased equipment and operating costs. However, the pressures are not out of the ordinary when compared to many industrial separation processes, as they can be kept in the range of 50-200 bar (Foster et al. 2003).

If the SCF is used as a solvent, then 100% of it can hypothetically be removed from the crystals simply by depressurizing. The SCF can then be easily collected and recycled, as it will already be purified. If a co-solvent is used the particles can be trapped on a filter, and the SCF/co-solvent mixture can be separated by depressurizing, purifying both, and allowing for reuse. If the SCF is used as an antisolvent, the increased solvating power at high pressures allows for high product purity, and the SCF/solvent can be separated and reused by depressurizing (Foster et al. 2003).

2.6.1. *Generic Pharmaceuticals*

Many different drugs have been processed using various technologies involving SCFs. Therefore, only a few studies have been reviewed here to outline some of the

progress made with more common drugs, such as aspirin, acetaminophen, etc. A brief

summary of a few of the drugs crystallized using SCFs is given in Table 2-4.

Table 2-4: Generic pharmaceuticals crystallized with SCFs

Drug	Method	Solvent	Size (μm)	Reference
Acetylsalicylic acid	RESS	-	2-5	(Domingo et al. 1997)
	RESS	-	0.1-0.3	(Huang et al. 2005)
Cyclosporine	RESSAS	Water / Tween 80	0.4-0.7	(Young et al. 2000)
Ibuprofen	RESS	-	2.5	(Charoenchaitrakool et al. 2000)
	RESSAS	Water / SDS	0.15-0.32	(Turk et al. 2002)
Paracetamol	SEDS	Ethanol	3-10	(Shekunov et al. 1999)
	GAS	Acetone	50 -250[7]	(Fusaro and Mazzotti 2004)

Paracetamol, a.k.a. acetaminophen or Tylenol, was originally processed with

SCFs using solution enhanced dispersion by supercritical fluids (SEDS)[8] with ethanol as

a solvent (Shekunov et al. 1999). It was found that the particle size increased as pressure

and/or temperature were increased. However, at lower pressures, the effect of increasing

temperature was almost negligible. Also, it was found that needles (instead of spheres)

were produced when the Tylenol was precipitated at higher temperatures and pressures.

This was attributed to the ethanol/CO_2 phase diagram, which has two distinct phases at

these conditions, allowing the particles to form at the phase interface, creating needles.

Paracetamol was also crystallized from acetone by the GAS process (Fusaro and

Mazzotti 2004). Generally, they found a decrease in particle size with a decrease in

temperature, an increase in initial solute concentration, or an increase in agitation rate.

However, the effect of these parameters on the final particle size was minor in

---

[7] Note that this particle size range is volume weighted, whereas the others listed in this table are number weighted. This is why the particles seem to be so much larger.

[8] The SEDS process uses CO_2 as an antisolvent. The liquid/solid solution is sprayed cocurrently with CO_2 into a pressure vessel, through two concentric nozzles. Normally, the liquid solution is sprayed through the inner nozzle, with CO_2 through the outer nozzle.

comparison to the antisolvent addition rate. The antisolvent addition rate was able to control the final particle size, which ranged between 50 and 250μm. They obtained similar results in two different reactors (400mL and 1,000mL) as long as the same specific antisolvent addition rates (defined as the mass flow rate of CO_2 divided by the initial mass of solvent) were used, indicating the possibility for scale-up of the GAS process.

It is worth noting, however, that the particle sizes reported in the work of Fusaro and Mazzotti (2004) were based on the volume fraction, whereas most papers report only the number fraction. A small amount of large agglomerates can cause the volume based diameter to be an order of magnitude higher than the number based diameter. Therefore, the results from this work may not actually be significantly different from those previously reported in the literature, despite their appearance. It should also be noted that the volume based diameter is much more important for delivery than the number based diameter because it is directly related to the mass of the drug within a certain size; e.g. it is much more important to have 80% of the mass of the particles within a certain size range than to have 80% of the number of particles within the same range.

Ibuprofen or Advil, was first micronized using the RESS process (Charoenchaitrakool et al. 2000), with the goal of increasing the dissolution rate and thus decreasing the dosage required. The micronized ibuprofen had an average diameter (~2.5μm) nearly twenty times smaller than the unprocessed material. Also, 90% of the micronized material had a diameter less than 5μm, while none of the unprocessed material had a diameter lower than 7.5μm. As would be expected, this decrease in particle size was accompanied by an increase in dissolution rate. The micronized

ibuprofen, without surfactant, exhibited a five-fold increase in dissolution rate over the original material, using a phosphate buffer solution. Coincidentally, the micronized ibuprofen exhibited a similar dissolution rate to the unprocessed ibuprofen with a surfactant. Therefore, by simply using the RESS process one can avoid the use of a surfactant while maintaining delivery efficiency.

In later experiments, an even lower particle diameter was obtained using RESSAS (rapid expansion from supercritical solutions into aqueous solutions). This method involves spraying a supercritical solution containing the drug into an aqueous solution containing a surfactant. The surfactant helps to prevent coagulation of the particles by stabilizing them in a micelle before they have time to grow. This method was able to produce ibuprofen, griseofulvin, cholesterol, benzoic acid and β-sitosterol nanoparticles with an average diameter less than 320nm. Some agglomeration was seen at higher surfactant concentrations due to foaming, where a distinctly bimodal size distribution was obtained. However, the particles remained in all cases below 1μm (Turk et al. 2002).

Acetylsalicylic acid, or Aspirin has been precipitated using RESS, along with benzoic acid, salicylic acid and phenanthrene (Domingo et al. 1997). A special nozzle with a frit at the end was used for spraying, which essentially provides several nozzles with very small diameters instead of one nozzle with a (relatively) large diameter. Using a standard capillary nozzle, the various solutes crystallized with a size range on the order of 1-8μm. However, when the frit nozzle was used the particles were an order of magnitude lower, with diameters around 100-500nm.

These results were later improved upon with RESS using much higher extraction temperatures (Huang et al. 2005). Aspirin particles smaller than 100nm could be

obtained, and most of the particles produced were in the 100-300nm range. This represents a decrease in particle size of about four orders of magnitude from the starting materials, and should allow for a substantial decrease in the dissolution profile.

2.6.2. *Proteins*

The GAS process was first used on proteins with insulin in 1993 (Yeo et al. 1993). DMSO and DMFA were used as the solvents, and the temperature and initial concentration of insulin were varied. In all experiments a median particle diameter of around 2μm was obtained, with 80% of the particles between 1 and 4μm. In this set of experiments, the particle size was found to be independent of the temperature and initial concentration, though it was postulated that the pressurization rate could have an effect. The processed insulin was injected into rats, and the blood glucose control was identical to that with unprocessed insulin. Therefore it was concluded that the processing did not affect insulin activity.

The GAS process involves operating conditions that seem likely to denature proteins, such as high pressure and shear forces, so it is quite surprising that the insulin powders were able to recoup their biological activity. Therefore, the protein structure was studied to determine how it was affected by GAS processing using Raman amide I band spectroscopy (Yeo et al. 1994). The spectra showed a $10cm^{-1}$ shift between the commercial powder and the GAS processed material, which implies significant distortion of the secondary structure. This was confirmed using spectral analysis, which showed a large decrease in α-helix content, and a corresponding increase in β-sheet content. However, after the protein was placed in a 0.01M HCl solution it completely regained its secondary structure (and thus biological activity, as seen in (Yeo et al. 1993)), indicating

that the protein was not irreversibly denatured. This is particularly surprising because even under normal crystallization techniques, insulin will only regain ~80% of its biological activity. Therefore, the GAS process was able to produce finer particles with a higher recovery of biological activity than traditional crystallization techniques.

Given these results, it was desirable to ensure that other proteins could also be renatured after supercritical antisolvent (SAS) processing[9] (Winters et al. 1996). Lysozyme, trypsin, and insulin were precipitated over a wide range of conditions. FTIR, amide I band Raman spectroscopy and biological activity tests were used to evaluate the extent of protein denaturation. In all cases, it was found that the SAS produced powder was denatured, but that placement in water allowed most of the biological activity to return; up to 100% for lysozyme, and up to 94% for trypsin. Some of this denaturation can be attributed to the solvent used (DMSO), and not the actual SAS process itself, as it was found that DMSO had a significant effect on structure due to its high hydrogen bonding capabilities. This result was very encouraging for SCF processing of proteins, although it is not universal to all proteins as alkaline phosphatase was irreversibly denatured in later experiments (Winters et al. 1999).

In a follow-up study, Winters et al. tested the effect of SAS processing conditions on the long term stability of the proteins (Winters et al. 1997). Lysozyme was stored as a dry powder for up to two years at various temperature ranging from -25°C to 60°C. The lysozyme crystals studied were all formed under identical processing conditions. Trypsin and insulin were stored at -15°C for two years, but the particles were formed under different conditions, allowing the study of how SAS process parameters affect long term

---

[9] The SAS process is similar to the GAS process, except that the solid/solvent mixture is added to a vessel containing pressurized CO_2, instead of adding CO_2 to a vessel with the solvent/solid mixture.

stability. In all cases biological activity was recovered to the same level as in (Winters et al. 1996), allowing the conclusion that SCF processing techniques and storage temperature have no significant effect on protein stability, and proteins formed in such a manner have a significant shelf-life.

Given the negative results of Winters et al., 1999 with alkaline phosphatase, it is desirable to obtain a method to prevent protein unfolding during SCF processing. This was first approached with lysozyme and lactate dehydrogenase (LDH) by using sucrose as a stabilizer (Sellers et al. 2001). Two interesting results were observed. First, the presence of sucrose significantly increased the sphericity of the resulting powder, which was further increased by the addition of Tween-20 (a surfactant). Second, while the lysozyme recovered nearly all biological activity after processing (confirming the result of Winters et al. 1999) without sucrose, the LDH recovered less than 20% of its activity. However, the addition of sucrose raised this value to nearly 70%, while the use of sucrose + Tween-20 allowed the recovery of activity to rise to almost 100%.

The work on proteins that has been reviewed so far produced particles within the 1-5µm range, which is suitable for inhalation therapy but not for many other types of drug delivery.   The first work to produce submicron protein particles used the supercritical antisolvent (SAS) method to process lysozyme in DMSO (Chattopadhyay and Gupta 2002). An ultrasonic horn was used to create high levels of turbulence at the solution inlet to the precipitation vessel, thereby increasing mass transfer and thus decreasing the particle sizes. When the horn was not turned on, the average particle size produced was on the order of 2µm, with similar results already in the literature (Winters et al. 1996). However, significantly smaller particles were obtained when the horn was

operating, with a minimum average particle diameter of 190nm for a horn power of 90W. At higher powers the particle size increased because, while high turbulence causes an increase in mass transfer, it also causes an increase in particle collisions and therefore agglomeration.

Many other reports on supercritical protein precipitation have also been made, some of which are highlighted in Table 2-5. The next stage is to begin encapsulating the proteins so they can be used in controlled release applications, as oral formulations, etc. This topic is briefly discussed in Section 2.6.4.

Table 2-5: Proteins precipitated using SCFs

Protein	Method	Solvent	Size (µm)	Reference
Albumin	ASES	Ethanol	0.1-0.5	(Bustami et al. 2000)
α-Chymotrypsin	SAS	Ethanol/water	0.2-0.6	(Sarkari et al. 2003)
Human growth hormone	SEDS	Isopropanol	1-6	(Velaga and Carlfors 2005)
Insulin	GAS	DMSO	1 - 4	(Yeo et al. 1993)
	SAS	DMSO	1-5	(Winters et al. 1996)
	ASES	Ethanol	0.1-0.5	(Bustami et al. 2000)
	SFL	Water	3	(Rogers et al. 2002)
	SFL	Water	1-10	(Yu et al. 2002)
Lysozyme	SAS	DMSO	1-5	(Winters et al. 1996)
	ASES	Ethanol	0.1-0.5	(Bustami et al. 2000)
	SAS-EM	DMSO	0.1-1	(Chattopadhyay and Gupta 2002)
	GAS	DMSO	1-5	(Muhrer and Mazzotti 2003)
rhDNase	ASES	Ethanol	0.1-0.5	(Bustami et al. 2000)
Trypsin	SAS	DMSO	1-5	(Winters et al. 1996)

2.6.3. *Steroids & Hormones*

The first work using supercritical fluids on steroids was in the mid 1990's (Allesi et al. 1996), where progesterone and medroxyprogesterone acetate were precipitated using the RESS process. It was found that progesterone was more soluble in CO_2, reaching up to nearly 0.1 wt% at 60°C and 240 bar, allowing for larger sample sizes.

Several different processing conditions were analyzed, finding that lower particle diameters were obtained upon a decrease in nozzle diameter, an increase in pre-expansion pressure, a decrease in the post-expansion temperature or a decrease in the post-expansion pressure. Also, at a higher post-expansion pressure dendritic particles were formed, most likely due to increased mass transfer. All average particle diameters listed were well below 10μm. The particles from RESS were compared to those obtained through jet milling, and it was concluded that RESS made smaller particles with a greater surface area. However, it should be noted that this is a difficult comparison to make because there is no way to compare process conditions. Not all RESS results showed improvements over the jet milled product; in some cases, the RESS product was worse.

To verify the suitability of SCF processing on steroids, the aerosol solvent extraction system (ASES)[10] was applied to: BDP, betamethasone-17-valerate, budesonide, dexamethasone-21-acetate, flunisolide, fluticasone-17-propionate, prednisolone, triamcinolone acetonide, all corticosteroids (Steckel et al. 1997). With the eventual application to inhalation therapy in mind, the drugs were co-precipitated with the surfactant phosphatidylcholine, which is able to improve the flow properties of the processed powder. No precipitates of BDP or betamethasone were formed in the experiments, and dexamethasone formed only as a film. However, of the remaining steroids tested, 90% of the particles were found in the range 1 to 10μm in all cases except the budesonide/phosphatidylcholine mixture which in some experiments reached particle sizes of 15μm. Additionally, in most cases 90% of the particles fell in the 1 to 5μm range, making them ideal for inhalation therapy. The addition and ability of co-

---

[10] The ASES is essentially the continuous version of SAS, i.e. the solid/solvent mixture is sprayed into pressurized CO_2, with an effluent line at the bottom of the vessel to allow continuous precipitation.

precipitating the steroid with a surfactant increases the drug delivery efficiency for inhalation, and increases the particle size only slightly.

Budesonide and flunisolide anhydrate were later processed using SEDS (Velaga et al. 2002). It was found that the solvent used had a strong effect on the budesonide particle morphology, with small (1-5μm) spherical particles produced with acetone, and large (5 – 30μm) plate-like particles produced with methanol. Similar results were seen with flunisolide. Also, it was discovered that the operating conditions could be used to control which polymorph was obtained in the flunisolide particles, allowing good control of the final product polymorphism.

Budesonide was also precipitated using ASES to obtain particles with an average size of ~2μm, and with nearly all the particles less than 5μm (Martin et al. 2002). The budesonide was also co-precipitated with poly(lactic acid) (PLA) as an encapsulation matrix. It is interesting to note that the precipitated PLA-budesonide particles, with an average diameter of 0.536μm, were much smaller than the pure budesonide particles (~2μm) or the PLA particles (~1.27μm). However, no explanation of this phenomenon was given. The ASES process was able to achieve a high encapsulation efficiency of about 80% compared to solvent evaporation, which could only obtain encapsulation efficiencies of 65%. Also, the budesonide maintained its biological activity, and was able to exhibit a controlled release pattern for up to four weeks.

Due to the poor water solubility of budesonide, it was co-precipitated with hydroxypropyl-β-cyclodextrin (HPBCD), which is able to improve drug dissolution (Bandi et al. 2004). The approach taken was similar to the GAS process, but no solvent was used. Instead, a mixture of the budesonide and HPBCD powders was placed in a

precipitation vessel, which then had CO_2 added. It was proposed that the addition of CO_2 lowered the glass transition temperature and melting point of the HPBCD, causing the formation of a liquid phase. This liquid phase was then able to exhibit increased interactions with the drug, as compared to the solid HPBCD phase, allowing the drug to diffuse through the liquid HPBCD. This precipitation resulted in a twenty-five fold increase in the aqueous solubility of budesonide. Also, 87% of the budesonide was released into an aqueous solution after 45 minutes, which was significantly higher than the peak of around 25% obtained for unprocessed budesonide. This would allow for a more potent fast acting drug.

To expand on the initial results in the precipitation of fluticasone (Steckel et al. 1997), it was desired to compare the powder produced by ASES to the traditional powder produced by jet milling (Steckel and Muller 1998). Fluticasone was precipitated from a DCM solution, with 5% lecithin added in some experiments. The median particle size found was smaller than that obtained by jet-milling, 1.7μm vs. 2.28μm. However, SEM revealed that while the jet-milled powder was irregular in shape, the ASES powder was made up of fibres with small spherical particles on either end. This effectively lowered the fine particle fraction as measured using a twin size impinger. However, the use of lecithin was able to significantly increase the fraction of fines. Generally, it was found that the ASES method was able to reproduce the particle inhalation characteristics obtained through jet milling, but was also able to micronize the particles while combining them with a surfactant, all in one phase.

While the focus of this section has been on asthma drugs, several other steroids have also been crystallized with SCFs. A brief list of these works is given in Table 2-6.

Also, several reports have been published on encapsulation of steroids and are described in Section 2.6.42.6.3.

Table 2-6: Steroids micronized by SCFs

Steroid	Method	Solvent	Size (μm)	Reference
Budesonide	ASES	Phosphatidylcholine	1-15	(Steckel et al. 1997)
	ASES	DCM	1-5	(Martin et al. 2002)
	SEDS	Acetone	1-5	(Velaga et al. 2002)
	SEDS	Methanol	5-30	(Velaga et al. 2002)
Dexamethasone	ASES	Phosphatidylcholine	1-5	(Steckel et al. 1997)
Flunisolide anhydrate	SEDS	Acetone	1-5	(Velaga et al. 2002)
	SEDS	Methanol	5-30	(Velaga et al. 2002)
Fluticasone	ASES	DCM	1-10	(Steckel and Muller 1998)
Hydrocortisone	SEDS	Acetone, methanol	> 2	(Velaga et al. 2002)
Medroxyprogesterone	RESS	-	1-10	(Allesi et al. 1996)
Prednisolone	ASES	Phosphatidylcholine	1-5	(Steckel et al. 1997)
Progesterone	RESS	-	1-10	(Allesi et al. 1996)

2.6.4. *Encapsulation*

One of the most interesting areas of study involving supercritical fluids is the encapsulation of pharmaceuticals in polymer matrices, usually for controlled release purposes. These matrices can be formed in a wide variety of shapes, and can be implanted in the body or administered orally, subcutaneously, or through the lungs. The ability to tightly control the final particle morphology size distribution, which allows for reproducibility of drug dissolution, makes SCFs excellent candidates as solvents/antisolvents to create polymer microspheres. The ability to completely remove the SCF, allowing a high degree of purity in the final product, is also a large reason to use SCFs. A brief list of some of the results on encapsulation can be found in Table 2-7.

Table 2-7: Polymer capsules using SCFs

Polymer	Drug	Method	Solvent	Size (μm)	Reference
PEG	Lipase	RESS	Ethanol[11]	10-20	(Mishima et al. 2000)
	Lysozyme	RESS	Ethanol[11]	10-20	(Mishima et al. 2000)
PEG / PLA	Insulin	GAS	DCM / DMSO	0.4-0.6	(Elvassore et al. 2001)
PLA	-	RESS	-	< 20	(Tom and Debenedetti 1991)
	-	GAS	DCM	0.5-3	(Randolph et al. 1993)
	Lysozyme	SAS	DCM	250-500	(Young et al. 1999)
	Insulin	GAS	DCM / DMSO	0.5-5	(Elvassore et al. 2001)
	Budesonide	ASES	DCM	0.54	(Martin et al. 2002)
PGLA	Lysozyme	SAS	DCM	5-60	(Young et al. 1999)

Encapsulation of pharmaceuticals was first done using SAS to encapsulate lysozyme within L-PLA and PGLA (Young et al. 1999). The lysozyme was initially suspended (not dissolved) in the polymer solution, which was then pumped into a vessel containing liquid CO_2. There appeared to be two major hurdles in precipitating the encapsulated proteins. First, to encapsulate the protein particles the polymer particles needed to be larger than the protein. Therefore, they found very little encapsulation when small polymer particles were formed (i.e. 1-5μm). Second, if the temperature was too high, significant agglomeration was seen due to softening of the polymer. However, if the temperature was too low, then mixing was poor and large particles were obtained. An optimal operating temperature of -20°C was found to balance these two effects.

Another study was performed around the same time using RESS to encapsulate lipase and lysozyme in PEG (Mishima et al. 2000). It was noted that the polymer concentration alone could be used to control the particle size, as well as the thickness of

---

[11] In this study methanol, propanol, acetone, and toluene were also used. However, the best results were obtained for ethanol, so that is what is shown here.

the polymer layer in the capsule. This allows for better control and prediction of the dissolution characteristics in the final product. Finally, it was noted that ethanol was the optimal solvent for this system, as it exhibited the highest solubility in the polymer + solvent + CO_2 mixture. This is particularly interesting because ethanol is a very poor solvent for the pure polymer. Additionally, because ethanol is volatile and not soluble in the polymer, after RESS processing the ethanol quickly evaporated instead of dissolving into the microcapsules.

The first studies to ensure that biological activity of the proteins remained after SCF processing was in 2001. Insulin was precipitated from a DCM/DMSO mixture using the GAS process, and encapsulated in L-PLA (Elvassore et al. 2001). The protein loaded capsules were quite a bit smaller than in previous experiments (Young et al. 1999; Mishima et al. 2000), with an average particle diameter ranging from 0.5 to 5μm. It was found that approximately 80% of the protein was encapsulated, and when injected into mice it maintained its biological activity.

In a second study (Elvassore et al. 2001), precipitated PEG/PLA capsules of insulin from DCM or DMSO using the GAS process. PLA biodegrades slowly and is hydrophobic, and thus is not optimal for controlled release applications. Therefore, PEG was added to increase drug delivery and biodegradation rates. In these experiments even smaller particles were obtained, with 90% of the material in the range of 400 to 600nm. Higher encapsulation efficiencies were also seen, with average values around 90%. The solvent remaining within the capsules was found to be ~10ppm for DCM and 300ppm for DMSO. Both values are well below the accepted limits of 300 and 600ppm, respectively. Finally, the insulin release profiles were evaluated, and it was discovered that high

molecular weight PEG capsules released their insulin as a quick initial burst, whereas low molecular weight PEG provides a slow and steady release rate that could be maintained for up to 1500 hours. This shows how the SCF processing conditions can be used to optimize the release profiles for one particular application.

A rather significant problem with controlled release formulations delivered to the lungs is the immune system. Drug particles that cannot diffuse into the blood quickly are either swept away by cilia or degraded by macrophages, in addition to the low delivery efficiency of drugs to the alveoli. One possible solution to this problem is to make particles too large to be digested by macrophages (geometric diameter > 5μm) that are highly porous (and thus have low density, < 0.1g/cm^3) so that they can still be delivered to the deep lung (Koushik and Kompella 2004).

To create porous particles, supercritical CO_2 can be used to expand existing polymer/drug composites (Koushik and Kompella 2004). PLGA-deslorin particles were formed as 1-2μm spheres in DCM using solvent evaporation techniques. CO_2 was then added to the particles to expand them, increasing the geometric diameter to 10-15μm and creating a highly porous, irregular surface. Additionally, the residual DCM was lowered from 4500ppm (an order of magnitude above the allowable limit) to < 25ppm. Deslorin was released steadily for 7 days, though depending on the CO_2 expansion conditions the initial burst varied from 7% to 50%, and the final delivered dose from 40% to nearly 100%, allowing the expansion conditions to be used as a means of controlling drug release characteristics for a particular application. Finally, the cellular uptake of the composite particles was found to be significantly reduced after CO_2 processing, ranging from a 50 to 90% reduction as compared to the particles that were not expanded.

3. Experimental Procedures

3.1. *GAS experiments*

3.1.1. *Materials*

Gas antisolvent experiments were performed using instrument grade carbon dioxide (99.99% purity, Praxair gases), which was further purified with a 2µm filter (HIP). The solvent used was HPLC grade acetone (99.9% purity, Sigma-Aldrich chemicals). The solute used in the GAS experiments was beclomethasone-17,21-dipropionate monohydrate, donated by GlaxoSmithKline, without any further purification. The system was washed with ACS grade acetone (99.5% purity, EMD chemicals) in between every experiment.

3.1.2. *Apparatus*

All GAS experiments were carried out in a 100mL high pressure vessel (rated to 3,300 psi), designed and built by Autoclave Engineers. The vessel was constructed from 316 stainless steel. CO_2 was supplied to the vessel by an Isco 260D syringe pump. The temperature in the pump was controlled using a VWR chiller/circulator (Model 1180A), which used water to keep the pump contents at a constant temperature. Backflow of CO_2 from the vessel into the pump was prevented using an HIP check valve (model 15-41AF1, rated to 15,000 psi). The flow of CO_2 into the vessel was controlled using a pneumatic Badger Meter control valve, type 759, and a 100psig air line was used to operate the valve pneumatically (see Section 3.2.1).

The CO_2 exit gas flow rate from the vessel was controlled manually using an HIP needle valve (model 15-11AF2, graded to 15,000 psi), and adjusted as required throughout the experiment. As the valve throttled the gas down to atmospheric pressure

rather significant cooling was observed as the gas was throttled. This led to the freezing of the solvent, causing clogging of the tubing. To avoid this undesirable effect, the valve was immersed in a 2L water bath (Fisher Scientific, Isotemp 202), which was maintained at approximately 55°C for the duration of the experiment.

Agitation was provided by a Carter 90V motor, attached to a MagneDrive II magnetic agitator. The motor speed was controlled using a Hall sensor attached to an Autoclave Engineers motor control (model MSC40H1100100). The complete apparatus is shown in Figure 3-1 and schematically in Figure 3-2. However, the Badger Meter control valve was not shown in detail in Figure 3-2 for the sake of simplicity.

Figure 3-1: Apparatus used for GAS experiments
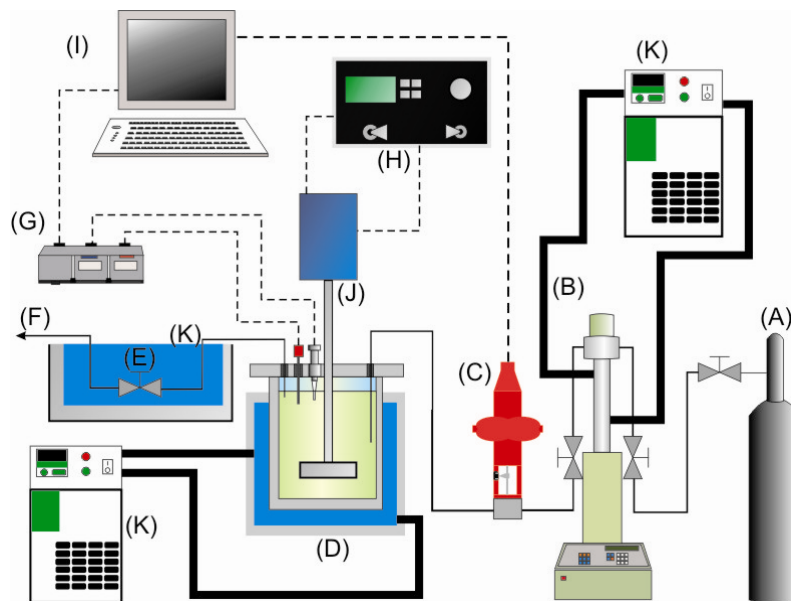
Figure 3-2: Schematic of the apparatus used for GAS experiments, with a CO_2 cylinder (A), syringe pump (B), pneumatic control valve (C), high pressure vessel (D), needle valve (E), 1/16" exit line (F), FieldPoint unit (G), motor control (H), computer (I), motor (J), and water baths (K).

The temperature in the vessel was measured using a T-type thermocouple. The temperature signal was input to a FieldPoint module (FP-TC-120), where it was monitored using LabView software. This allowed the temperature to be controlled using standard PID control logic, as discussed in Section 4.1. The vessel temperature and CO_2 addition rate were controlled using LabView, as described in Section 3.2.1. LabView was also used to monitor the pressure in the vessel as well as the pump pressure, volume and flowrate.

The syringe pump was connected directly to the computer through an RS-232 serial port, which allowed control of the pump using a LabView virtual instrument (VI). The vessel pressure signal was amplified with an FP-AI-V100m FieldPoint card, and fed to LabView through an FP-TB-10 FieldPoint module. The LabView VI developed in this work is shown in Figure 3-3.
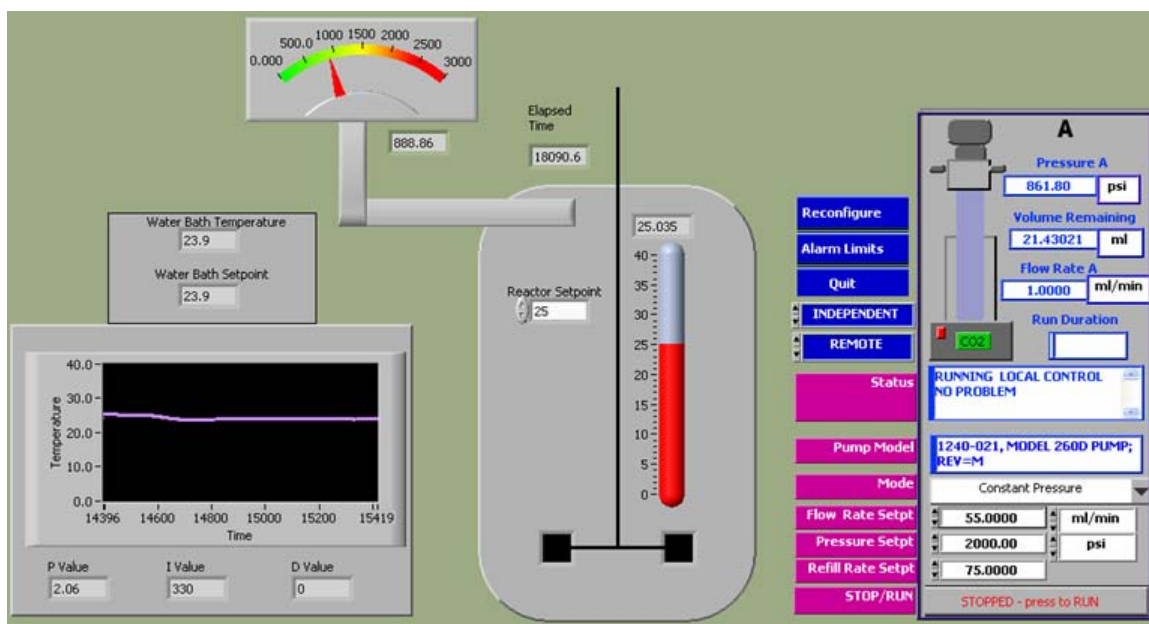
Figure 3-3: LabView VI

3.1.3. *GAS crystallization procedure*

The desired amount of drug was initially dissolved into 10mL of acetone in a glass vial and mixed vigorously to ensure that the solute was fully dissolved. This mixture was placed in the precipitation vessel which was then sealed. The system temperature and agitation rate were set, and maintained for approximately thirty minutes in order to reach steady state. At the same time, the pump temperature was set to the same value as the vessel temperature, and the pump was pressurized to 2000psig for each experiment. The experiment was not started until the pump had reached equilibrium, which was indicated by an approximately zero flow rate on the pump controller.

Once both the vessel and pump were equilibrated, the desired (volumetric) flowrate was set, and the pneumatic control valve was controlled using LabView to maintain the flowrate throughout the pressurization phase. CO_2 was added until the vessel reached 1000psig, at which point the control valve was shut. To ensure that the system reached equilibrium before rinsing, agitation was continued for forty-five minutes

after pressurization. Then, to allow the particles to settle before rinsing, the system was allowed to sit without agitation for another ten to fifteen minutes. Both of these steps were performed with the vessel inlet and outlet closed.

The precipitated solute was then rinsed with CO_2 for approximately six hours. The pressure was maintained constant throughout this phase by using the backpressure provided by the CO_2 cylinder. This allowed the rinsing to proceed at constant pressure and constant flow. Due to the nature of the antisolvent system, it is important to maintain the pressure while rinsing above the pressure required for phase inversion. If this is not done, then the solvent will form a pure liquid phase and the solute could re-dissolve. At $25^{o}C$, this corresponds to a pressure of approximately 750psi.

After rinsing the particles, the vessel was depressurized and the sample collected, weighed, and stored for further analysis. Particles were found to be dry in all reported cases. The total run time of an experiment was usually between 6 and 10 hours, including time allowed for the sample preparation, system equilibration, rinsing, etc.

3.2. *Controller tuning*

3.2.1. *Apparatus*

The apparatus used was described in detail in Section 3.1.2. The flowrate of CO_2 into the vessel was controlled using a Badger Meter pneumatic control valve (Type 759). Air was supplied to the valve using a 100psi air line from a fume hood. This air was put through a regulator which output a constant pressure of 60psig, so that fluctuations in the fume hood pressure would not affect the control valve. The valve was controlled pneumatically using a pressure between 3 and 15psi. Both the water bath and the control valve were controlled using LabView.

3.2.2. *Procedure*

In order to develop temperature control for the vessel, the following procedure was used. To simulate the approximate conditions during GAS operation, the vessel was first pressurized and maintained at 1000psig with CO_2, while the agitation was set to 1000RPM. The water bath was then started and the temperature in the bath was set, while LabView was used to monitor the temperature in the vessel and in the bath. Once the temperature in the vessel had maintained the same value of temperature for at least 5 minutes, the set point on the water bath was changed. The temperatures of both the water bath and the pressure vessel were monitored until the vessel temperature had maintained the same value for at least 5 minutes. At this point, another step change could be performed. Once this was performed, a process model was constructed and the tuning parameters were obtained (see Section 4.1).

A similar procedure was followed for the control valve tuning. The vessel was kept open, as the conditions within the vessel were assumed to have little effect on the ability of the valve to control the flow. This allowed the pump to operate for long periods of time without worry of over-pressurizing the vessel. The control valve was operated by manually changing the signal current between 4 and 20mA, with 20mA closing the valve completely and 4mA opening the valve completely. The current signal and the flowrate of CO_2 were both monitored using LabView. The valve position was maintained until a steady flowrate was obtained, which took approximately one minute. When a steady flowrate was obtained, the position was changed and the new position and flowrate were monitored until a steady value was achieved. Once this was performed, the tuning parameters were obtained assuming a first order system model (see Section 4.1).

3.3. *Particle characterization*

3.3.1. *Laser diffraction particle sizing*

To obtain the particle size distribution (PSD) a Malvern Mastersizer 2000 with a Hydro S dispersing unit was used (see Figure 3-4). The Mastersizer measures particle size using laser diffraction (see Figure 3-5). The operating principle behind this technique is that a laser is shined into a cell which contains the particles whose sizes are to be measured. As the laser reflects off of the individual particles, it creates a scattering pattern which is acquired by detectors. This process takes approximately 1 ms and is repeated over 2000 times to ensure that a large amount of particles are measured for statistical purposes (Malvern 1999).

Figure 3-4: Malvern Mastersizer 2000 with Hydro S attachment
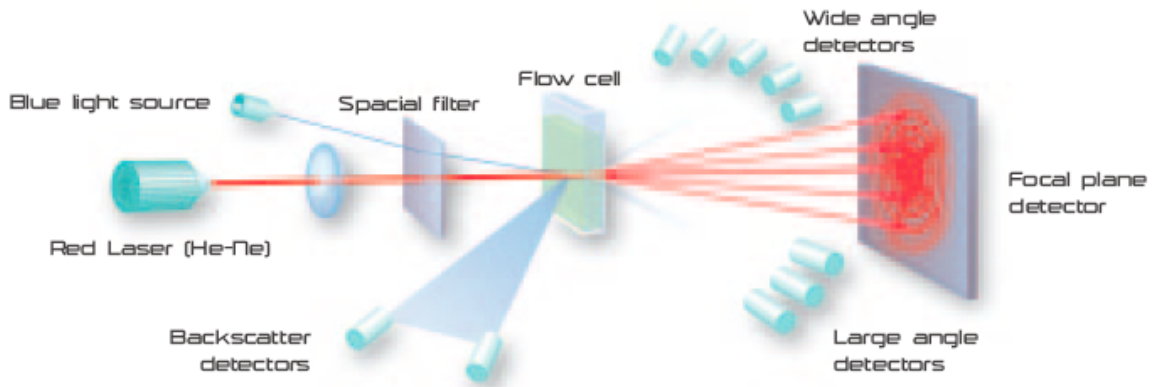
Figure 3-5: Detection schematic in Mastersizer (Malvern 1999)

Once the scattering pattern has been determined, it can be converted into a particle size distribution using Mie theory, which was developed to calculate scattering patterns for particles given the size, refractive index, and adsorption. It should be noted that this theory assumes that the particles analyzed are perfect spheres. Since this is not normally true, the Mastersizer takes the volume it measures and converts this into an equivalent diameter for a sphere (Malvern 1999).

Before each analysis, the Mastersizer was rinsed thoroughly with distilled water and some surfactant to remove any residual particles. The system was then de-gassed twice to remove any bubbles present in the system. The agitation was then set to 2975RPM and the sample was added until an appropriate obscuration level was achieved (normally 2-5%). A few drops of a dilute Triton X-100 surfactant solution was added to lower the liquid surface tension, allowing the particles to disperse throughout the liquid.

After the sample was added and dispersed, it was analyzed 7 times at 30 second intervals to ensure that the measured distribution reached a steady state. Ultrasound was then turned up to 30% to break up any aggregates, and the sample was measured another 7 times at 30 second intervals. By measuring the samples in this manner, we were able to determine both the size of the aggregates as well as of the individual particles. Each GAS experiment was analyzed twice to ensure reproducibility.

3.3.2. *Scanning Electron Microscopy (SEM)*

SEM was used for two reasons: to visually confirm the particle sizes obtained using laser diffraction, and to observe the crystal shape, structure, and agglomeration. Electrons are produced for the SEM using an electron gun. After the electrons leave the

gun, they pass through a condenser lens which focuses the beam and allows a small are of the sample to be observed. The beam is then deflected across the sample so that a large area can be observed. As the electrons travel towards the sample, a significant repulsive force will occur due to interactions with electrons within the sample. If this force is strong enough, electrons from the sample will be ejected (called secondary electrons), which are then observed by a secondary electron detector. As these electrons are emitted from the sample surface, the SEM is able to create pictures with depth (Dykstra 1992).

As the images are produced by electrons ejected from the sample, it is important that the sample is conductive. However, this is not the case in many systems of interest in biology/pharmacy. Therefore, non-conductive specimens are often coated with a thin layer of gold. For this work, though, BDP was found to be conductive enough to provide good images at low voltages (1-1.5kV), therefore the samples were loaded directly onto carbon tape and analyzed.

3.3.3. *Differential Scanning Calorimetry (DSC)*

DSC is a simple technique most commonly used to observe phase changes, such as melting or glass transition. DSC works by raising the temperature of two samples, a reference sample and the sample of interest, linearly with time while monitoring the heat flux provided to both. When a phase change in the sample occurs, the heat flux required to increase the temperature will be increased or decreased, depending on the nature of the phase change, from that required for the reference sample. For example, when a solid melts it will require a great deal more heat to maintain the same rate of temperature increase as the reference. Therefore, there will be a large spike in the heat provided, which can be used to estimate the melting point of a sample (Ehrenstein et al. 2004).

A small aluminum tray was filled with sample (usually 8-10mg), and was sealed with a perforated aluminum lid to allow any vapours to escape. Once the DSC instrument had reached its initial temperature of 50°C, the sample was placed in the heating chamber opposite the reference sample. The temperature was then increased at a rate of 10°C/min to a final temperature of 250°C, after which the unit was cooled and the sample removed. The melting point and heat of fusion were then determined by interpolating the temperature at the peak and integrating the area beneath the peak, respectively.

3.3.4. *High Performance Liquid Chromatography (HPLC)*

Chromatography can generally be defined as a technique which separates mixtures by passing them over a stationary phase with a particular quality such as charge or polarity. As an example, ion exchange chromatography involves passing a mixture over a column packed with charged beads. Therefore, an oppositely charged molecule will travel through the column quickly, while a molecule with the same charge as the column will be retained. HPLC is essentially liquid chromatography performed at higher pressures, which allows for greater resolution by decreasing diffusion within the column. Normally, polarity is the criterion for separation in HPLC analysis. In this work, HPLC was used to determine the purity of the GAS processed samples (Walsh 2003).

A few milligrams of BDP was dissolved in 5mL of acetonitrile and run through a single reversed phase C_{18} HPLC column. The mobile phase employed was a mixture of methanol, acetonitrile and water (30%, 60%, 10%), with a flowrate of 1mL/min. The analyte was detected using a UV detector at 254nm.

4. Experimental Results

4.1. *PID controller tuning*

The effect of temperature on the final particle size distribution using the GAS process is very important (Bakhbakhi 2004), so a good temperature controller needed to be developed using the techniques of process control. To determine the control parameters, several open loop tests were performed. In these tests the vessel was filled with CO_2 to 1000psi and the agitation was set to 1000RPM in an attempt to roughly simulate the conditions during a GAS experiment. Once this was done, the temperature of the water bath was changed, and the temperature of both the bath and the vessel were monitored until both had stabilized (see Section 3.2 and Figure 4-1). It was found that this system could be approximated as a first order system with dead time, which has the following general equation (Seborg et al. 2004):

$$\Delta T^{vessel} = KM \left(1 - e^{\frac{(t-\theta)}{\tau}} \right) \tag{4.1}$$

where ΔT^{vessel} is the temperature change in the vessel, K is the steady state gain constant, M is the magnitude of the step change, t is the time, θ is the dead time, and τ is the time constant. The data from the step change was fit to this model, and the three parameters were regressed. Several runs were performed, and are given with their associated K, τ and θ values in Table 4-1. Therefore, the process model determined for this system was:

$$\Delta T^{vessel} = 0.91134M \left(1 - e^{\frac{(t-55.612)}{329.514}} \right) \tag{4.2}$$
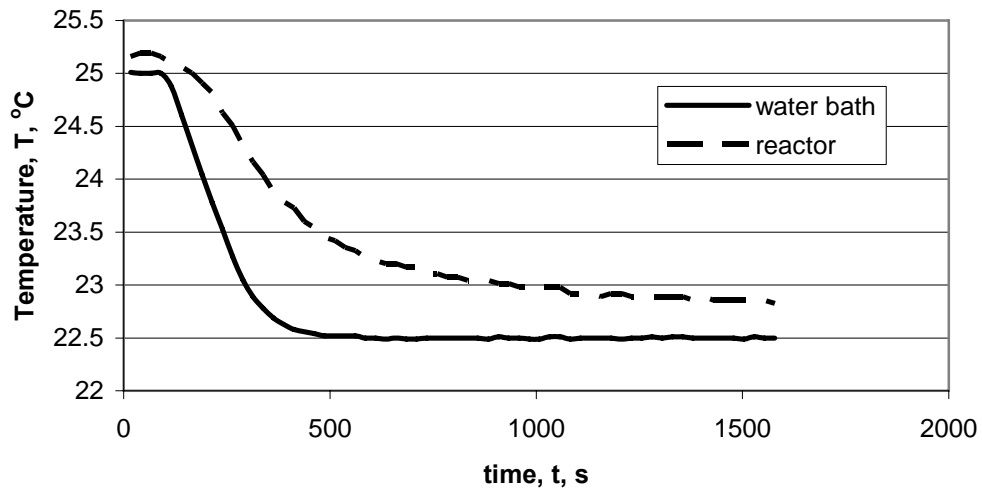
Figure 4-1: Sample of vessel step change profile

Table 4-1: System parameters for PID tuning

Step Change (^{o}C)	25-30	25-27.5	25-22.5	22.5-25	25-20	20-25	Mean
K	0.90799	0.87677	0.96281	0.87777	0.93644	0.90625	0.91134
τ	396.633	311.054	375.543	234.674	425.749	233.433	329.514
θ	67.3747	72.5339	76.0792	27.4178	69.7382	20.5297	55.6122

These parameters were input into the Matlab file recipe.m (Jutan 2004), which determines appropriate values for the control law parameters K_c, τ_I and τ_D based on 8 different tuning methods. Each of these sets of tuning parameters was tested with the system model in Simulink as a closed system (see Figure 4-2 and Figure 4-3) to determine which gave the best response. It was found that the direct synthesis PI method ($K_c = 2.06$, $\tau_I = 330$, $\tau_D = 0$) gave the best response to a step change, hence these were the control parameters used for the experiments reported in this work.
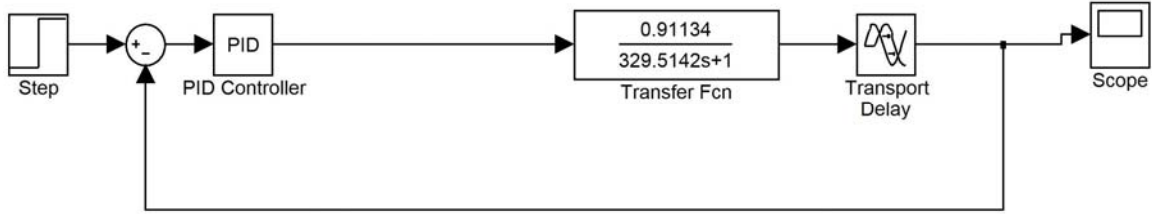
Figure 4-2: Simulink block diagram
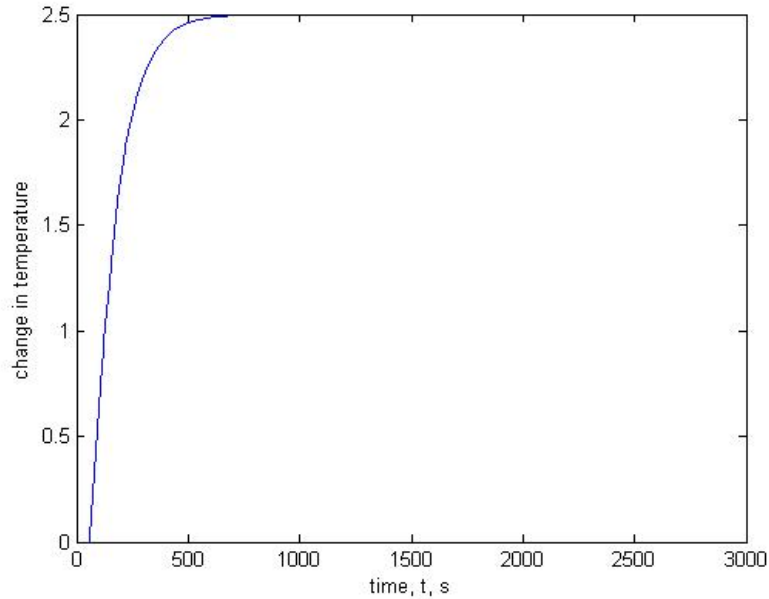
Figure 4-3: Closed loop test of system using direct synthesis PI control parameters

Once the control parameters were determined, the actual control law needed to be implemented in LabView. This was done using the LabView/Matlab interface in the block diagram, which allows Matlab code to be used within a LabView program. The Matlab block takes in values for K_c, τ_I, τ_D, the current temperature setpoint, and the current reactor temperature. The block implements the velocity form of the standard control algorithm (Seborg et al. 2004), and updates the water bath set-point temperature:

$$T_{new} = T_{last} + K_C\left(e_2 - e_1\right) + \frac{K_C}{\tau_I}e_2\left(t_2 - t_1\right) + \frac{K_C}{\left(t_2 - t_1\right)}\tau_D\left(e_2 - 2e_1 + e_0\right) \qquad (4.3)$$

where T_{new} represents the new water bath set-point, T_{last} represents the old water bath set point, t_i represents the time at i, e_i represents the error between the reactor set point and

the reactor temperature at i, and the subscript i represents the order of the measurement, i.e. e_2 is the current value for error, e_1 is the prior value for the error and e_0 is the error value prior to e_1. It should be noted that the control law was given a minimum water bath set-point temperature of 10°C, and a maximum of 40°C, to prevent damage to the equipment.

Due to of the importance of the flowrate to the obtained crystal size distribution, a control valve was used so that the pump could be run at a constant pressure and flowrate. The same general method was used to tune the control valve as with the water bath, and the results from several step changes along with the corresponding K and τ values are given in Table 4-2, and a sample step change is shown in Figure 4-4. The process dead time observed was negligible, and therefore was not considered.

Table 4-2: Model parameters for the control valve

	step 3	step 7	step 8	step 10	step 11	step 12	average
current (mA)	$15 \rightarrow 17$	$17 \rightarrow 16$	$16 \rightarrow 15$	$13 \rightarrow 16$	$16 \rightarrow 14$	$14 \rightarrow 12$	
K	-9.96	-13.25	-9.659	-11.67	-9.57	-10.90	-11.58
τ	0.955	1.609	2.791	1.380	1.954	1.244	1.456
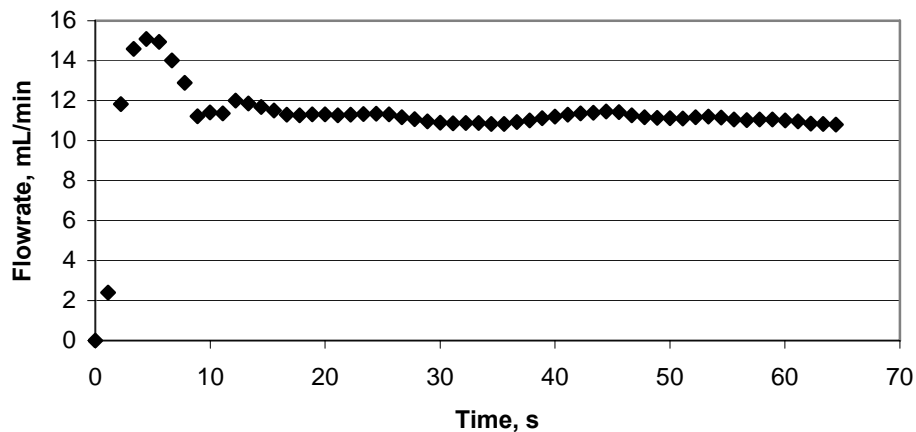
Figure 4-4: Step change in the current sent to the control valve

The program recipe.m (Jutan 2004), described earlier, was used to determine values of K_c, τ_I and τ_D. The Ciancone (set point) method was found to give the best response upon simulation in Simulink, as described above, with tunning parameters $K_c = -0.122$, $\tau_I = 1.09$ and $\tau_D = 0$. However, as can be seen in Figure 4-4, valve action is inherently a second order process. Therefore, the assumption of a first order process was chosen for simplicity, and used to determine an "initial guess" of the values for K_c, τ_I and τ_D, which were then tuned manually. The final values used were $K_c = -0.015$, $\tau_I = 0.95$ and $\tau_D = 0$, and were implemented using Equation (4.3), as with the water bath.
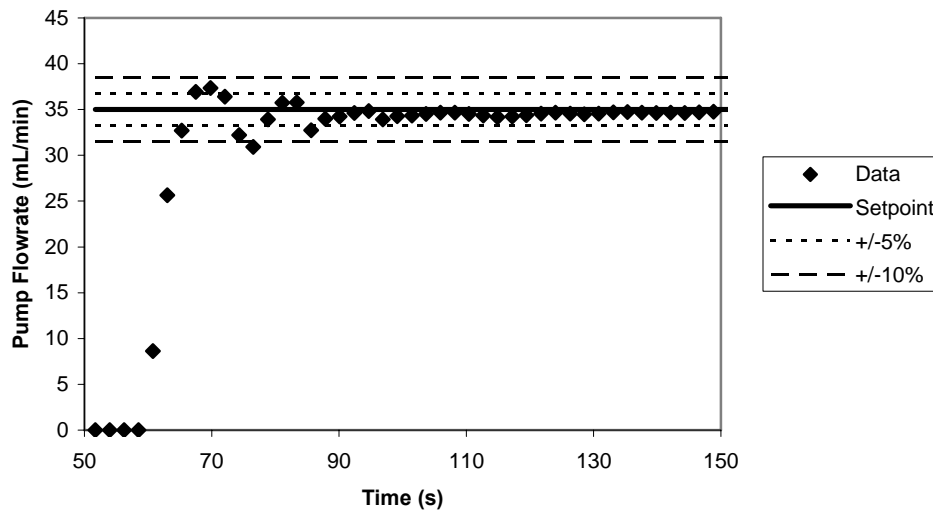
Figure 4-5: Pump flowrate (mL/min) vs. time while running at constant pressure with control valve
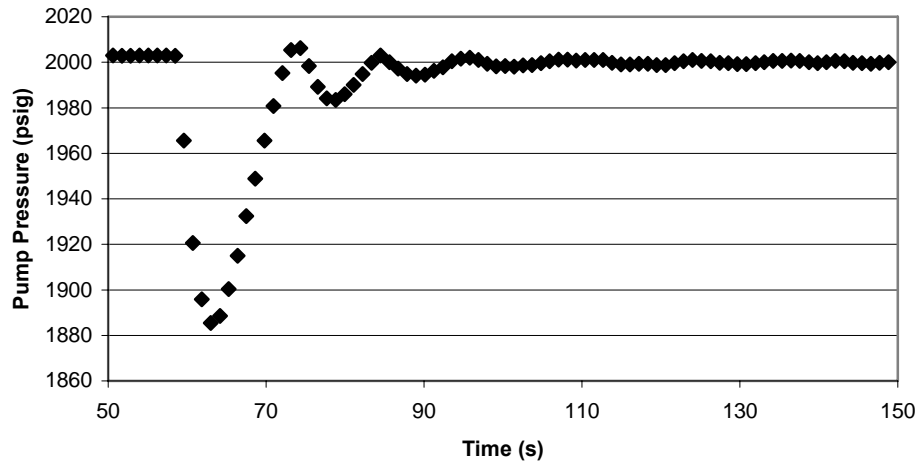
Figure 4-6: Pump pressure vs. time while running at constant pressure with control valve

As can be seen in Figure 4-5, the valve was able to control the flow reasonably well, achieving a steady value within 10% of the set-point fairly quickly. Also, the pressure was maintained within +/- 10% of 2000psig (Figure 4-6). This slight pressure fluctuation has a negligible effect on the mass flowrate of CO_2, as can be seen in Figure 4-7. The mass flowrate was calculated using pressure-density data from the NIST database (NIST 2003) to obtain the density as a function of pressure for CO_2.
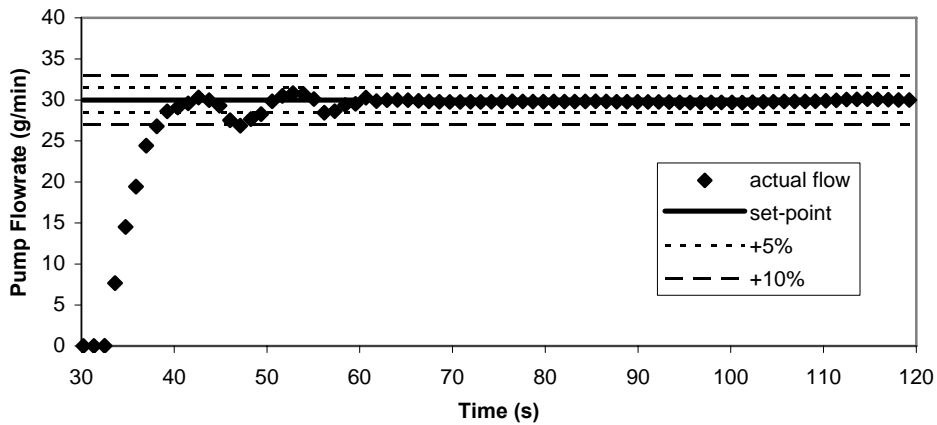
Figure 4-7: Pump flowrate (g/min) vs. time while running at constant pressure with control valve

While the flowrate control was found adequate for the current study, future work could be done to improve control. As the pump adjusts the flowrate to maintain a

constant pressure of 2000psig, once that setpoint is reached, the pump lowers the flowrate to maintain it (see Figure 4-8); this is what causes the oscillatory behaviour in the flow. If the controller were made to monitor the pump pressure as well, though, then it should be possible to account for this and adjust the flowrate accordingly to avoid any oscillations.
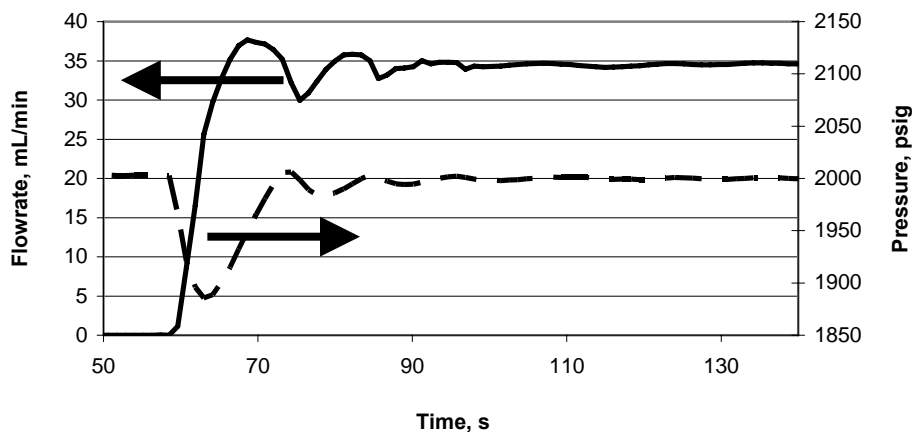
Figure 4-8: Flowrate and pressure profiles at the pump during pressurization at 25°C

4.2. GAS experiments

The gas antisolvent apparatus described in Section 3.1 was used to perform several experiments, with the conditions summarized in Table 4-3. The parameters studied were agitation, temperature and CO_2 addition rate in an attempt to better understand the effect of each variable on the crystal size distribution produced. The agitation rate and CO_2 addition rate were chosen to span the working limits of the equipment. The temperature was chosen to expand upon the work done by Bakhbakhi (2004). All experiments were performed using 10mL of acetone and 300mg of beclomethasone. Also, the vessel was pressurized to approximately 1000psi in every experiment.

It must be stressed that all particle sizes are reported as volume weighted diameters instead of number weighted diameters. This is why there is such a large discrepancy between the results reported in the literature for GAS (see Section 2.6), which are given as number densities, and the results reported here. Volume weighted distributions are given because they are more relevant to drug delivery, as knowledge of the mass of drug in a particular size range is very important, as discussed earlier in Section 2.

The purpose of the experimental study was two-fold. To process BDP using the GAS process it is important to understand how the process variables affect the particle size distribution. This way the product can be optimized for a particular use, such as inhalation therapy, and good control of the final particle size can be obtained. A model of the GAS crystallization process is also desirable, as it will yield a better understanding of how the particles form, and so can also be used to optimize the particle size distribution for a particular application. Additionally, a model can lower the number of required experiments by providing some predictive capabilities. Therefore, experimental data is also needed for determination of the kinetic constants involved in GAS crystallization modelling, as discussed in Section 6.

The flowrates in Table 4-3 were listed in mL/min because the pump records the volumetric flowrate. However, because the control valve maintained a pressure close to 2000psig in the pump during pressurization (see Section 4.1), the mass flowrate is essentially constant and was not shown in the interests of space. However, it must be noted that the same volumetric flowrates were used at the different temperatures, and therefore the mass flowrate was not consistent from one temperature to the next, because

the density was different. This approach is justified because the change in density is not large enough to significantly affect the experimental outcome, with only a 3% difference between the mass flowrates observed at 20 and 25°C for the same volumetric flowrate.

Table 4-3: Summary of experimental conditions studied

Run	Temperature (^{o}C)	Agitation (RPM)	Flowrate (mL/min)
F1	25	1000	25
F2	25	1000	50
F3	25	1000	75
A1	25	200	50
A2	25	1800	50
A3	20	200	50
A4	20	1000	50
A5	20	1800	50
F4	20	1000	25
F5	20	1000	75
T1	30	1000	50

Both HPLC and DSC were used to verify the purity of the GAS processed powders. Using HPLC, the purity of the unprocessed BDP was found to be 99.9%, and a retention time of 3.48 minutes was observed (the time corresponding to the BDP peak, see

Figure 4-9). Four samples were chosen from the GAS processed powder to check the purity, and determine if there was any obvious effect of process conditions. The average purity was found to be 99.5%, so the processed powder was essentially pure. Additionally, the relative standard deviation[12] of the purity for the GAS processed samples was 0.14%, indicating that the experimental conditions had very little effect on the purity of the final product.

The purity of the samples was also verified using DSC to obtain the melting temperature and the heat of fusion for BDP. The original and GAS processed BDP were

---

[12] The relative standard deviation is defined as the standard deviation of a set divided by the average.

both found to have an extrapolated melting point of 211°C (at16.1 minutes), which was verified visually with a hot stage microscope. As the unprocessed beclomethasone obtained from GlaxoSmithKlein is a monohydrate, the drop around 100°C (at 5 minutes) is presumed to be crystal lattice restructuring due to the evaporation of water.

Retention time, min
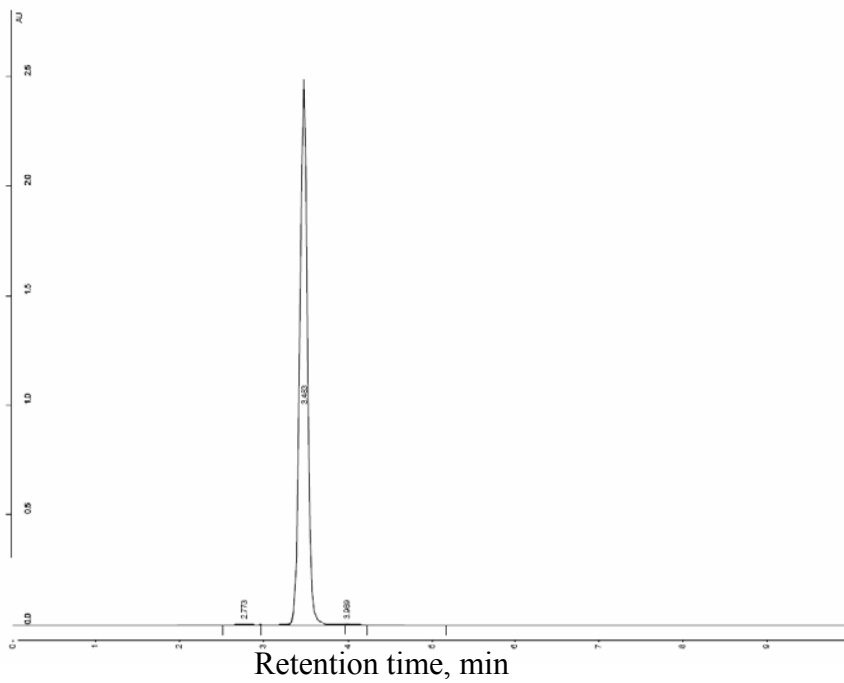
Figure 4-9: HPLC profile of pure BDP

Retention time, min
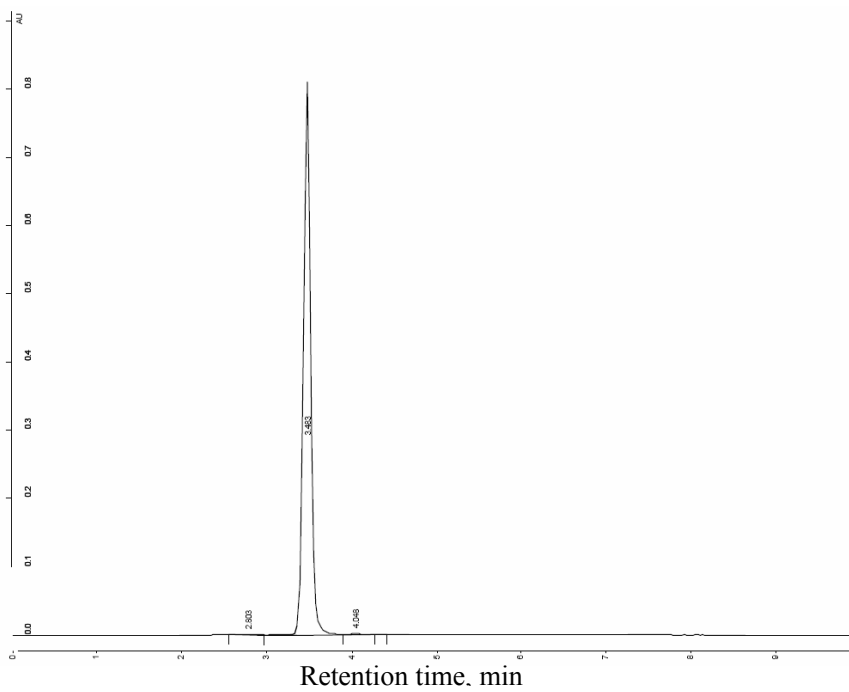
Figure 4-10: HPLC profile of GAS processed BDP (run F2)

10
mW

0   2   4   6   8   10   12   14   16   18   min

Time, min
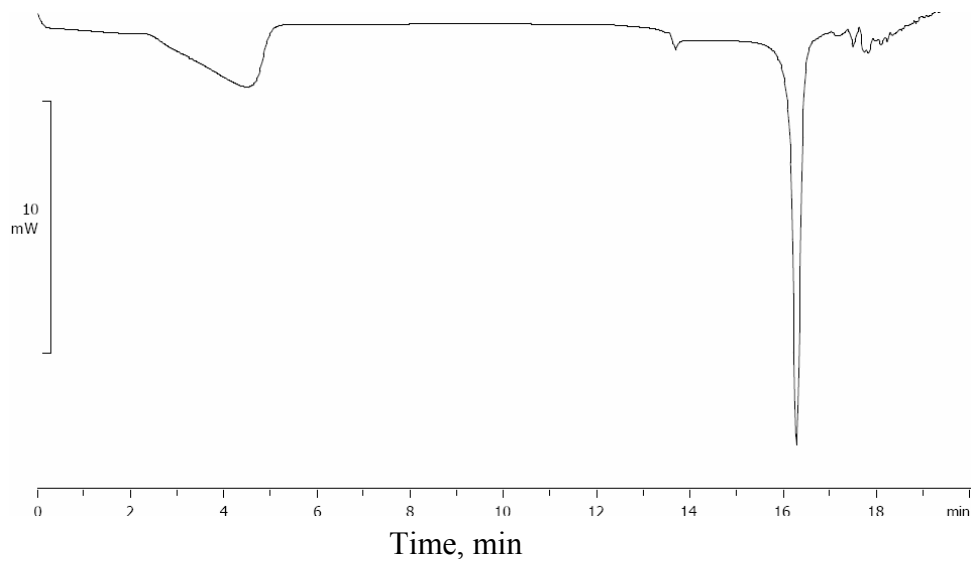
Figure 4-11: DSC profile of pure BDP

10
mW

0   2   4   6   8   10   12   14   16   18   min

Time, min
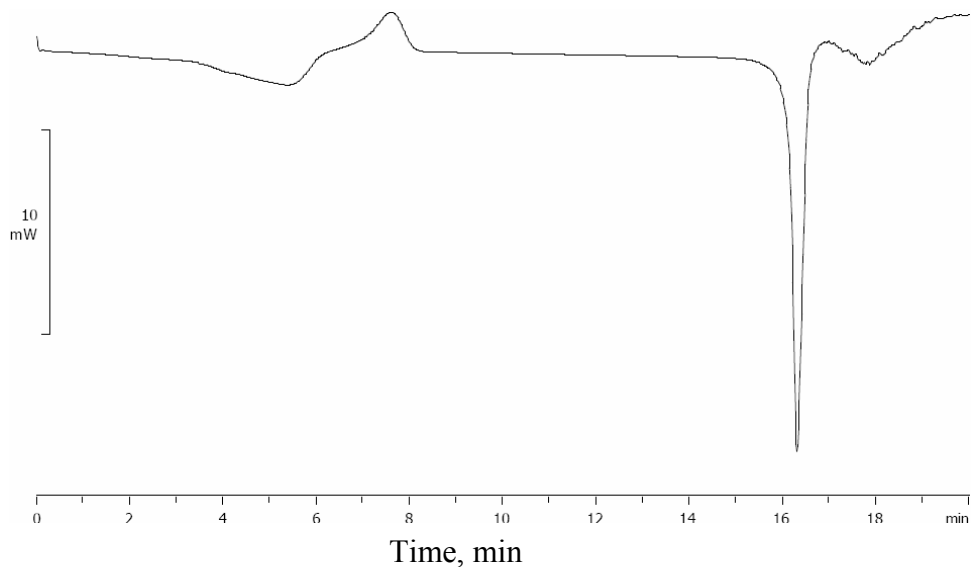
Figure 4-12: DSC profile of GAS processed BDP (run F2)

4.2.1. *Effect of agitation rate*

In this work, three different agitation rates at two temperatures were studied, namely 200, 1000 and 1800 RPM at 20 and 25°C. In all cases, a flowrate of 50mL/min was used. The particles were analyzed both with and without sonication so that a better indication of the level of aggregation could be obtained. The results are summarized in Table B1-1 for analysis without sonication, and in Table B1-2 when sonication was used.

In the tables, $d_p(10\%)$ represents the diameter at which all smaller particles take up 10% of the total volume, while $d_p(50\%)$ and $d_p(90\%)$ have analogous definitions. $d_p(4,3)$ represents the volumetric mean diameter, and is written as such because the volumetric mean is defined as the fourth moment of the particle size distribution divided by the third moment, thus 4,3. The relative standard deviation of each result is given in brackets next to the particle size as a percent.

Sonication was used on the powders to break up any loose aggregates, ideally allowing individual particles to be studied. However, sonication will not break up any agglomerated particles[13], which are held together by strong bonds. Also, as the crystallization model described in Section 6 did not account for aggregation, sonication was required in order to make a comparison between experimental and predicted particle size distributions. The size of the sonicated particles is given in Table B1-2 and Figure 4-13. The figure describes the $d_p(10\%)$, $d_p(50\%)$ and $d_p(90\%)$ of the particle size distribution individually instead of by providing the volumetric mean to give a better indication of the full range of the distribution.

---

[13] An aggregate is a collection of particles held by weak forces, such as van der Walls forces, while an agglomerate is a collection of particles held by strong forces, such as chemical bond.

The sonicated samples exhibited an interesting trend. While a decrease in particle size with an increase in agitation was observed at 20°C, the particle size appears to have increased with an increase in agitation at 25°C (see Figure 4-13). Generally, the effect of agitation is believed to improve mass transfer (Lin et al. 2003). However, if too much energy is input to the system there can be an increase in particle-particle collisions, causing larger particle sizes to be observed as the particles agglomerate (Chattopadhyay and Gupta 2002). Therefore, it is possible that at 25°C mass transfer was not a limiting factor and interparticle collisions dominated, causing an increase in particle size (due to agglomeration) with an increase in agitation rate. However, at 20°C a decrease in mass transfer limitation due to an increase in the agitation rate led to smaller particles. This could also explain why the result at 200RPM was larger for 20 than 25°C, where the mass transfer limitations were strong enough to counteract the effect of operating at a lower temperature.
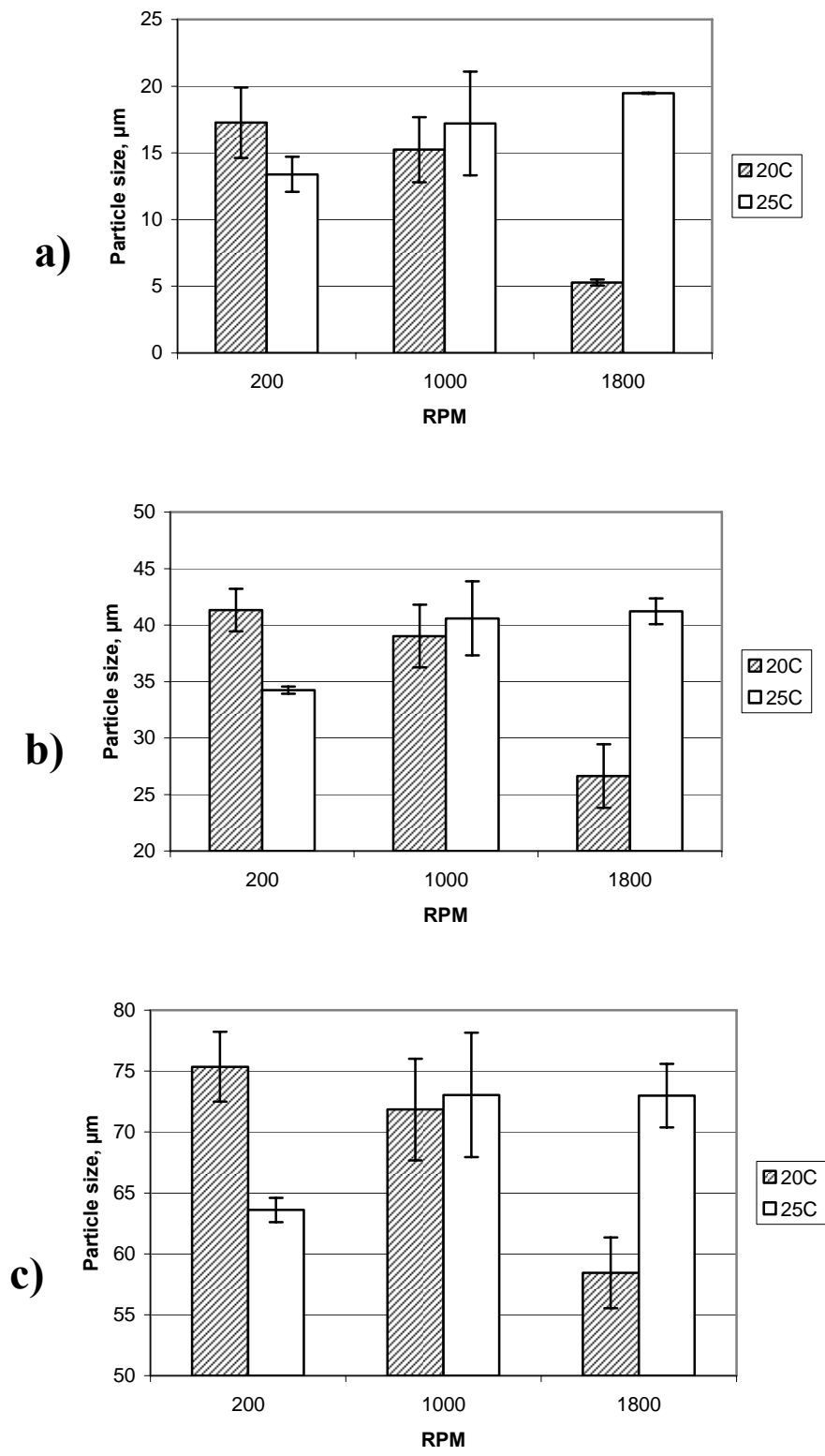
Figure 4-13: Effect of agitation on particle size with sonication for: a) $d_p(10\%)$, b) $d_p(50\%)$, c) $d_p(90\%)$

It is also possible that there was in fact no significant effect of increased agitation rate on the sonicated particles at $25^{\circ}C$, given the overlap of the error bars and data points seen in Figure 4-13, at 1000 and 1800RPM in particular. This would also be consistent with the hypothesis that CO_2 mass transfer is not limiting at $25^{\circ}C$, because the increased agitation speed should improve CO_2 dissolution into the liquid phase, and thus create smaller particles. Therefore, as the particles did not get smaller with an increase in agitation rate, the maximum mass transfer rate had likely already been obtained.

The sizes for the unsonicated particles, which represent the aggregates, are shown in Figure 4-14. When sonication was not used, there was a clear decrease in the size of the aggregates when the agitation was increased at both temperatures studied (see Figure 4-14). Also, the aggregates formed at $20^{\circ}C$ were found to be smaller than those formed at $25^{\circ}C$. At $25^{\circ}C$ the size of the aggregates decreased (Figure 4-14) while the size of the individual particles remained essentially the same (Figure 4-13). Therefore, at $25^{\circ}C$ the effect of an increase in agitation rate was simply to decrease the level of aggregation.
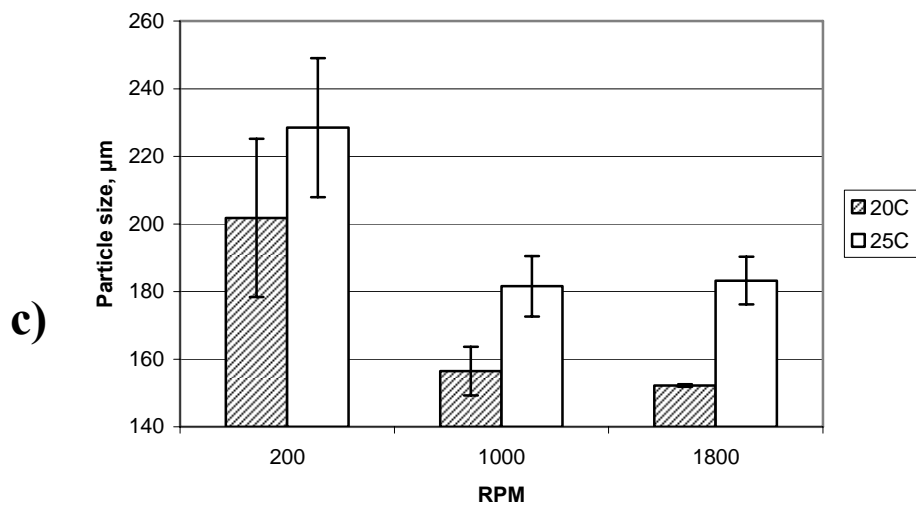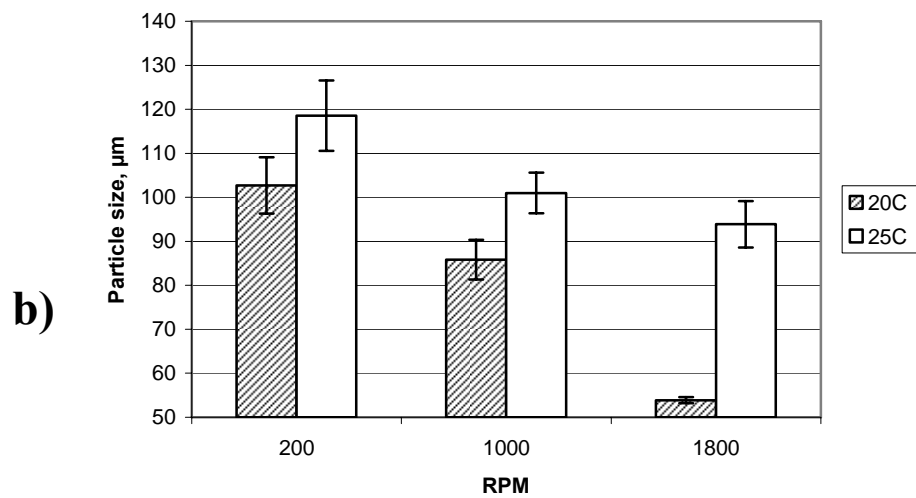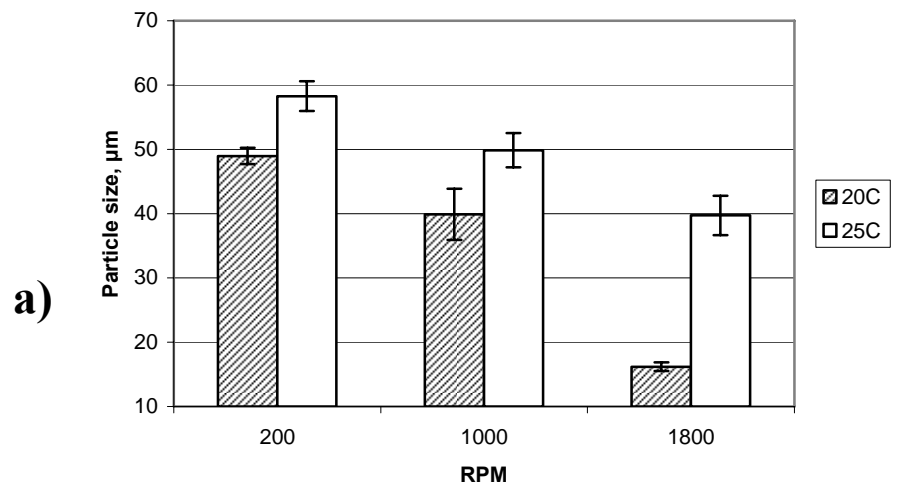
Figure 4-14: Effect of agitation on particle size without sonication for: a) $d_p(10\%)$, b) $d_p(50\%)$, c) $d_p(90\%)$

SEM was performed to obtain visual confirmation of the trends observed through particle size analysis. At 25°C there is an obvious decrease in the size of the aggregates from 200 to 1800 RPM (Figure 4-15), which agrees with the results presented in Figure 4-14. However, the SEM results do not seem to match the individual particle size results obtained using laser diffraction (Figure 4-13), which showed that at 25°C there was an increase in size with an increase in agitation rate. It is possible that the large clumps observed at very low agitation rates[14] broke apart during sonication, yielding smaller particle size measurements. The same can be said of the dense particle clusters observed at 1000RPM (Figure 4-15b). However, given the varying degrees of aggregation/agglomeration in the samples, it is difficult to determine any conclusive trends relating to the size of individual particles from the SEM data at 25°C.

At 20°C (see Figure 4-16) the SEMs correspond to the trend observed in Figure 4-13, i.e. there is an obvious decrease in the particle size with an increase in agitation rate. Also, as the agitation rate was increased, there appears to be a decrease in the level of aggregation, which agrees well with Figure 4-14.

---

[14] See, for example, the cluster in the upper-left corner of Figure 4-15a.
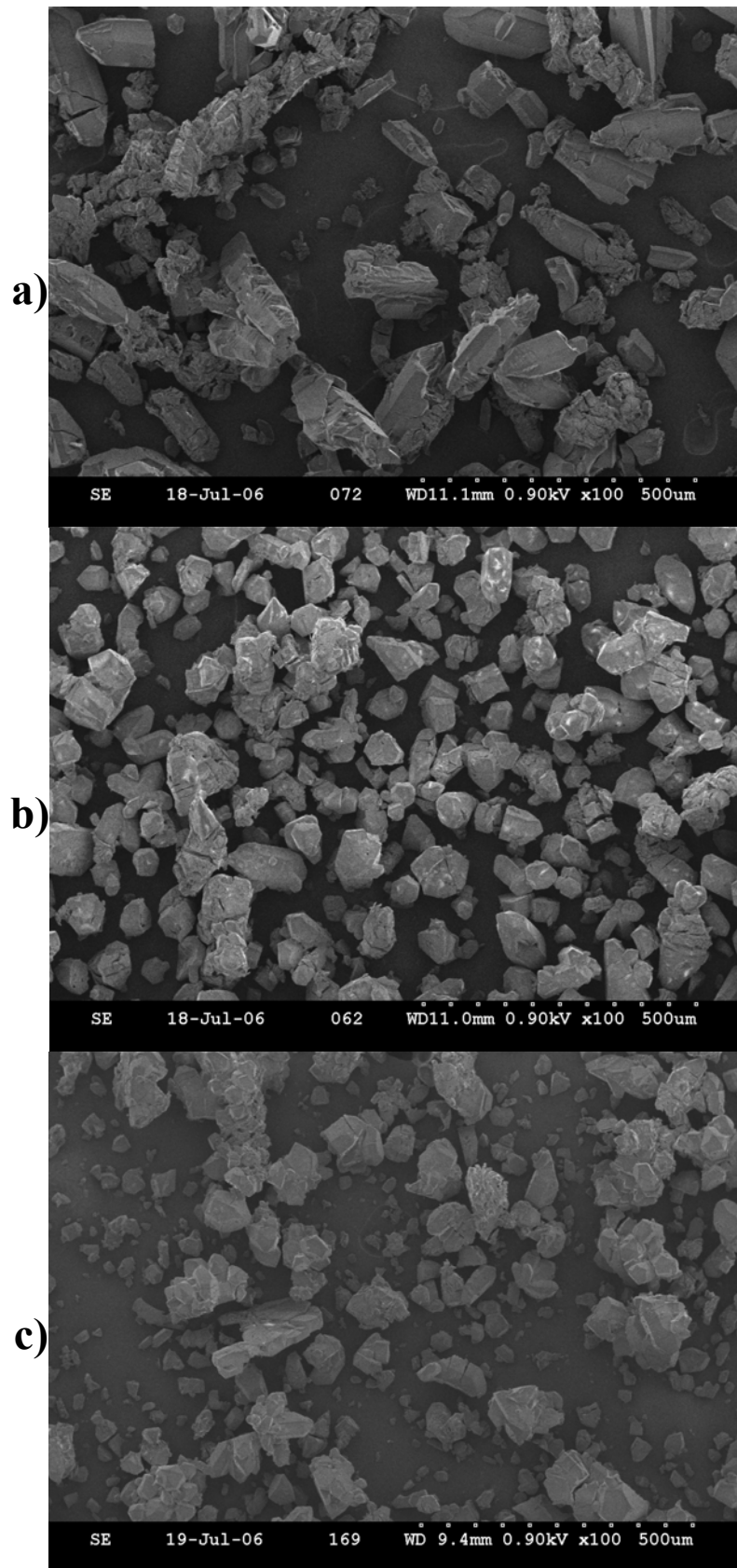
Figure 4-15: SEM of GAS runs at 25°C, 50 mL/min, and a) 200RPM, b) 1000RPM and c) 1800RPM
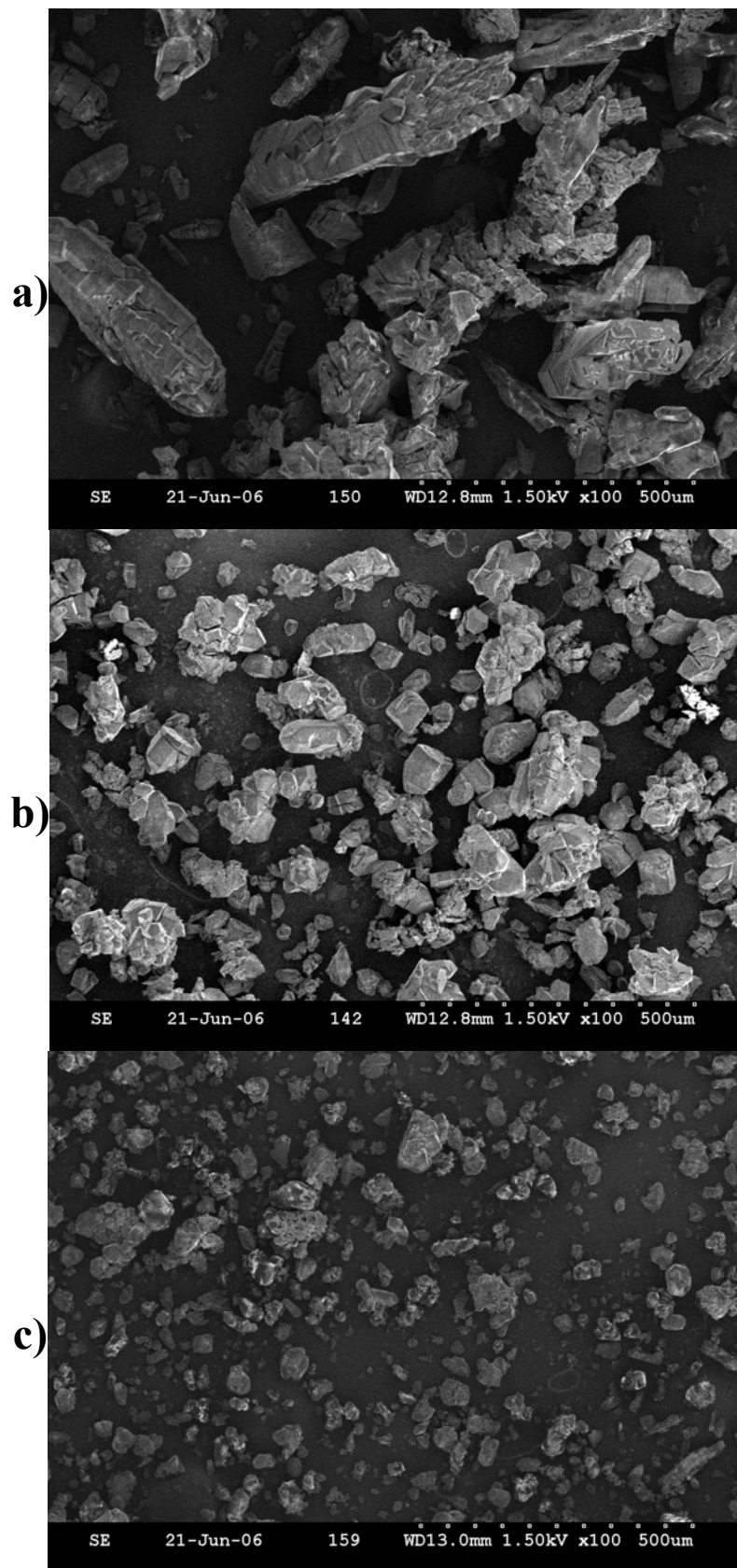
Figure 4-16: SEM of GAS runs at 20°C, 50 mL/min, and a) 200RPM, b) 1000RPM and c) 1800 RPM

4.2.2. *Effect of CO₂ Addition Rate*

Three different CO_2 addition rates were studied at two separate temperatures, i.e. 25, 50, and 75 mL/min at both 20 and 25°C. In all cases an agitation rate of 1000RPM was used. The results are tabulated for analysis with and without sonication in Table B2-1 and Table B2-2, respectively, along with the relative standard deviation of each experiment in brackets.

The sonicated samples show a clear decrease in particle size with an increase in CO_2 addition rate (Figure 4-17). However, there are two important points to note: First, the increase in addition rate does not have much of an effect on $d_p(10\%)$ for the sonicated particles. Therefore, adding CO_2 more quickly did not create smaller nuclei, but instead decreased the fraction of large particles obtained, most likely by increasing nucleation rates and hindering growth rates[15].

Second, there did not appear to be a strong temperature effect when the flowrate was varied. This is particularly interesting given that there was a temperature effect when the agitation rate was varied (see Section 4.2.1). This can be explained by noting that there is little difference in density between CO_2 at 20 and 25°C (see Figure 2-3 on page 7). Therefore, the mass flow rates of CO_2 at either temperature will be essentially the same. So, as the mass of CO_2 added per unit time to the vessel is not affected by temperature, it is logical that the particles produced will also not be affected.

---

[15] It should be noted here that these two effects are intertwined. As there are a finite number of solid molecules in solution, a particular molecule can either nucleate or grow. Therefore, if the nucleation rate is increased the growth rate will decrease. It should be noted that this result was hinted at by Muhrer et al. (2002), but their work was not compared to experimental data, so no concrete conclusions were given.

This argument implies that an increased flowrate has very little effect on CO_2 mass transfer, which is surprising given that an increased addition rate should increase turbulence and mixing within the reactor. However, previous work has shown that an increase in addition rate causes only slight improvements to mass transfer, which are insignificant when compared to the effect of agitation (Lin et al. 2003). Therefore, the effect of increased flowrate on the particle size is likely due entirely to the decreased time scale for pressurization, leading to higher nucleation rates and lower growth rates.

It is also possible that no temperature effect was observed due to the high agitation rate (1000RPM), which might provide adequate mass transfer. However, this contradicts the results presented in Section 4.2.1 at 20°C, where an increase in agitation rate from 1000 to 18000RPM still produced a large decrease in particle size. Therefore, mass transfer improvements are still possible at 1000RPM.
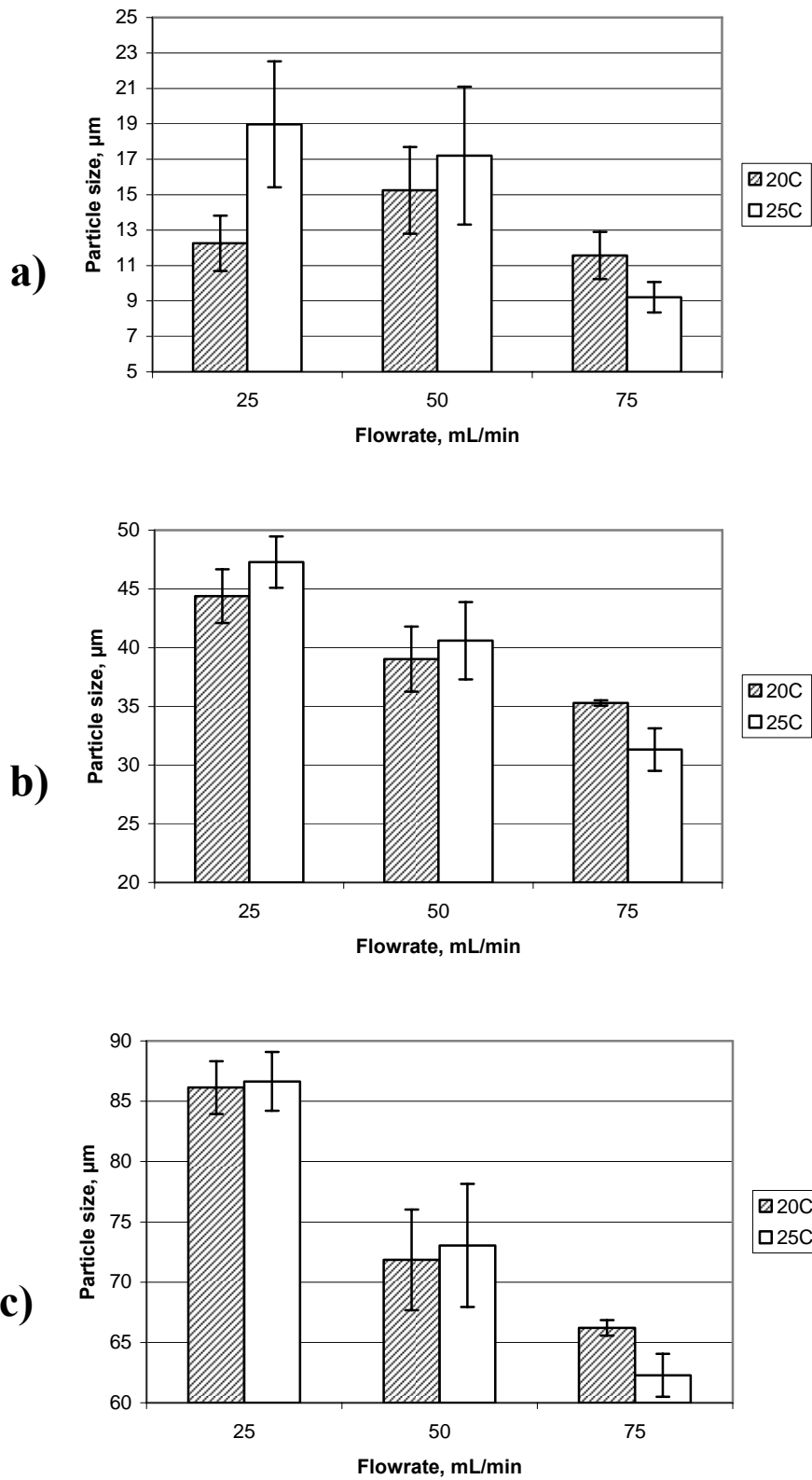
Figure 4-17: Effect of CO_2 flowrate on particle size with sonication: a) $d_p(10\%)$, b) $d_p(50\%)$, c) $d_p(90\%)$

An increase in flowrate caused a clear decrease in aggregate size at $d_p(10\%)$, $d_p(50\%)$ and $d_p(90\%)$ for the unsonicated samples at both temperatures (see Figure 4-18). Also, it appears that at a lower temperature, smaller aggregates were obtained, although at 25 mL/min the results appear to be essentially the same. As the sonicated samples showed a similar aggregate size regardless of temperature, the difference between the results at 20 and 25°C when no sonication was applied (Figure 4-18) can be attributed entirely to aggregation. Therefore, higher temperatures promoted the formation of aggregation, most likely because of the increased energy of the system, creating favourable kinetics for aggregation.

SEM was performed for visual confirmation of the results obtained through particle size analysis in Figure 4-17 and Figure 4-18. At 25°C there is a clear decrease in the particle size with an increase in the addition rate (Figure 4-19). Additionally, there is a noticeable difference in the size and makeup of the aggregates. At 75 mL/min (Figure 4-19a), there is very little aggregation, with mostly distinct crystals present. At 50 mL/min (Figure 4-19b) there is some aggregation of smaller particles, for example at the top of the SEM, but the aggregates are collections of only a few particles. However, at 25mL/min (Figure 4-19c), there is a large degree of aggregation creating very large particles, as seen at the right of the SEM. Therefore, the increase in flowrate not only lowers the size of the individual particles, but also the size and extent of aggregation. The same trends were observed at 20°C, as shown in Figure 4-20.
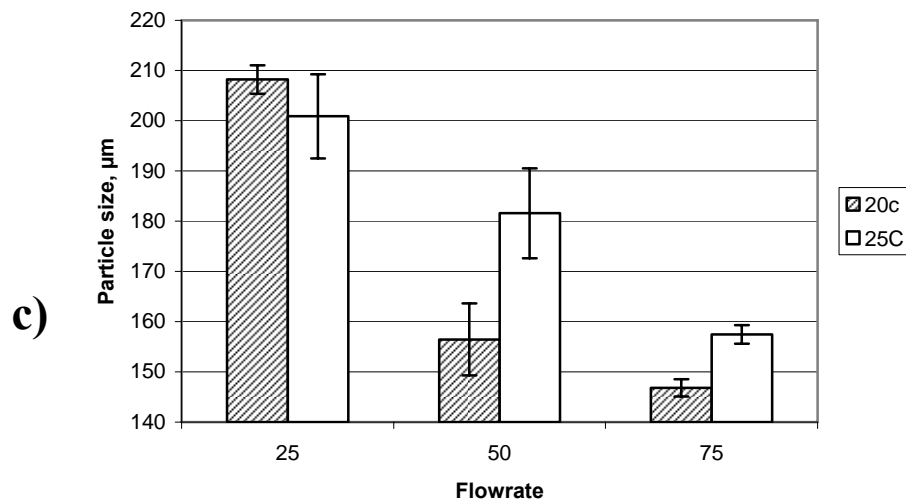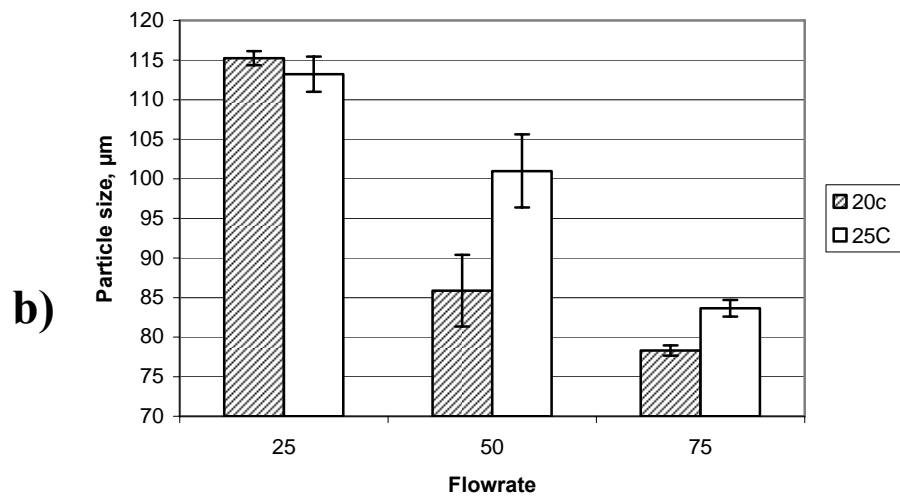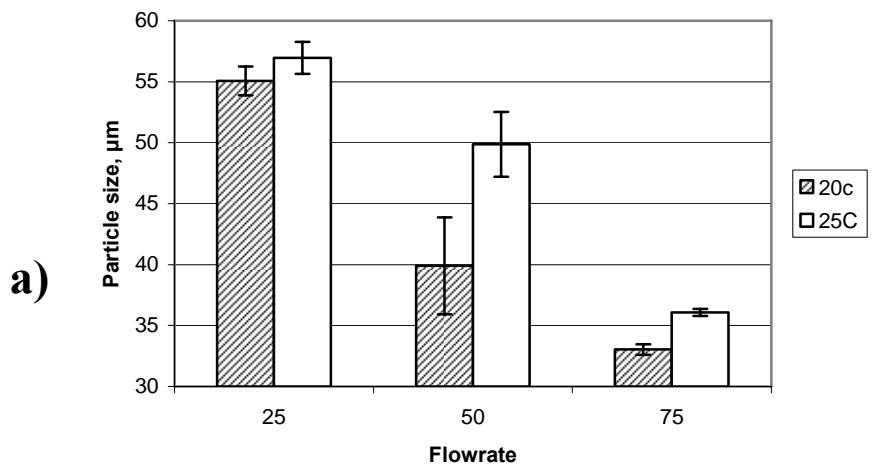
Figure 4-18: Effect of CO_2 flowrate on particle size without sonication: a) $d_p(10\%)$, b) $d_p(50\%)$, c) $d_p(90\%)$
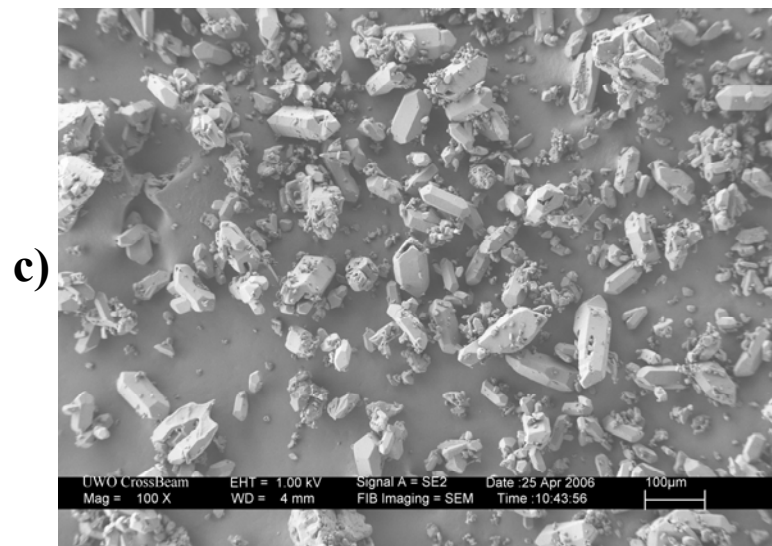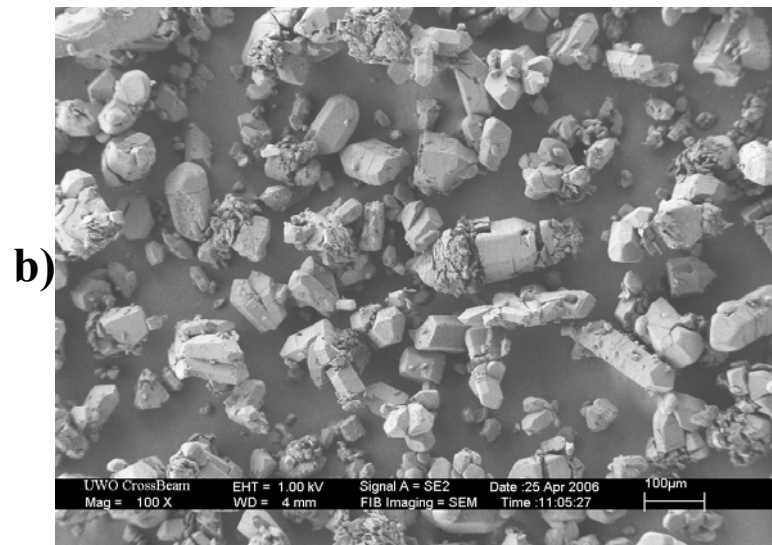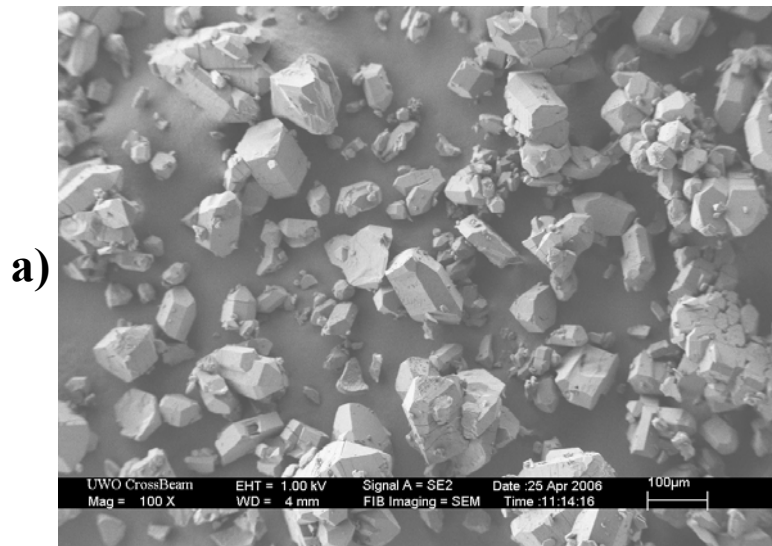
Figure 4-19: SEM of GAS runs at 25°C, 1000RPM, and a) 25 mL/min, b) 50 mL/min and c) 75 mL/min
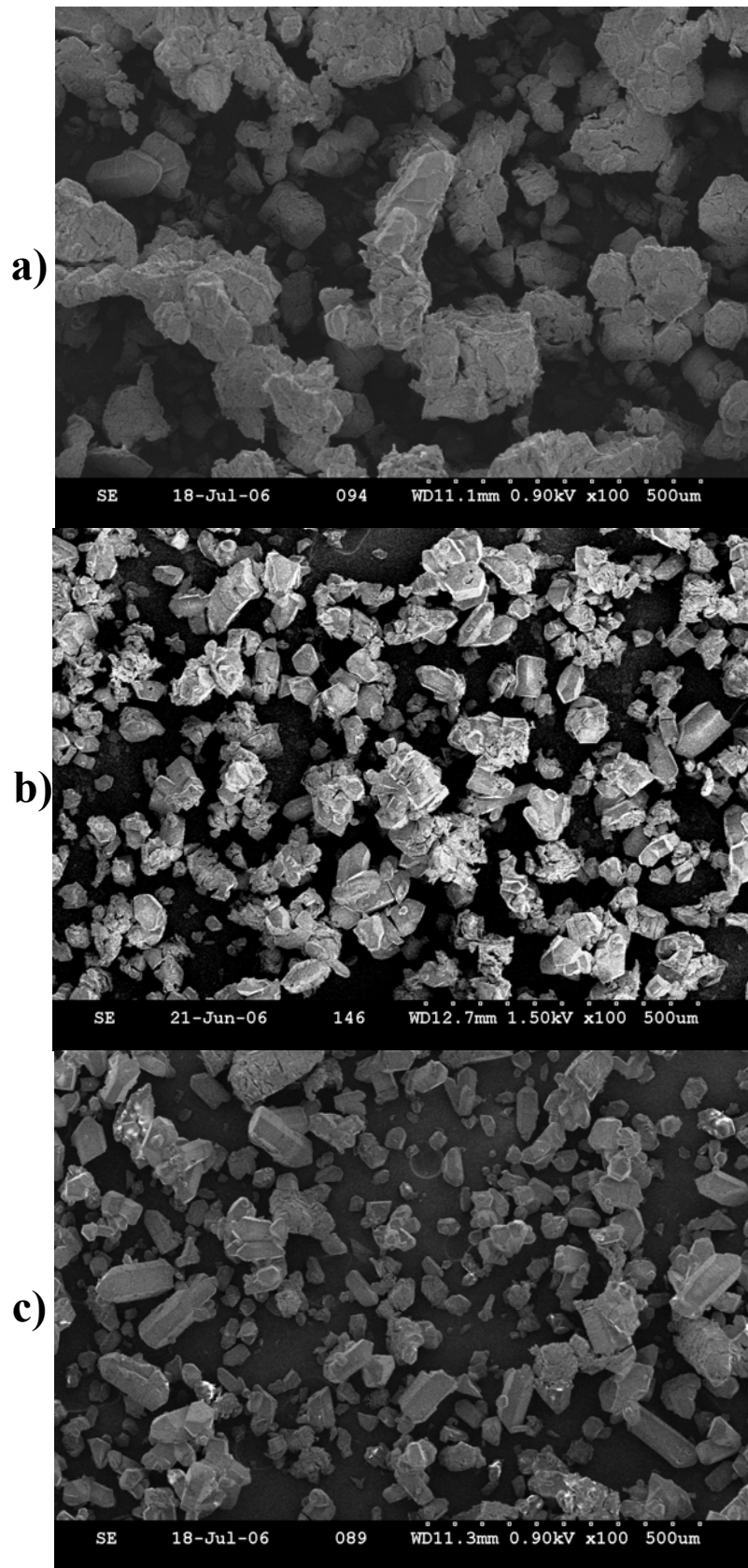
Figure 4-20: SEM of GAS runs at 20°C, 1000RPM, and a) 25 mL/min, b) 50 mL/min and c) 75 mL/min

4.2.3. *Effect of Temperature*

To further evaluate the effect of temperature, an additional GAS experiment was performed at 30°C, 50mL/min and 1000RPM. The results are tabulated in Table B3-1 and Table B3-2, along with the associated results at 20 and 25°C, for analysis without and with sonication, respectively. The relative standard deviation at each experimental condition has been included in brackets. Also, the results have been presented graphically in Figure 4-21 and Figure 4-22.

When sonication was not used (Figure 4-21), there was a slight increase in particle size from 20 to 25°C, but not from 25 to 30°C, although little change in size was observed from 25 to 30°C. However, when sonication was employed (Figure 4-22), there was virtually no difference between the results regardless of the temperature.
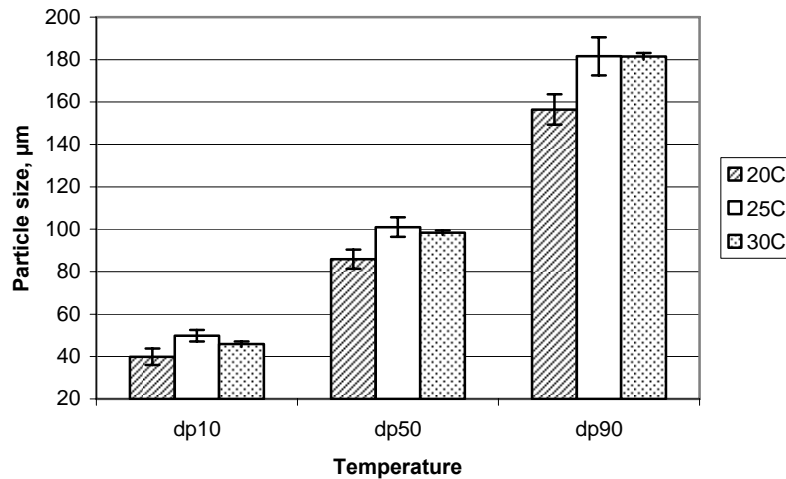
Figure 4-21: Effect of temperature on particle size without sonication
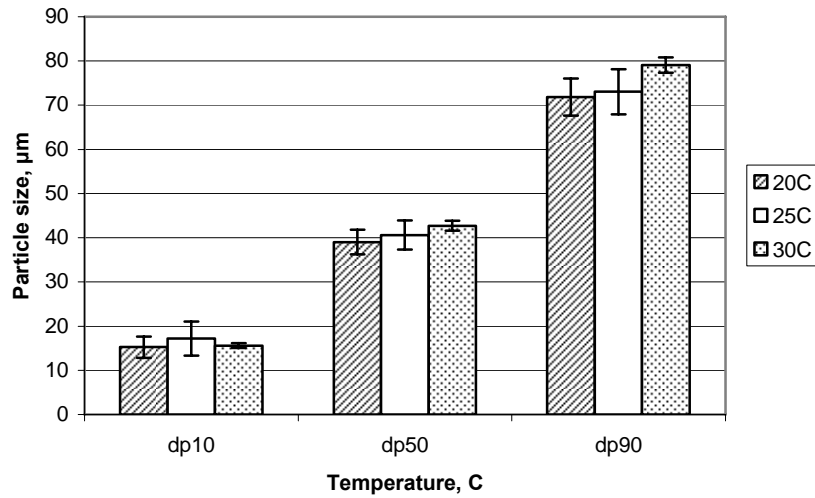
Figure 4-22: Effect of temperature on particle size with sonication

It is difficult to make concrete conclusions without having more data at 30°C to observe the effect of flowrate and agitation. However, given the scale of the project and the time required to perform the experiments, another set of runs was not feasible. It appears that any effects due to temperature can be attributed to the agitation rate of the system (see Section 4.2.1), as a result of the increased mass transfer.

SEM was performed to obtain visual confirmation of the trends observed in Figure 4-21 and Figure 4-22 through particle size analysis. There does not appear to be any noticeable difference between the crystals produced at the three different temperatures. Therefore, the trends observed in Figure 4-21 and Figure 4-22 appear to be correct, and temperature has little effect on the particle size distributions produced at 1000RPM and 50mL/min. However, it clearly had an effect at 200RPM and 1800RPM, as seen in Section 4.2.1. Therefore, in this study temperature likely only played a role in determining particle size through mass transfer effects.
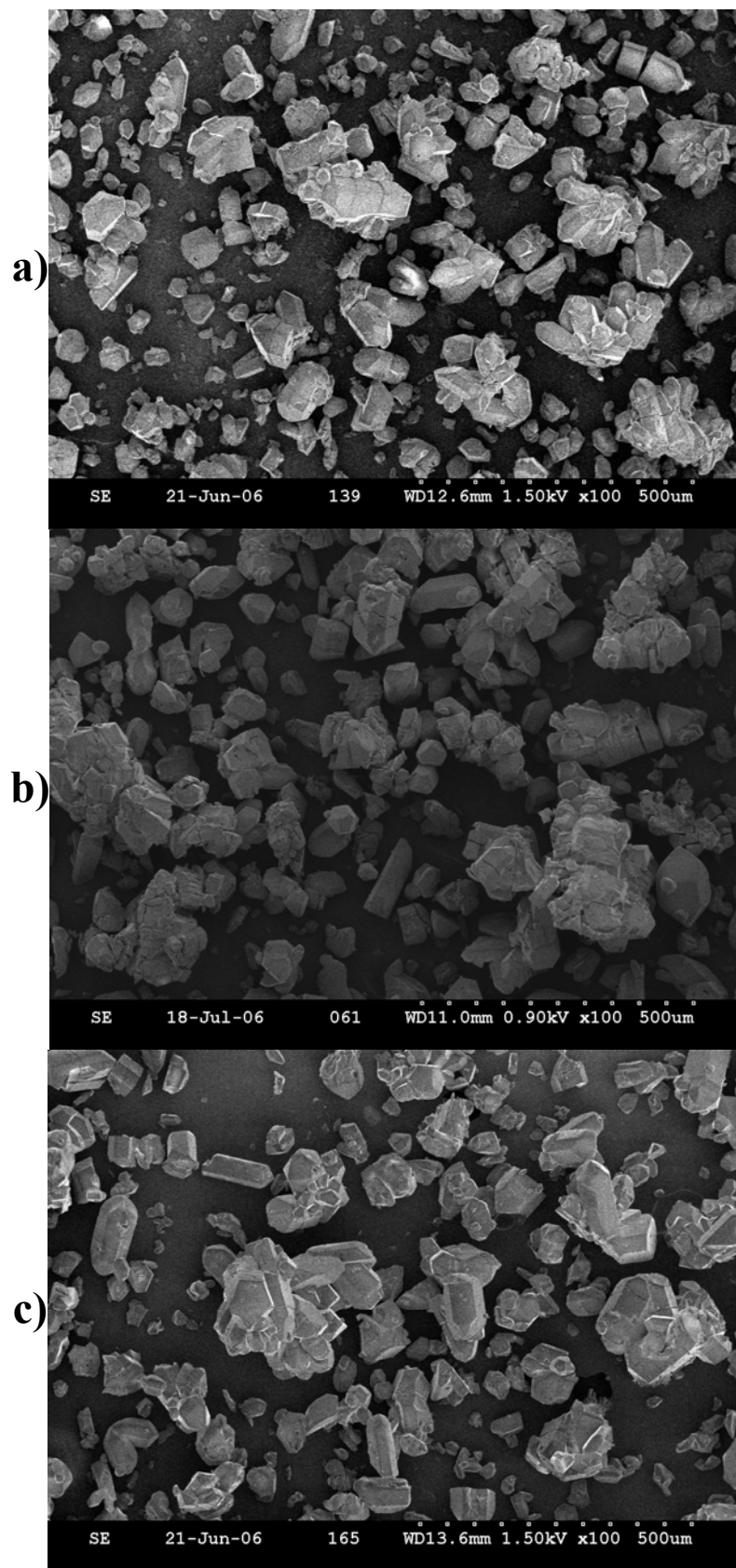
Figure 4-23: SEM of GAS runs at 50 mL/min, and a) 20°C, b) 25°C and c) 30°C

5. Thermodynamics of the GAS process

The precipitation of solids in the GAS process is governed by two general phenomena: phase equilibrium and kinetics. A good understanding of the phase equilibrium underlying the GAS process can help one to select appropriate solvents, operating temperatures, pressures, etc. before performing any actual GAS experiments.

Additionally, the kinetic model presented in Section 6 requires information about the equilibrium concentration of solute in the liquid phase, as well as the volume of the liquid phase, as a function of time. Therefore, a thermodynamic model of the volume expansion process (discussed in Section 2.2) was developed.

5.1. *Expanded liquid phase model (ELPM)*

The first step in modelling the volume expansion process is to consider the system in question. The temperature change in the crystallization vessel was normally small, so that the system can be considered isothermal. The GAS process involves a precipitation vessel, with constant volume V, which has one inlet for CO_2 addition and no outlets. This setup implies the following mass-balance equations (Muhrer et al. 2002):

$$\frac{d}{dt}\left(N_V y_a + N_L x_a\right) = \dot{Q}_a \qquad (5.1)$$

$$\frac{d}{dt}\left(N_V y_s + N_L x_s\right) = 0 \qquad (5.2)$$

where N_V is the molar hold-up of the vapour phase, $\dot{Q}_a$ is the molar flow rate of antisolvent into the reactor, and y_i, x_i represent the mole fractions of components A (antisolvent) and S (solvent) in the vapour and liquid phases, respectively. As no solvent is able to enter or leave the system, we know that the total amount of solvent stays

constant. Therefore, if we assume that CO_2 is added at a constant mass flowrate[16], then the mass balances become:

$$N_V y_a + N_L x_a = N_a^0 + \dot{Q}_a t \qquad (5.3)$$

$$N_V y_s + N_L x_s = N_S^0 \qquad (5.4)$$

where the ^{o} superscript represents the initial value for each parameter. It should be noted that the initial vapour phase is assumed to contain CO_2 at atmospheric pressure, which implies a small amount of CO_2 is also initially present in the liquid phase. This is why there is an N_a^0 term in Equation (5.3). Also, the total volume of the system must remain constant because the precipitation occurs in a rigid vessel:

$$N_V v_V + N_L v_L = V \qquad (5.5)$$

where V is the total reactor volume. Finally, to solve the mass balance we require an equation of state (EOS). The Peng-Robinson EOS was chosen to represent the compressibility Z (Smith et al. 2004):

$$Z = 1 + B - AB \frac{Z - B}{Z^2 + 2BZ - B^2} \qquad (5.6)$$

where A and B represent the (dimensionless) excluded volume and intermolecular force terms, and are described mathematically as (Smith et al. 2004):

$$B = \frac{bP}{RT} \qquad (5.7)$$

$$b = \sum_i \sum_j x_i x_j b_{ij} \qquad (5.8)$$

---

[16] It should be noted that in the experiments performed, the mass flowrate of CO_2 was not constant throughout the process, due to start-up conditions (see Figure 4-7 for an example). However, because the start up phase only takes a few seconds before the CO_2 flowrate is within 10% of the set point, it was assumed to have negligible effect on the predicted particle size.

$$b_{ii} = 0.07779 \frac{RT_{c,i}}{P_{c,i}} \tag{5.9}$$

$$b_{ij} = \frac{\left(b_{ii} + b_{jj} \right)}{2} \left(1 - l_{ij} \right) \text{ for } i \neq j \tag{5.10}$$

and

$$A = \frac{aP}{\left(RT \right)^2} \tag{5.11}$$

$$a = \sum_i \sum_j x_i x_j a_{ij} \tag{5.12}$$

$$a_{ii} = 0.45724 \frac{\alpha_i R^2 T_{c,i}^2}{P_{c,i}} \tag{5.13}$$

$$a_{ij} = \sqrt{a_{ii} a_{jj}} \left(1 - k_{ij} \right) \text{ for } i \neq j \tag{5.14}$$

$$\alpha = \left(1 + \left(0.37464 + 1.54226 \omega_i - 0.26992 \omega_i^2 \right) \left(1 - \sqrt{T_{r,i}} \right) \right) \tag{5.15}$$

where α_i is a temperature dependant correction for the vapour pressure, ω_i is the acentric factor, k_{ij} and l_{ij} are empirical interaction parameters describing how the presence of component i affects component j, and vice versa. $T_{c,i}$ and $P_{c,i}$ are the critical temperature and pressure of component i, $T_{r,i}$ is the reduced temperature of component i ($= T/T_{c,i}$), and R is the universal gas constant. Quadratic mixing rules were chosen for Equations (5.8) and (5.12) because they have shown good agreement with experimental liquid/gas phase equilibrium data and are quite common (Poling et al. 2001).

The system must also satisfy several physical restraints. First, the mole fractions must add up to 1 in each phase:

$$y_a + y_s = 1 \tag{5.16}$$

$$x_a + x_s + x_p = 1 \tag{5.17}$$

Second, the equifugacity condition must be satisfied for each component:

$$\hat{f}_a^V = \hat{f}_a^L \tag{5.18}$$

$$\hat{f}_s^V = \hat{f}_s^L \tag{5.19}$$

It should be noted that the use of these equations implies that an instantaneous equilibrium is obtained between the liquid and vapour phases. The fugacity of each component in each phase can be found using

$$\hat{f}_i^\alpha = x_i^\alpha \hat{\phi}_i^\alpha P \tag{5.20}$$

where the fugacity coefficient of component i in phase α, $\hat{\phi}_i^\alpha$, is defined as (Elliott and Lira 1999):

$$
\begin{aligned}
\ln \hat{\phi}_k^\alpha = {} & \frac{1}{B^\alpha} \frac{\partial\left(nB^\alpha\right)}{\partial n_k}\left(Z^\alpha - 1\right) - \ln\left(Z^\alpha - B^\alpha\right) \\
& - \frac{A^\alpha}{\sqrt{8}B^\alpha}\left(\frac{1}{A^\alpha}\frac{\partial\left(nA^\alpha\right)}{\partial n_k} - \frac{1}{B^\alpha}\frac{\partial\left(nB^\alpha\right)}{\partial n_k}\right)\ln\left(\frac{Z^\alpha + \left(1+\sqrt{2}\right)B^\alpha}{Z^\alpha + \left(1-\sqrt{2}\right)B^\alpha}\right)
\end{aligned}
\tag{5.21}
$$

Note that in Equations (5.20) and (5.21) only, x_i^α is used to define the mole fraction of component i in any phase α, as opposed to representing the composition of the liquid phase.

For the solid phase, the equifugacity condition cannot be applied since it is not at equilibrium during precipitation. However, to determine the supersaturation we must be able to determine the saturated concentration of solute in the liquid phase. Therefore, by assuming that the solid is in equilibrium during CO_2 addition, we can determine its

equilibrium (or saturated) mole fraction. When combined with the population balance, the mass of solute still in solution can be determined, and thus the supersaturation can be calculated as well. Therefore, we can apply a third isofugacity relation:

$$\hat{f}_p^S = \hat{f}_p^L \tag{5.22}$$

It should be noted that the mole fraction of solid present should have an effect on the mole fractions of the other components in the liquid phase. However, because the solubility of the solid is normally rather low, especially during antisolvent addition, it can be neglected (Muhrer et al. 2002). To calculate the solute fugacity, the following method was used (Dixon and Johnston 1991). First, the solid phase was assumed to be pure solute. This allows us to treat the solid phase fugacity as:

$$\hat{f}_p^S = f_p^{OS} \exp\left(\int_{P^o}^{P} \frac{v_p^s}{RT} dP \right) \tag{5.23}$$

where f_p^{OS} is the solid fugacity of the pure solute, and the exponential term is the Poynting factor. The liquid phase fugacity can be obtained by

$$\hat{f}_p^L = x_p P \hat{\phi}_p^L \tag{5.24}$$

While this equation was able to describe the solute dissolved in the liquid phase reasonably well at low and medium pressures, it was not able to do so at high pressures because the order of $\hat{\phi}_p^L$ becomes very small, creating numerical problems (Dixon and Johnston 1991). Therefore, a correction factor is used which has the effect of normalizing $\hat{\phi}_p^L$, enabling more accurate calculations (Dixon and Johnston 1991):

$$\hat{f}_p^L = x_p P \hat{\phi}_p^L \left(\frac{f_p^{OL} \gamma_3^o}{P^o \phi_p^o} \right) \tag{5.25}$$

where f_p^{OL} is the fugacity of a hypothetical pure liquid solute, γ_3^o is the activity of the solute at a reference pressure P^o, and ϕ_p^o is the fugacity coefficient at the same reference pressure. As the system is initially at a low pressure, γ_3^o can be found using regular solution theory or a software package (such as Aspen).

When Equations (5.23) and (5.25) are entered into Equation (5.22) and rearranged, the term f_p^{OL} / f_p^{OS} appears. This term can be written as (Prausnitz et al. 1986):

$$\ln\left(\frac{f_p^{OL}}{f_p^{OS}}\right) = \frac{\Delta H_{fusion}}{RT_m}\left(\frac{T_m}{T} - 1\right) \tag{5.26}$$

We have now introduced enough equations to match the number of system unknowns, so solution is possible. The volume expansion model was solved using Matlab, and the solution algorithm has been given in Appendix A-1.

5.2. *Relative partial molar volume fraction (RPMVF) model*

While the model described in the previous section is a straightforward application of classical thermodynamic principles, it is somewhat limited in its application. To be implemented, the critical constants for all three components must be known. While this is true for nearly all solvents and antisolvents, it is rarely true for the choice of solid. In fact, quite often the solid critical point has no physical meaning as the compound will decompose before reaching the critical temperature. While there are ways to determine physical constants even if they do not exist, such as group contribution methods (see Section 4.2), they may not always provide physically realistic predictions for the phase equilibrium. Therefore, an alternative method would be beneficial.

As was discussed in Section 2.2, precipitation in the GAS process occurs because the CO_2 dissolves into the liquid phase, expanding the phase and causing a decrease in the solvents solvating power. Therefore, it seems intuitive that a description of the volume expansion process should be able to account for the drop in saturation of the solute in the liquid phase. Several attempts have been made by describing the relative volume expansion in terms of the change in total volume of the liquid phase divided by the initial volume of the liquid phase (Kordikowski et al. 1995), the ratio of the current and initial molar volumes of the liquid phase (de la Fuente et al. 2000), and the partial molar volume fraction (PMVF) (Mukhopadhyay 2003), described as:

$$PMVF\left(T,P,X_S\right) = \frac{X_S \overline{v}_{L,S}}{v_L} \tag{5.27}$$

where X_s is the mole fraction of solvent on a solute free basis, $\overline{v}_{L,s}$ is the partial molar volume of the solvent in the liquid phase, and v_L is the molar volume of the liquid phase, all of which are calculated for the binary solvent-antisolvent system. It is important to note that this method still requires an EOS to calculate the molar volumes for the solvent and CO_2.

The PMVF represents the contribution of the solvent to the total volume of the liquid phase, and thus is related to the solvent power of that phase. Therefore, it has been proposed that the solubility of the solute is proportional to the relative partial molar volume fraction (RPMVF), which is the PMVF of the binary solution at a particular pressure/composition to the initial PMVF of the binary system (Mukhopadhyay and Dalvi 2004):

$$x_P = \frac{PMVF\left(T,P,X_S\right)}{PMVF\left(T,P^o,X_{SO}\right)} x_P^o \tag{5.28}$$

where x_P^o is the initial mole fraction of solute dissolved in the liquid phase of the ternary system. As this method does not incorporate the solid into the molar volume calculations, it does not require any of the physical constants for the solute that are needed for the expanded liquid phase model presented in Section 5.1.

Implementation of the RPMVF model is straightforward, and follows the same general procedure given in Section 5.1, with the exception that the solute is ignored in the equilibrium calculations. The partial molar volume can be obtained from the Peng-Robinson equation of state:

$$P = \frac{RT}{v-b} - \frac{a}{v^2 + 2bv - b^2} \tag{5.29}$$

$$\bar{v}_i = \left(\frac{\partial\left(nv\right)}{n_i}\right)_{T,P,n_j \neq n_i} \tag{5.30}$$

$$0 = \frac{RT\left[\left(v-b\right)-\left(\bar{v}_i-\bar{b}_i\right)\right]}{\left(v-b\right)^2} - \frac{\bar{a}_i}{\left(v^2+2bv-b^2\right)} + \frac{2a\left[v\left(\bar{v}_i+\bar{b}_i\right)+b\left(\bar{v}_i-\bar{b}_i\right)\right]}{\left(v^2+2bv-b^2\right)^2} \tag{5.31}$$

where

$$\bar{b}_i = \left(\frac{\partial\left(nb\right)}{n_i}\right)_{T,P,n_j \neq n_i} \tag{5.32}$$

$$\bar{a}_i = \frac{1}{n}\left(\frac{\partial\left(n^2 a\right)}{n_i}\right)_{T,P,n_j \neq n_i} \tag{5.33}$$

Equation (5.31) can be solved explicitly for $\overline{v}_i$, or a solver (such as fsolve in Matlab) can be used instead. The algorithm used to implement the RPMVF model in Matlab is given in Appendix A-2

5.3. *Parameter estimation*

Before the expanded liquid phase GAS model described in Section 5.1 could be implemented in Matlab, the physical parameters that describe the system (i.e. critical point, interaction parameters, etc.) must first be determined. While there is data available for nearly all solvent and antisolvent choices (see Table 5-1), there is little to no available data on the physicochemical properties of most solids of interest (including BDP). Therefore the desired properties must be obtained using correlations such as group contribution methods. The various methods and results are discussed here, and a summary is given in Table 5-2.

Table 5-1: Summary of acetone/CO_2 physical parameters found in literature

Parameter	Symbol	Value	Reference
CO_2 critical temperature	$T_{c,1}$	304.2K	(Smith et al. 2004)
CO_2 critical pressure	$P_{c,1}$	73.83bar	(Smith et al. 2004)
CO_2 acentric factor	ω_1	0.225	(Smith et al. 2004)
CO_2 liquid molar volume	$v_{L,1}$	55 (cm^3/mol)	(Dixon and Johnston 1991)
CO_2 solubility parameter	δ_1	6.014 (cal/cm^3)$^{1/2}$	(Dixon and Johnston 1991)
Acetone critical temperature	$T_{c,2}$	508.1K	(Smith et al. 2004)
Acetone critical pressure	$P_{c,2}$	47.00bar	(Smith et al. 2004)
Acetone acentric factor	ω_2	0.304	(Smith et al. 2004)
Acetone liquid molar volume	$v_{L,2}$	73.427 (cm^3/mol)	(NIST 2003)
Acetone solubility parameter	δ_2	9.823 (cal/cm^3)$^{1/2}$	(Sepassi and Yalkowsky 2006)

Table 5-2: Summary of estimated parameters for acetone/CO_2

Parameter	Symbol	Method of estimation	Result	Reference
BDP critical temperature	$T_{c,3}$	Group contribution	977.24K	(Marrero and Gani 2001)
BDP critical pressure	$P_{c,3}$	Group contribution	12.58bar	(Marrero and Gani 2001)
BDP acentric factor	ω_3	Group contribution	1.665	(Constantinou et al. 1995)
Acetone-CO_2 interaction parameter	k_{12}	Regression of phase data	0.0194	(Day et al. 1996)
Acetone-CO_2 interaction parameter	l_{12}	Regression of phase data	0.0142	(Day et al. 1996)
BDP-CO_2 interaction parameter	k_{13}	Regression of phase data	0.0325	(Dean et al. 1995; Vatanara et al. 2005)
BDP liquid molar volume	$v_{L,3}$	Group contribution	427.84 (cm^3/mol)	(Constantinou et al. 1995)
BDP solubility parameter	δ_3	Group contribution	11.26 $(cal/cm^3)^{1/2}$	(Stefanis et al. 2004)

5.3.1. *Group contribution methods*

Some of the simplest methods for performing parameter estimation are the group contribution methods. The Constantinou-Gani method (Constantinou and Gani 1994) has gained recognition as an easy and quick method for obtaining properties while maintaining good accuracy, especially for large molecules (Gordillo et al. 2005).

Group contribution methods attempt to estimate physical properties based solely on the molecular structure of the compound in question. The various functional groups are assigned a weighting (or contribution) that is regressed from available data on hundreds of different compounds. The property of the molecule, then, is related to the sum of the contribution multiplied by the number of times each group occurs (Marrero and Gani 2001).

There are three levels of groups that can be considered. The first and simplest level accounts for the contribution of each functional group in the molecule as if it were totally isolated, i.e. the groups in the molecule do not interact. Therefore, they are not normally able to predict properties for complex molecules where the effect of group interactions cannot be ignored. The second order groups consider the effect of proximity by incorporating large clusters of functional groups, and also allowing for distinction between isomers. However, the second order groups are still not always reliable when considering multifunctional or polycyclic/polyaromatic compounds, so a third level can be incorporated for these effects. Each atom in the group must be described by one (and only one) first order group, whereas second and third order groups do not need to account for every atom, and are allowed to overlap (Marrero and Gani 2001).

The overall contribution of the molecular structure to any property P can be written as:

$$f(P) = \sum_i M_i F_i + \sum_i N_i S_i + \sum_i O_i T_i \qquad (5.34)$$

where f is a function that incorporates the property P and several constants. M_i, N_i, O_i are the number of occurrences of each first, second and third order group respectively, and F_i, S_i, T_i are the contributions from the first, second, and third order groups respectively. Once the function f is obtained, property P can be calculated using the appropriate equation relating f to P. The various functions f used in this work are listed in Table 5-3.

Table 5-3: Equations used for group contribution property estimation

P	$f(P)$	Reference
$T_m(K)$	$\exp\left(T_m/147.45\right)$	(Marrero and Gani 2001)
$T_c(K)$	$\exp\left(T_m/231.239\right)$	(Marrero and Gani 2001)
$P_c(bar)$	$\left(P_c - 5.9827\right)^{-0.5} - 0.108998$	(Marrero and Gani 2001)
$v_l\left(m^3/kmol\right)$	$v_l - 0.01211$	(Constantinou et al. 1995)
ω	$\exp\left(\omega/0.4085\right)^{0.5050} - 1.1507$	(Constantinou et al. 1995)
$\delta\left(J/cm^3\right)^{1/2}$	$\left(\delta + 56.14\right)^{2.605273} - 75954.1$	(Stefanis et al. 2004)

The results for beclomethasone are shown in Table 5-4 and Table 5-5, along with a listing of groups used. The results are given as two separate tables because the Marrero and Gani (2001) paper presented slightly different groups from Constantinou et al. (1995) and Stefanis et al. (2004). The melting temperature was estimated to provide some validation of the method since the experimental value is known through DSC.

The melting point of BDP was found to be approximately 484K using differential scanning calorimetry (see Section 4.2). This agrees well with the estimated melting temperature listed in Table 5-4, with an error of 2.23%. It should also be noted that the estimated parameters are similar in magnitude to those reported for cholesterol, progesterone and testosterone (Kosal et al. 1992), which is expected given the structural similarity between different steroids.

Table 5-4: Group assignment for T_m, T_c and P_c (Marrero and Gani 2001)

Group	# of occurrences	$T_{m,i}$	$T_{c,i}$	$P_{c,i}$
First order groups				
CH_3	5	0.6953	1.7506	0.018615
OH	1	2.7888	5.2188	-0.0054
CH_2CO	1	2.5232	5.7157	0.019619
CH_2COO	2	1.6329	5.9619	0.026983
CCl	1	1.8424	3.7063	0.009187
$CH_2(cyclic)$	4	0.5699	1.8815	0.009884
$CH(cyclic)$	4	0.0335	1.102	0.007596
$C(cyclic)$	3	0.1695	-0.2399	0.003268
$(CH=CH)_{cyclic}$	1	1.1936	3.6426	0.013815
$(CH=C)_{cyclic}$	1	0.4344	3.5475	0.010576
$(C=O)_{cyclic}$	1	3.2119	12.6396	-0.00021
Second order groups				
$CH_{cyclic}-CH_3$	1	-0.1326	-0.1233	0.000779
$CH_{cyclic}-OH$	1	1.3691	0.8973	0.00464
$C_{cyclic}-CH_3$	2	0.1737	0.1607	0.001235
Third order groups				
$CH_{multi-ring}$	2	0.6647	0.4963	-0.00099
$C_{multi-ring}$	4	0.0792	-	-
	$f(P)$	**24.8888**	**68.4496**	**0.280273**
	P	**473.97 K**	**977.24 K**	**12.58 bar**

Table 5-5: Group assignment for ω, v_l and δ (Constantinou et al. 1995; Stefanis et al. 2004)

Group	# of occurrences	ω_i	$v_{l,i}$	δ_i
First order groups				
CH_3	5	0.29602	0.02614	-2308.6
CH_2	4	0.14691	0.01641	-277.1
CH	4	-0.07063	0.00711	-355.5
C	3	-0.35125	-0.0038	-176.2
CH_2CO	1	0.25224	0.02692	7274.2
CH_2COO	2	0.23492	0.0161	5194.2
OH	1	1.5237	0.00551	12228.9
CCl	1	0.63264	0.02816	-1415.6
$CH=CH$	1	0.75574	0.03567	-381.9
$CH=C$	1	0.57021	0.0202	1887.1
CHO [17]	1	0.96265	0.03371	5398.2
Second order groups				
5 member ring	1	0.16284	0.00213	-2637.7
6 member ring	2	-0.03065	0.00063	-524.2
$C_{cyclic}=O$	1	-	-0.00111	-3745
$CH_{cyclic}-OH$	1	-	-0.0025	-359.5
$f(P)$		**6.4902**	**0.41573**	**12986.7**
P		**1.67**	**0.4278 m³/kmol**	**23.23 (J/cm³)¹ᐟ²**

5.3.2. *Peng-Robinson interaction parameters*

The Peng-Robinson interaction terms, k_{12}, k_{13}, and l_{12}, all needed to be obtained to model the GAS process. The simplest way to do this is to regress the values from binary phase data with CO_2, which is available for both acetone and beclomethasone (Dean et al. 1995; Day et al. 1996; Vatanara et al. 2005).

The thermodynamics required are quite similar to that presented in Section 5.1, except that we need only consider a binary system instead of a ternary system. In the

---

[17] While BDP actually contains a CO group, CHO was used instead as no results for CO were reported for these properties. While this will certainly affect the estimation, it should not do so significantly because of the size of the molecule relative to the slight difference in the contribution of a single group.

case of acetone-CO_2, the liquid and gas phases are both binary so there are two fugacity conditions that need to be satisfied, Equations (5.18) and (5.19). The fugacity coefficient was calculated using Equation (5.21) for both phases. The value of k_{12} could then be regressed from experimental pressure and liquid/gas phase compositions. The algorithm for solution, along with the Matlab code developed, is provided in Appendix A-4.

To ensure that the code worked properly, k_{12} was first regressed from CO_2 – toluene data and compared to the literature data (Ng and Robinson 1978). The results are shown in Figure 5-1 at 38°C, and the value of k_{12} and l_{12} were found to be 0.0405 and - 0.0565 respectively, with an AARD of 5.98% between experimental and calculated bubble pressures. Ng and Robinson considered linear mixing rules in b (i.e $b = \sum x_i b_i$), and therefore are not directly comparable to the result obtained here. However, when the program was modified to use linear mixing rules in b then we get $k_{12} = 0.08$, which is very close to the literature value of 0.09 (Ng and Robinson 1978). Therefore, it was assumed that the algorithm and code were correct. Phase data for the acetone-CO_2 mixture was obtained from the literature (Day et al. 1996), and the values of k_{12} and l_{12} were found to be 0.0194 and 0.0142 respectively, with an AARD of 0.72% between experimental and calculated bubble pressures (see Figure 5-2).
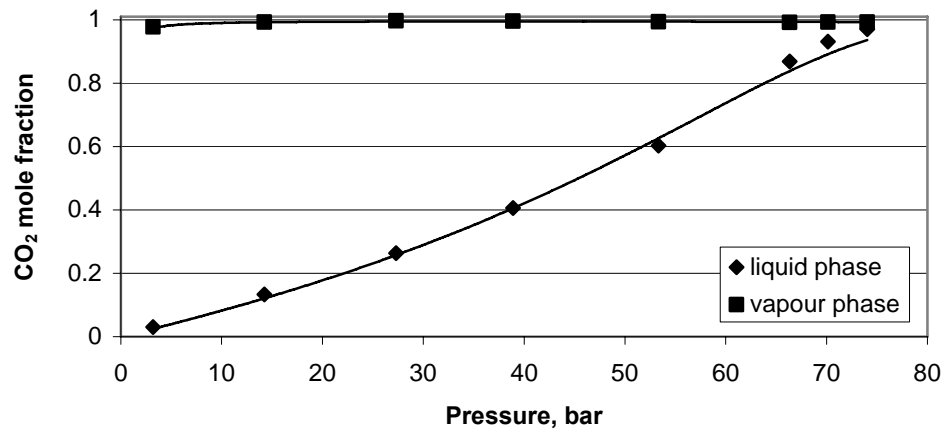
Figure 5-1: CO_2 dissolved in toluene at 38°C (data from Ng and Robinson, 1978)
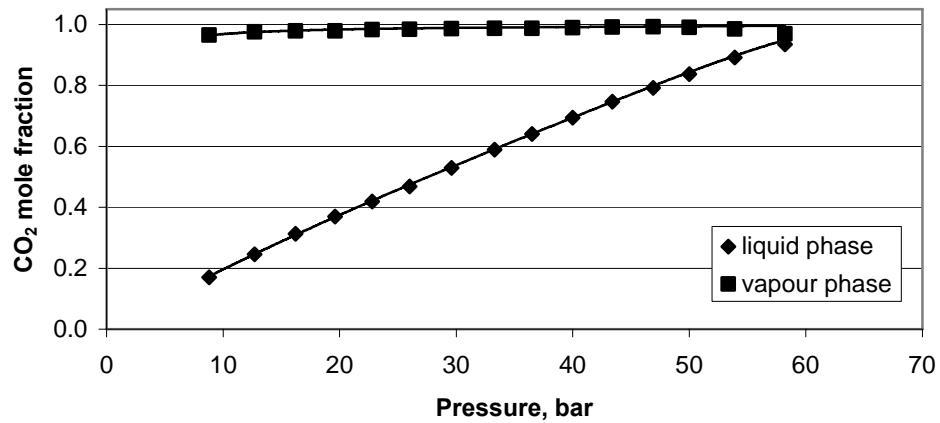
Figure 5-2: CO_2 dissolved in acetone at 25°C (data from Day et al. 1996)

The same general procedure was followed in the case of solid/gas equilibrium, with a few minor changes. It was assumed that the gas did not dissolve into the solid phase, which means that there was only one equilibrium relation to satisfy:

$$\hat{f}_3^V = f_3^S \tag{5.35}$$

The form of the vapour phase fugacity still follows Equation (5.20). However, the solid phase fugacity has the following general form:

$$f^S = \phi^{sat} P^{sat} e^{\frac{v^s}{RT}\left(P - P^{sat}\right)} \tag{5.36}$$

As the solid vapour pressure is normally quite low (on the order of 10^{-10} Pa), it was assumed that the vapours behave ideally and so the fugacity coefficient is approximately 1. Therefore, combination of Equations (5.35) and (5.20) into Equation (5.36) yields:

$$y_3 = \left(\frac{1}{\hat{\phi}_3^V} \right) \left(\frac{P^{sat}}{P} \right) e^{\frac{v^s}{RT}\left(P - P^{sat} \right)}$$

$$(5.37)$$

To ensure that the algorithm/code was implemented properly, the CO_2/phenanthrene system was studied first. The results are shown in Figure 5-3 at 45°C where the points represent the experimental data (Kurnik et al. 1981) and the lines represent the model predictions. For the phenanthrene/CO_2 system, the value of k_{13} was found to be 0.119 with an AARD of 16.34% between the experimental and model solute mole fractions, which agrees with the literature value of 0.113 (Kurnik et al. 1981).
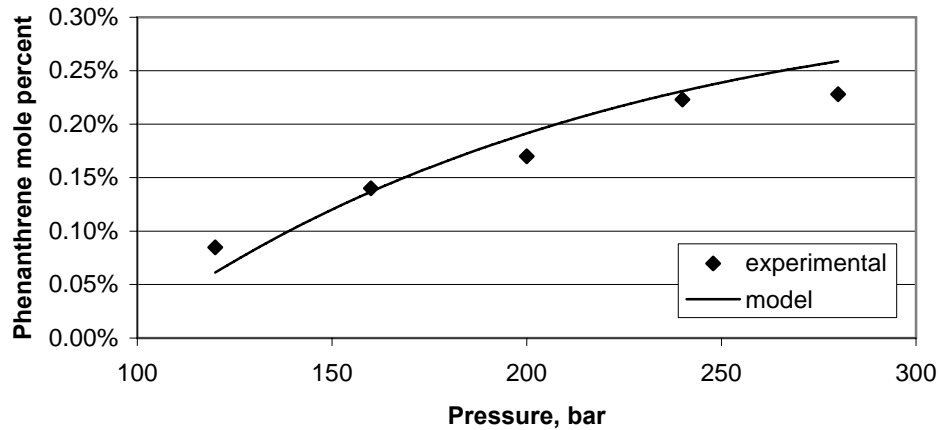
Figure 5-3: Phenanthrene solubility in CO_2 at 45°C (data from Kurnik et al. 1981)

The BDP/CO_2 system was then evaluated to obtain the interaction parameter using the estimated parameters obtained in Section 5.3.1, and data from (Vatanara et al. 2005). The saturation pressure was estimated using the Ambrose-Walton method, which uses the following equations (Poling et al. 2001):

$$\ln\left(\frac{P_{vap}}{P_c}\right) = f^{(0)}(T_r) + \omega f^{(1)}(T_r) + \omega^2 f^{(2)}(T_r) \qquad (5.38)$$

where,

$$f^{(0)}(T_r) = \frac{-5.97616\tau + 1.29874\tau^{1.5} - 0.60394\tau^{2.5} - 1.06841\tau^5}{T_r} \qquad (5.39)$$

$$f^{(1)}(T_r) = \frac{-5.03365\tau + 1.11505\tau^{1.5} - 5.41217\tau^{2.5} - 7.46628\tau^5}{T_r} \qquad (5.40)$$

$$f^{(2)}(T_r) = \frac{-0.64771\tau + 2.41539\tau^{1.5} - 4.26979\tau^{2.5} + 3.25259\tau^5}{T_r} \qquad (5.41)$$

$$\tau = 1 - T_r \qquad (5.42)$$

Using this method, the saturation pressure could be estimated at each temperature for which data was available. Once the saturation pressure was found, the interaction parameter could then be regressed. The result is shown in Figure 5-4 for 35°C, where k_{13} was found to be 0.0325 with an AARD of 26.53%. While this AARD value seems somewhat high, literature values for AARD can often be above 40% depending on the estimation technique used for the critical parameters, the equation of state, the mixing rules, the method of calculation for the sublimation pressure, and of course the solid (Coimbra et al. 2006).
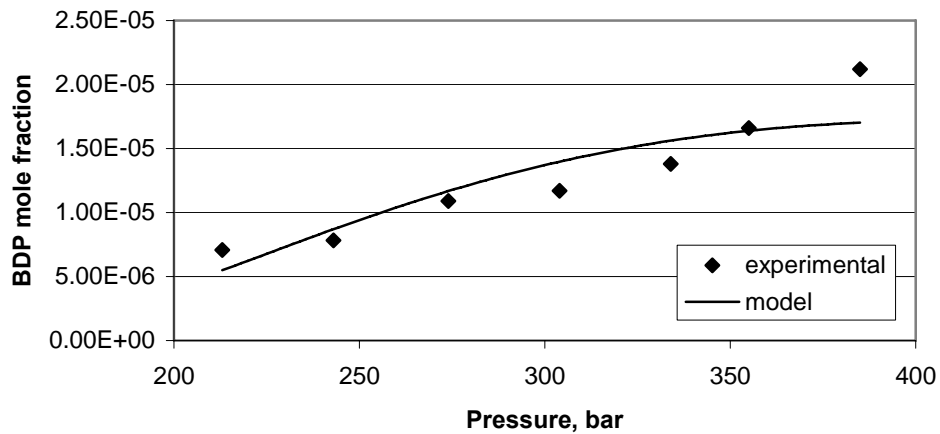
Figure 5-4: Solubility of BDP in CO$_2$ at 65°C (data from Vatanara et al., 2005)

5.4. *Phase equilibrium model*

5.4.1. *Expanded liquid phase model*

Once all the required parameters were estimated, the expanded liquid phase model discussed in Section 5.1 could be implemented (see Appendix A-1). To ensure that the model worked properly, the equilibrium liquid mole fractions calculated in the model were compared to experimental data for the phenanthrene/toluene/CO_2 (see Figure 5-5) and naphthalene/toluene/CO_2 systems (see Figure 5-6). Good agreement was obtained between the experimental data and the model results, indicating that the model was able to handle these systems. It is important to note the sudden increase in CO_2 mole fraction, along with the associated decreases in solute and toluene mole fractions, at around 55bar. This drop in solid solubility is what creates the driving force for crystallization.
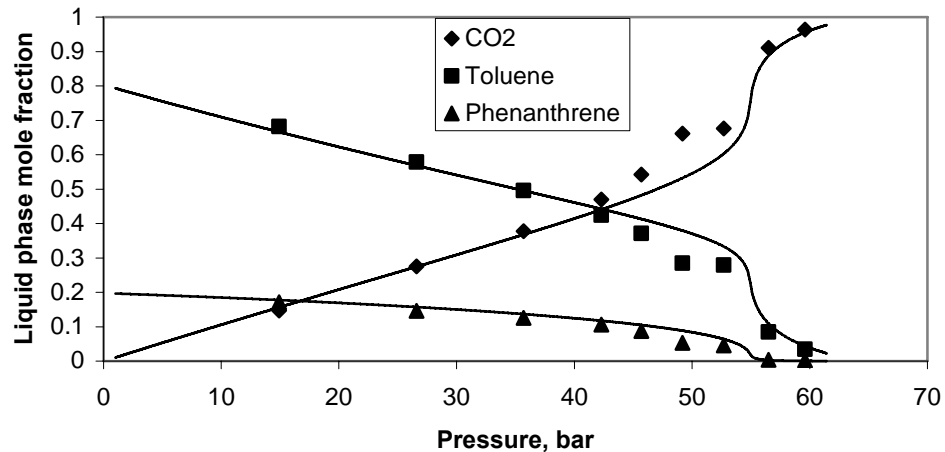
Figure 5-5: Liquid phase composition of the phenanthrene/toluene/CO_2 ternary system at 25°C (data from Dixon and Johnston 1991)
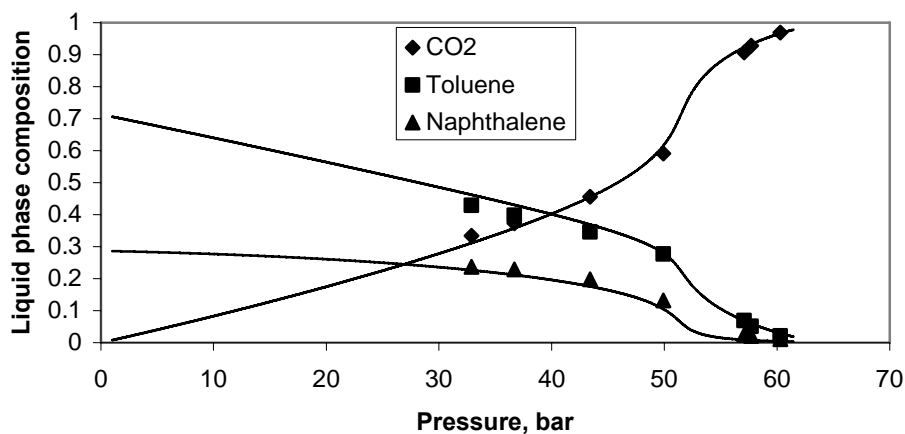
Figure 5-6: Liquid phase composition of the naphthalene/toluene/CO_2 ternary system at 25°C (data from Dixon and Johnston 1991)

The end point for the simulation was determined by examining the results of the mass balance, namely the moles in the vapour phase, and the time (see Figure 5-7). Initially, as CO_2 is added, the number of moles in the vapour phase (N_V) increases because the CO_2 stays mainly in the vapour phase. However, once the liquid phase begins to expand (around 58.5 bar in Figure 5-7a), N_V decreases quickly as the CO_2 liquefies.

If the model is allowed to run to higher pressures, as seen in Figure 5-7b which caries the simulation up to a pressure of 60.5bar, the number of moles in the vapour phase dips well below zero. The physical interpretation of this is that the liquid phase takes up the entire vessel, so trying to perform gas-liquid equilibrium calculations no longer has meaning and the mass balance gives erroneous results. It was found for this system that the maximum pressure we could achieve while maintaining physically realistic results was 58.5bar in the CO_2-toluene system at 25°C.
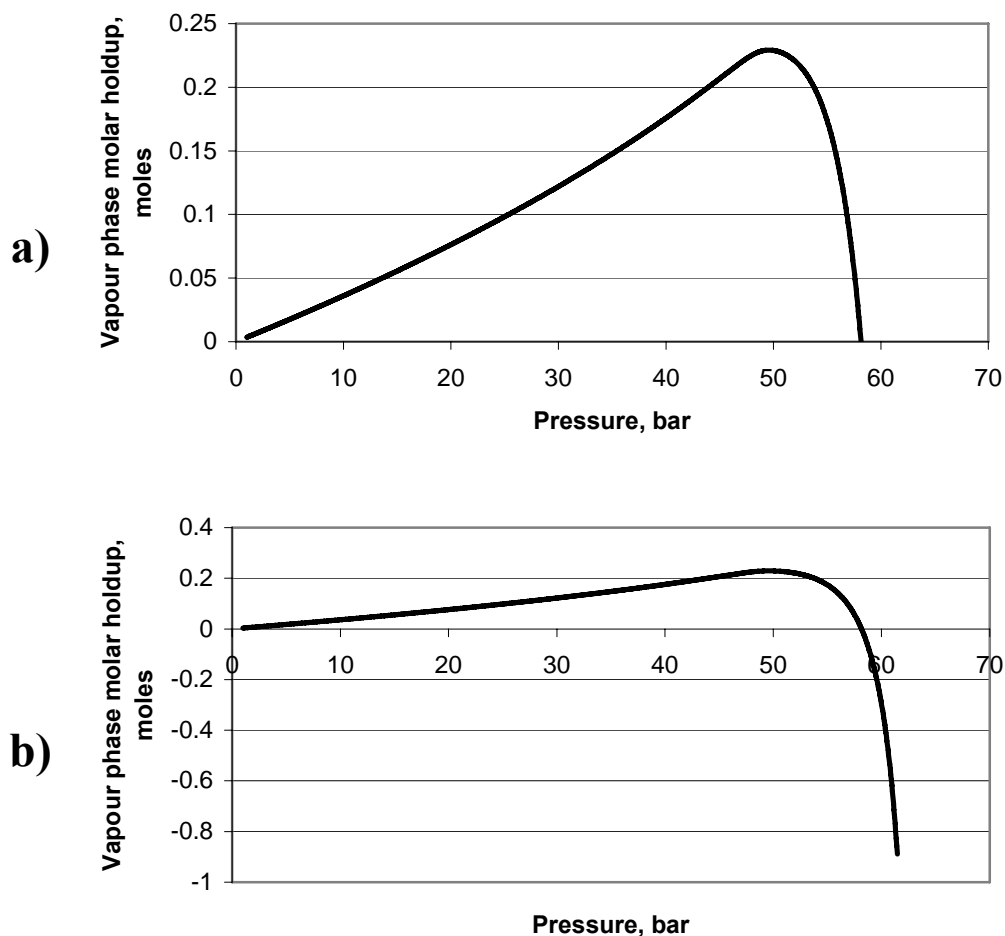
Figure 5-7: Model results for N_V vs. P up to (a) 58.5bar and (b) 60.5bar

It is important to test how the use of estimated parameters (using the methods outlined in Section 5.3.1) alters the predicted compositions so that some level of confidence can be given to the model when applying it to beclomethasone. Therefore, the physical properties of phenanthrene and naphthalene were estimated using the techniques outlined in Section 5.3.1 and applied to the equilibrium in toluene and CO_2. The results of the estimation are shown in Table 5-6 and Table 5-7, and it can be seen that most of the parameters were in reasonable agreement with the actual values.

Table 5-6: Estimated parameters for phenanthrene

Parameter	Actual Value[18]	Estimated Value	% difference
Critical temperature	869.2K	870.80K	0.18%
Critical pressure	33.5bar	30.9bar	7.86%
Acentric factor	0.536	0.399	25.55%
Liquid molar volume	151.2 cm^3/mol	163.3 cm^3/mol	8.00%
Solubility parameter	9.774 (cal/cm^3)$^{1/2}$	9.535 (cal/cm^3)$^{1/2}$	2.45%

Table 5-7: Estimated parameters for naphthalene

Parameter	Actual Value[18]	Estimated Value	% difference
Critical temperature	748.35K	746.6	0.19%
Critical pressure	39.7bar	39.96	0.67%
Acentric factor	0.302	0.302	0.07%
Liquid molar volume	131.2 cm^3/mol	127.53 cm^3/mol	2.80%
Solubility parameter	9.921 (cal/cm^3)$^{1/2}$	9.300 (cal/cm^3)$^{1/2}$	6.25%

These values were used in the expansion model, and the results are shown in Figure 5-8 and Figure 5-9. In both cases the model was able to predict the behaviour of all three components, though the accuracy of the prediction is slightly better in the naphthalene system. This is most likely due to the large error in the acentric factor estimation for phenanthrene, whereas the estimated values for naphthalene were all quite good. Both sets of predictions are able to represent the trends observed in the data, so it appears that some level of confidence can be given to the estimation techniques.

---

[18] From Dixon and Johnston, 1991
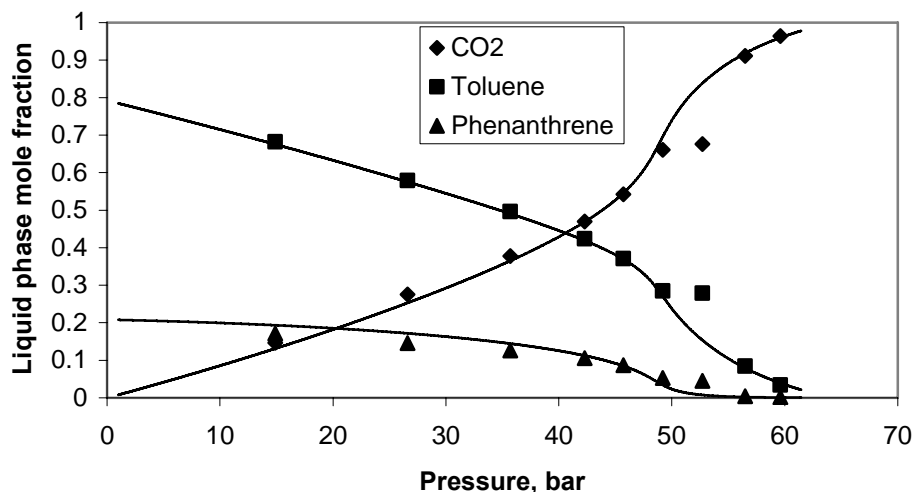
Figure 5-8: Liquid phase composition for the phenanthrene/toluene/CO_2 system using estimated properties for phenanthrene (data from Dixon and Johnston 1991)
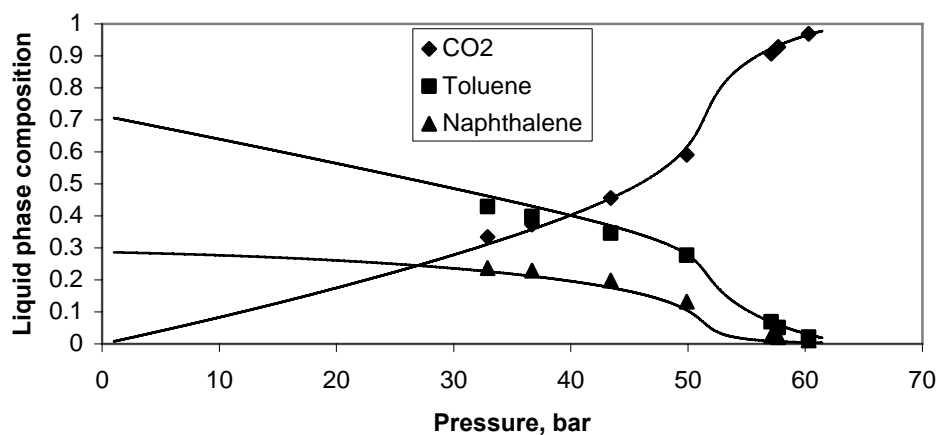
Figure 5-9: Liquid phase compositions for the naphthalene/toluene/CO_2 system using estimated properties for naphthalene (data from Dixon and Johnston 1991)

Based on these results, it can be concluded that the expansion model was implemented properly and was able to accurately predict the equilibrium data in two model systems. However, both naphthalene and phenanthrene are relatively small, simple compounds whereas beclomethasone is not. Therefore, it seemed prudent to test the model against a different system with a large, complex molecule. Cholesterol was chosen because it is a frequently studied steroid with phase data available, and therefore

should be able to give an indication of how reliable the model will be for beclomethasone.

The physical parameters for cholesterol were estimated using the techniques outlined in Section 5.3.1 and are shown in Table 5-8, although in this case it was not possible to compare to experimental values, since none were available in the literature. However, the parameters were similar to those previously estimated using different techniques (Kosal et al. 1992), so they are considered to be reasonable estimates.

Table 5-8: Estimated parameters for cholesterol

Parameter	Estimated Value
Critical temperature	883.12K
Critical pressure	12.5bar
Acentric factor	0.993
Liquid molar volume	388.88 cm^3/mol
Solubility parameter	8.562 $(cal/cm^3)^{1/2}$

The results from the phase equilibrium model are shown in Figure 5-10, where the data was obtained from (Liu et al. 2002). The predictions for both acetone and CO_2 mole fractions in the liquid phase are quite good. However, as can be seen in Figure 5-11, the prediction is not able to capture the behaviour of cholesterol whatsoever. The initial concentration is overestimated by a factor of roughly 4, and the model predicts an exponential decrease in solubility as pressure is increased, which is not consistent with physical reality. Therefore, the expanded liquid phase model cannot be used in the cholesterol-acetone-CO_2 system, which does not give any confidence to the possibility of using it on the BDP-acetone-CO_2 system.
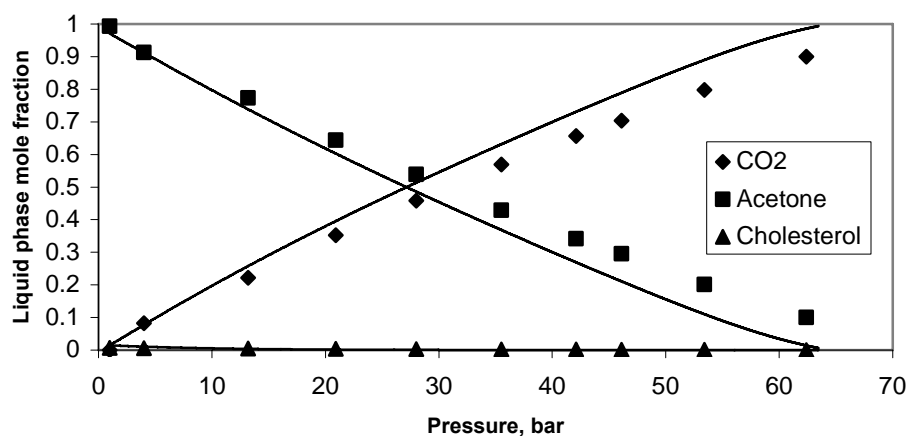
Figure 5-10: Liquid phase composition for the cholesterol/acetone/CO_2 system at 308K (data from Liu et al. 2002)
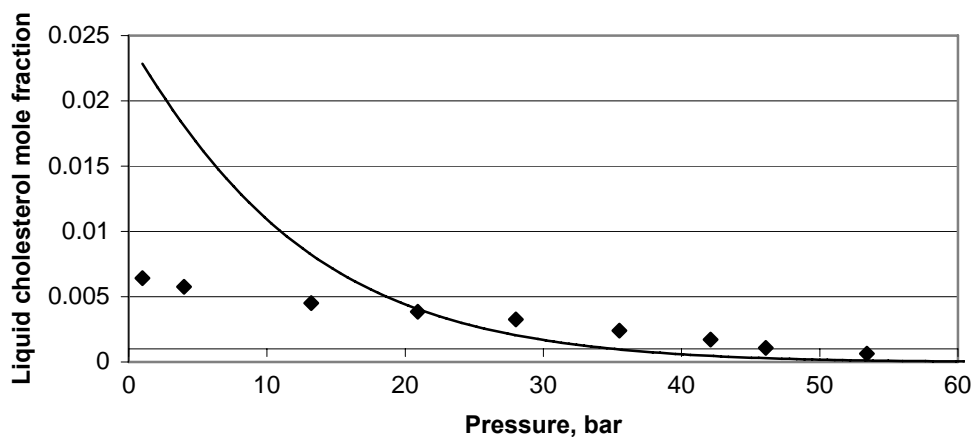
Figure 5-11: Liquid cholesterol mole fraction in the cholesterol/acetone/CO_2 at 308K (data from Liu et al. 2002)

There are several possibilities for why this model was able to handle the equilibrium in the phenanthrene and naphthalene systems, but was not satisfactory in the cholesterol system. First, the cholesterol mole fractions measured were on the order of 10^{-5}, with measured vapour pressures on the order of 10^{-9} bar (Kosal et al. 1992). Values at this order of magnitude can be very difficult to measure, and thus often exhibit large errors, which will propagate to significant error in the regressed parameters. When combined with the errors incorporated by estimating the critical point (instead of

obtaining an experimental value), it is possible that the regressed value of k_{13} is quite different from the "actual" value.

Also, because cholesterol does not actually exhibit a critical point[19], the definition of one through the mathematical methods provided in Section 5.3.1 is somewhat arbitrary. It can be thought of more as a tool to allow classical thermodynamics to work on compounds which lie outside its normal range of application. Therefore this approach is quite limited in its application. It is useful when modelling binary phase data because a k_{13} can be regressed to force the model to fit the data. However, when trying to apply these values to prediction of a system without empirical constants, this approach is more problematic.

Finally, quadratic mixing rules such as Equations (5.8) and (5.12) are not normally suitable for complex or polar systems. In these cases the dependence of the liquid phase fugacity on composition is often not so simple, especially when mixing polar (i.e. acetone) and non-polar (i.e. cholesterol/BDP) components, or for large compounds. This is usually overcome by incorporating an activity model into the mixing rules, such as with the Wong-Sandler mixing rules. However, this approach is quite time consuming and often requires regression of several parameters from experimental data in the system of interest, which is difficult to do accurately when dealing with small data sets and impossible to do when the data is not present (Poling et al. 2001). Therefore, this approach is not practical for the BDP/cholesterol-acetone-CO_2 system.

Despite these problems, the expanded liquid phase model was still applied to the BDP/acetone/CO_2 system, as shown in Figure 5-12. While it is difficult to make concrete

---

[19] The compound will decompose thermally before reaching a critical point. This is often the case with solids

conclusions on the suitability of the model without phase data for comparison, the results shown do not seem realistic. The actual initial mole fraction of BDP in acetone is approximately 0.01, so the expanded liquid phase model overestimates the solubility by over an order of magnitude. It initially seems to show an exponential decrease in solubility, as was the case with the model predictions for cholesterol. Also, at around 25 bar the solubility of BDP in the liquid phase is actually predicted to increase. It should be noted that, were this true, the GAS process would not work with beclomethasone since the solute would never precipitate, which was not observed to be the case (see Section 3.1). Finally, the code used for this model normally required 2-3 minutes to complete for simpler systems, yet took 8-10 hours when trying to predict the BDP-acetone-CO_2 equilibrium. This indicates that significant convergence issues were encountered when trying to calculate the phase equilibrium, which raises even more questions about the accuracy of the prediction. Given these observations, it can be concluded that this model is inadequate for representing the actual phase equilibrium in the BDP-acetone-CO_2 system, and therefore a different approach must be taken to model the phase data.
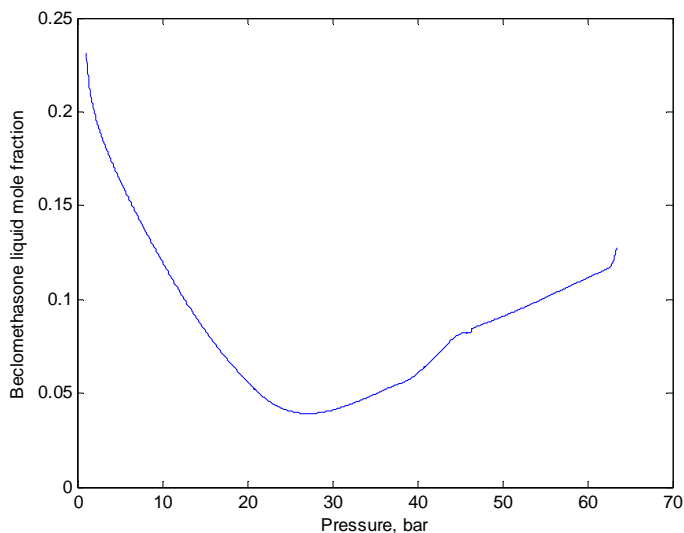
Figure 5-12: Liquid beclomethasone mole fraction in the beclomethasone/acetone/CO_2 at 298K

5.4.2. *RPMVF model*

The relative partial molar volume fraction (RPMVF) model described in Section 5.2 has the major advantage of not requiring any information about the solute in question, except its solubility in the solvent at atmospheric pressure, because the solute is neglected when calculating the partial molar volumes. Therefore, the problems involved in estimating critical properties etc. that were encountered in the previous section are eliminated. Also, as the solid is not considered in the phase equilibrium, no special considerations must be taken with the mixing rules.

The RPMVF model was applied to phenanthrene and naphthalene in toluene, as shown in Figure 5-13 and Figure 5-14. In both cases the model was able to predict the mole fractions of all three components reasonably well. It is important to note that this method will predict negative solid mole fractions at high pressures because the partial molar volume of the solvent becomes negative. Therefore, the "cut off" for the model is once the solute mole fraction becomes negative (see Figure 5-15). However, it is clear

from the results that up to this point the model is able to handle the phase equilibrium quite well.
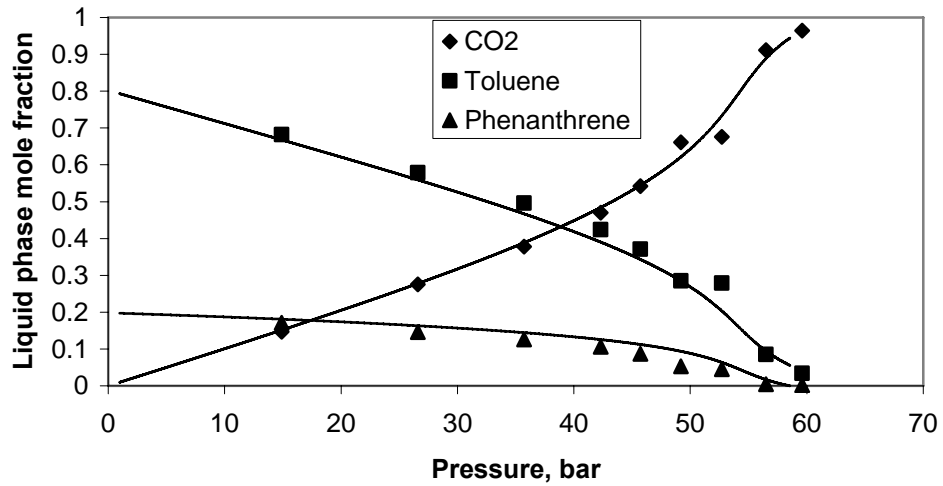
Figure 5-13: Liquid phase composition in phenanthrene/toluene/CO_2 system 298K using RPMVF model (data from Dixon and Johnston 1991)
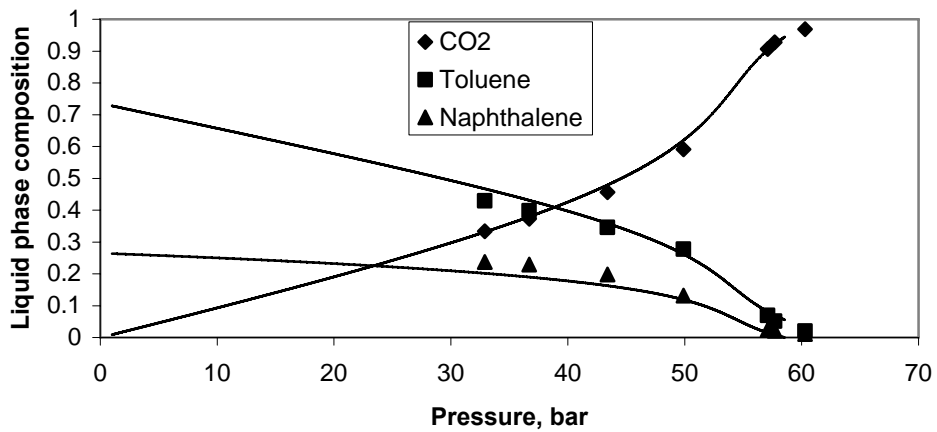
Figure 5-14: Liquid phase composition in naphthalene/toluene/CO_2 system at 298K using RPMVF model (data from Dixon and Johnston 1991)
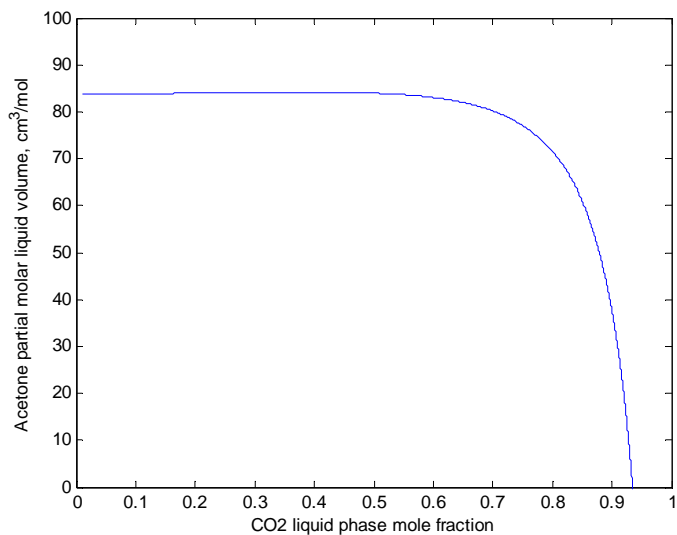
Figure 5-15: Acetone partial molar volume vs. CO_2 mole fraction

The RPMVF model was then applied to the cholesterol/acetone/CO_2 system, with the results shown in Figure 5-16 and Figure 5-17. The model was able to describe the equilibrium of all three components rather well. In particular, the solid predictions are very good, indicating that this method is able to work with large complex compounds as well as with small and simple compounds. The results from the ELPM and the RPMVF models are compared in Figure 5-18. It is clear that there is a significant improvement in the ability of the RPMVF model to predict the solubility of cholesterol in acetone.
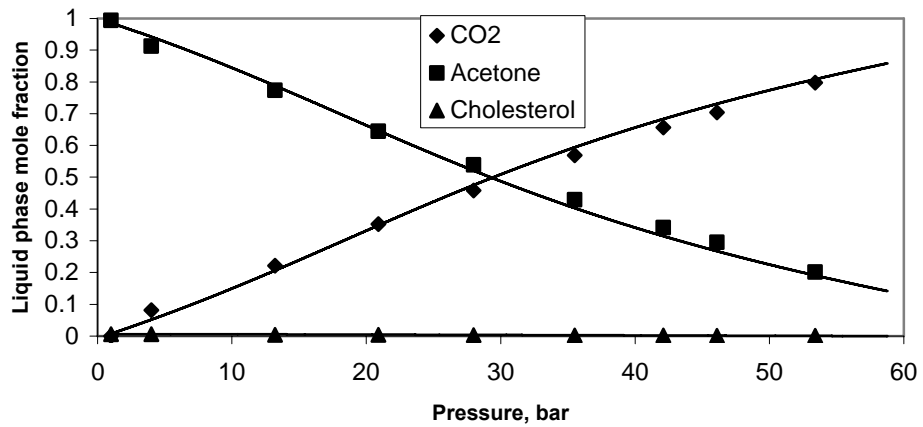
Figure 5-16: Liquid phase composition in cholesterol/acetone/CO_2 system at 308K using RPMVF model (data from Liu et al. 2002)
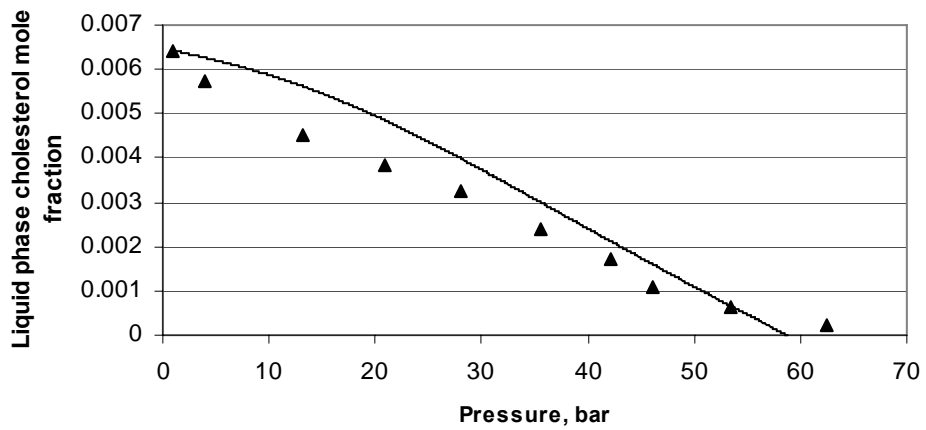
Figure 5-17: Liquid cholesterol mole fraction at 308K using RPMVF model (data from Liu et al. 2002)
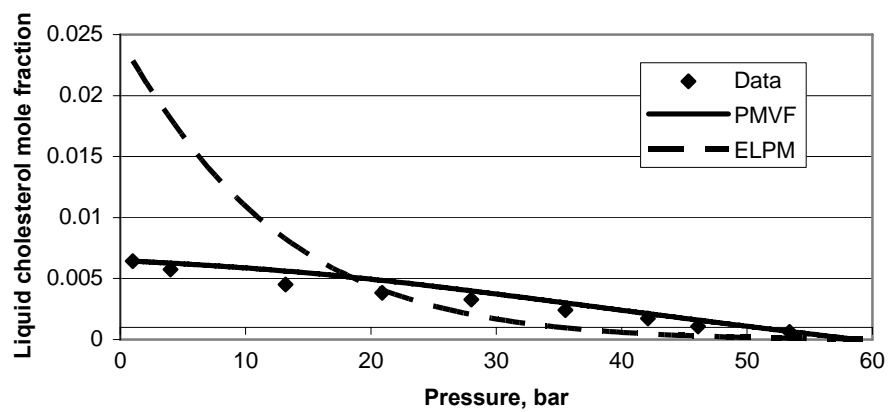
Figure 5-18: Comparison of results obtained between PMVF and ELPM models (data from Liu et al. 2002)

While the ELPM is based on well known thermodynamic concepts, with only the assumption of instantaneous equilibrium, the RPMVF model is justified on the assumption that it is the volumetric expansion which drives the increase in supersaturation. Therefore, this approach can be considered semi-empirical since it does not have a rigorous thermodynamic background, but is based on our current understanding of the GAS process. However, there is no denying the usefulness of this approach or its apparent success in describing three phase equilibrium.

Also, it is important to stress that this model does not consider the equilibrium of the solid phase, and therefore is not a true equilibrium model for the system, even though it does consider the solvent-CO_2 equilibrium. Also, it is interesting that Equation (5.28) relates the solute mole fraction linearly to the solvent's contribution to the molar volume. This implies that CO_2's role in the GAS process is not related directly to the antisolvent/solid interactions, but that it simply dilutes the liquid phase.

Once the phase equilibrium model was completed, it was possible to use the profile of solute saturation vs. time to obtain some preliminary results on how the various physical process conditions would affect the particle size. The effect of flowrate on the saturated solute concentration at $25^{o}C$ was examined (see Figure 5-19). It should be noted that the trend observed for 1g/min is the same as in the others, but that it took approximately 5000 seconds to approach zero, and so was truncated. At a low flowrate, the drop in mole fraction is quite gradual, thereby providing time for nuclei to grow. However, as the flowrate is increased, the mole fraction drops much more quickly. In these cases, the supersaturation will reach higher levels because the actual amount of solute dissolved cannot decrease fast enough. Therefore, under these conditions one

would expect much smaller particles, as they have little time to grow, which is the experimentally observed trend.
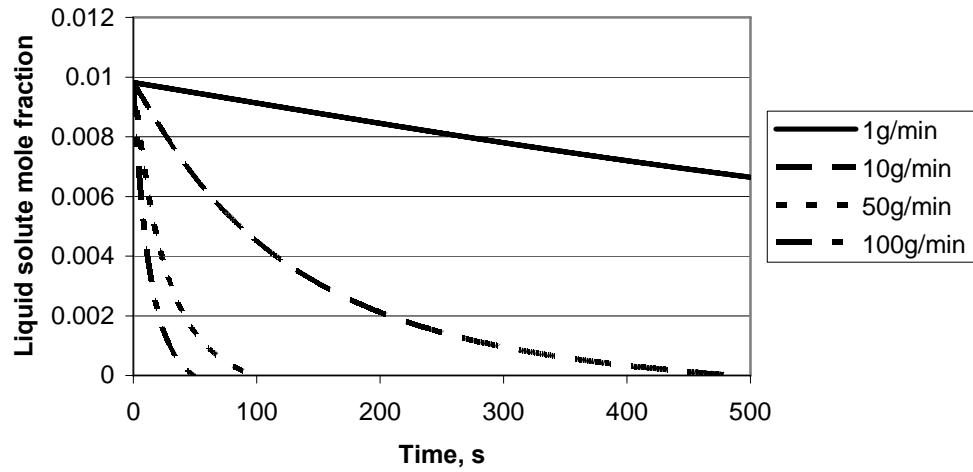
Figure 5-19: Effect of CO_2 addition rate on solute solubility

6. Kinetics of the GAS process

To understand the GAS crystallization procedure, and thus be better able to optimize process conditions to produce particles of a particular size, it is important to develop a model for the crystallization kinetics. The ultimate goal of this model is to accurately predict the final particle size distribution after GAS processing, based on system dependant physical constants (such as viscosity) and the initial experimental conditions. The commercial software packages Matlab (Mathworks) and FEMLAB (Comsol) were used to implement this model.

6.1. *Crystallization Model*

A population balance, i.e. a mass balance over an infinitely small subregion, is commonly used in crystallization kinetics. This type of model can be used as a predictive tool, as opposed to empirical models which are often limited to a specific application. The general form of the one dimensional population balance is as follows (Randolph and Larson 1988):

$$\frac{\partial n}{\partial t} + G\frac{\partial n}{\partial L} + \frac{n}{N_L v_L}\frac{d(N_L v_L)}{dt} = B(L) - D(L) \tag{6.1}$$

where $n = n(t,L)$ is the distribution function of the particles, L is the size of the particles, G is the growth rate of the particles, which is assumed to be independent of particle size, N_L is the liquid molar hold-up, v_L is the molar volume of the liquid phase in the vessel, $B(L)$ is the crystal birth rate, and $D(L)$ is the crystal death rate. It should be noted that the volume of the "reactor" was taken to be the liquid phase only, i.e. the vapour phase was ignored, because this is where the precipitation occurs. However, this

means that the volume of interest is not constant, despite performing the crystallizations in a rigid vessel.

The birth and death terms generally are used to account for any effect that creates unique particles or destroys existing particles, such as nucleation, aggregation, and breakage. However, if the nuclei are assumed to form with a zero radius then nucleation can be incorporated into the boundary condition for Equation (6.1) (Muhrer et al. 2002).

Agglomeration and breakage are somewhat more complicated because they inherently involve both birth and death of particles with a non-zero size, i.e. agglomeration involves the death of two small particles to create one large particle. However, it has been shown that in practice agglomeration and breakage do not play a significant role in the GAS process (Bakhbakhi 2004). Therefore, we are able to ignore the birth and death terms and the population balance takes on the following form:

$$\frac{\partial n}{\partial t} + G \frac{\partial n}{\partial L} + \frac{n}{N_L v_L} \frac{d\left(N_L v_L\right)}{dt} = 0 \tag{6.2}$$

We are now able to start defining the different terms in the population balance. First, it has been shown that the growth rate can be considered to be size independent while maintaining good agreement with experimental results (Bakhbakhi 2004). Therefore, we will use a relatively simple expression for the crystal growth (Muhrer et al. 2002):

$$G = \frac{dL}{dt} = k_g \left(S-1\right)^g \ \text{ for } S > 1 \tag{6.3}$$

where k_g and g are both system dependant empirical constants, and S is the supersaturation. The volume derivative in Equation (6.1) was calculated using the results from the volume expansion model discussed in Section 5.1.

There is no single strict definition for the supersaturation. Any form which is able to describe the amount of solute dissolved, to the amount of solute dissolved in a saturated solution at identical conditions seems to suffice. As such, the supersaturation S is often defined as the difference between current and saturated concentration $\left(S = \dfrac{\Delta C}{C^{sat}} = \dfrac{C - C^{sat}}{C^{sat}} \right)$, as the ratio of fugacities between current and saturated conditions $\left(S = \dfrac{\hat{f}_P^L}{\hat{f}_P^{L,sat}} \right)$, or simply as a ratio of mole fractions (Randolph and Larson 1988):

$$S = \frac{x_P}{x_P^{sat}} \tag{6.4}$$

Equation (6.4) was used in this work primarily for simplicity of calculation, since the equilibrium solid mole fractions are calculated directly, as discussed in Sections 5.1 and 5.2.

We now require one boundary and one initial condition to solve the population balance. First, we can assume that all of the solid in the system is initially dissolved, i.e. that

$$n(0, L) = 0 \tag{6.5}$$

For our boundary condition, we will make the assumption that the nuclei are formed with an initial diameter of 0, as stated above (Muhrer et al. 2002). Therefore, the nucleation rate can be considered as the rate of change of the particle distribution with respect to time at a size of zero, i.e:

$$B = \left(\frac{dn}{dt} \right)_{L \to 0} = \left(\frac{dL}{dt} \frac{dn}{dL} \right)_{L \to 0} \tag{6.6}$$

where B is the nucleation rate. However, the first derivative in the brackets is defined as the growth rate G (see Equation (6.3)), which is independent of size, so that the limit $L \rightarrow 0$ does not require special consideration. The second derivative represents the particles formed at length zero, and is therefore the distribution of the nuclei, $n(t,0)$. Once these observations are combined, we get our boundary condition (Randolph and Larson 1988):

$$n(t,0) = \frac{B}{G} \tag{6.7}$$

where B is defined by the following set of equations (Muhrer et al. 2002):

$$B = \begin{cases} B' + B'' & if \ S > 1 \\ 0 & if \ S \leq 1 \end{cases} \tag{6.8}$$

$$B' = 1.5 D_{AB} \left(c_p N_A \right)^{7/3} \sqrt{\frac{\gamma}{kT}} \frac{v_p}{N_A} \exp\left(-\frac{16\pi}{3} \left(\frac{\gamma}{kT} \right)^3 \left(\frac{v_p}{N_A \ln S} \right)^2 \right) \tag{6.9}$$

where B' and B'' are the rates of primary and secondary nucleation, respectively. In this thesis, two different equations for secondary nucleation will be evaluated (Muhrer et al. 2002). The first, Equation (6.10), has a theoretical basis but has not seen widespread use, whereas the second, Equation (6.11), is entirely empirical but is commonly used (Randolph and Larson 1988):

$$B'' = \frac{\alpha'' a_v D_{AB}}{d_M^4} \exp\left(\frac{-\pi}{\ln S} \left(\frac{\gamma d_M^2}{kT} \right)^2 \right) \tag{6.10}$$

$$B'' = k_s M_T^j (S-1)^i \tag{6.11}$$

where D_{AB} is the diffusion coefficient, c_p is the particle concentration in the liquid phase, N_A is Avogadro's number, γ is the solid-liquid interfacial tension, k is

Boltzmann's constant, T is the temperature, v_p is the molar volume of the solid particles, a_v is a volumetric shape factor, d_M is the molecular diameter, α'' is an empirical constant which determines the order of magnitude of secondary nucleation in Equation (6.10), k_s does the same in Equation (6.11), M_T is the suspension density, and i and j are empirical exponents. Several of these variables can be further defined as follows (Muhrer et al. 2002):

$$D_{AB} = \frac{kT}{2\pi\eta d_M} \tag{6.12}$$

$$d_M = \left(\frac{v_p}{N_A}\right)^{1/3} \tag{6.13}$$

$$a_v = k_a m_2$$

$$m_i = \int_0^\infty nL^i dL \tag{6.14}$$

$$c_p^L = \frac{x_p}{v_L} \tag{6.15}$$

where η is the dynamic viscosity of the liquid phase, k_a is a surface shape factor ($k_a = \pi$ for spherical molecules), m_i is the ith moment of the population density function $n(t,L)$, and x_p is the mole fraction of solid dissolved in the liquid phase.

The solid-liquid interfacial tension is an important parameter in crystallization because the particle that is forming must overcome this energetic barrier. However, the experimental determination of the interfacial tension, while possible, presents a significant challenge because the solid is soluble in the liquid, so traditional methods (such as contact angle) cannot be used. Mersmann developed a theoretical approach to

calculate the interfacial tension of binary solid/liquid systems based on a free energy balance over the interface, which leads to the equation (Mersmann 1990):

$$\gamma = 0.414 kT \left(c_p^S N_A\right)^{2/3} \ln\left(\frac{c_p^S}{c_p^L}\right)$$ (6.16)

where k is the Boltzmann constant, T is the temperature, N_A is Avogadro's number, and c_p^S and c_p^L are the (molar) solute concentration in the solid and liquid phases, respectively. It is important to note that this equation accounts for the change in interfacial tension as the system supersaturation increases, whereas the approach taken by Muhrer (Muhrer et al. 2002) does not.

Since Equation (6.16) was developed purely from theory, it should be able to represent the interfacial tension in most systems with reasonable accuracy. It was tested in 58 different binary systems and showed fairly good agreement in most cases (Mersmann 1990). Therefore, this method was used to provide an order of magnitude guess for the interfacial tension in the BDP/acetone binary system.

Finally, to determine the supersaturation, the amount of solute currently in solution is required. To determine this, we need to know how many moles of particles have precipitated in a given time. The volume of the precipitated particles can be found using the third moment of the particle density distribution, n, along with a shape factor. However, the third moment describes the volume of particles per unit volume of the liquid phase. Therefore, this moment must be multiplied by the total liquid volume to obtain the total crystal volume (Grosch and Briesen 2004):

$$V_{crystal} = k_v m_3 N_L v_L$$ (6.17)

where k_v is a volumetric shape factor ($= \dfrac{\pi}{6}$ for spherical crystals), and $V_{crystal}$ is the volume of the crystals. This can then be converted into the number of moles of particles by simply dividing by the molar volume of the solid, i.e.:

$$N_p = \frac{k_v m_3 N_L v_L}{v_p} \qquad (6.18)$$

so, the mole fraction of solute remaining in solution can be obtained by a simple mass balance:

$$x_p = \frac{N_p^o - N_p}{N_L} \qquad (6.19)$$

The commercial software package FEMLAB was used to solve the population balance, and the implementation can be found in Appendix A-3. However, to solve the population balance, the volume of the liquid phase and supersaturation must be known as a function of time. Therefore, a thermodynamic model of the equilibrium must also be performed. While the crystallization model and the thermodynamic model are both inherently linked, it has been previously shown that they can be decoupled without significant error (Muhrer et al. 2002). Therefore, the mass balance was solved independently of the population balance in this work.

6.2. *Model implementation*

The population balance, Equation (6.2), was implemented using the commercial software package FEMLAB, which uses the finite element method to solve partial differential equations. The population balance was implemented using the one-dimensional general coefficient mode, which gives a general second order PDE and allows the user to enter the coefficients:

$$e_a \frac{\partial^2 u}{\partial t^2} + d_a \frac{\partial u}{\partial t} + \nabla \cdot \left(-c\nabla u - \alpha u + \gamma \right) + au + \beta \cdot \nabla u = f \qquad (6.20)$$

where e_a, d_a, c, α, γ, a, β and f are the coefficients, and u is the function. The population balance was solved for particle sizes ranging from 1nm to 1mm. A dirichlet boundary condition was used, based on Equation (6.7), at the 1nm boundary, which implied that particles are formed with "zero" size, considering the actual particles formed were in the 1-100μm range. The variables input from the phase equilibrium model (see Sections 5.1, 5.2, and 5.4) were entered as Matlab .m files which, using time as an input, would interpolate to calculate the required value. The saturated mole fraction, liquid volume in the precipitation vessel, number of moles in the liquid phase, and the volume derivative in Equation (6.2) were all input in this manner.

The size of the mesh was chosen to balance computational time with numerical accuracy. This was done in two ways. First, particle size distributions normally scale logarithmically, with a large fraction occurring at smaller sizes (i.e. 1 μm) as opposed to bigger sizes (i.e. 1mm). Therefore, the mesh spacing was scaled to be very fine at the left end (1nm), and grow to a size of a few dozen microns by the right end (1mm). This allowed good numerical accuracy to be achieved without an excessive number of elements. Second, the simulation was run several times to determine acceptable values for the mesh growth rate and minimum mesh spacing. The solution time was normally 5-20 minutes, depending on the mesh spacing used, and little change in the predicted particle size distribution was observed when the mesh spacing/growth rate were decreased further. Therefore, a minimum mesh spacing of 1nm and a growth rate of 1.05 were used, giving 226 mesh elements over the region 1nm to 1mm.

6.3. _Model Results_

In this work, the crystallization kinetics were described by three kinetic terms: primary nucleation, secondary nucleation, and size-independent growth. Primary nucleation is described by Equation (6.9), which is a standard equation based on the free energy change when a crystal forms out of solution, and is fully described by the physical properties of the system being studied. The secondary nucleation was described by two equations separately, Equations (6.10) and (6.11). Equation (6.10) was developed based on the growth of a crystal on a smooth surface multiplied by the probability that this second crystal will dislodge, i.e. the parameter α'' (Worlitschek and Mazzotti 2004), while Equation (6.11) is empirical in nature, but is commonly used (Randolph and Larson 1988).

First, it is important to give some level of justification to why secondary nucleation was chosen to describe the bimodal distributions commonly encountered in GAS processed powders (Muhrer et al. 2002). The results shown in this section were obtained using Equation (6.10) to describe secondary nucleation, because it has only one empirical parameter to be adjusted and will still show the same general trends in an order of magnitude analysis as Equation (6.11). The model results were based on the BDP-acetone-CO_2 system at a temperature of $25^{\circ}C$, a CO_2 addition rate of 43.3g/min, and an initial solids loading of 0.3 g solute/mL solvent.

The basic effect of α'' is to adjust the order of magnitude of secondary nucleation. To maintain a general view of what is occurring, three values of α'' were evaluated. A high value of 10^{-15}, moderate value of 5×10^{-17} and a low value of 10^{-18} were chosen to illustrate the effect of the secondary nucleation parameter, and not because they

have any particular physical significance. As can be seen in Figure 6-1, an increase in the

secondary nucleation parameter decreases the particle size estimated by the model.
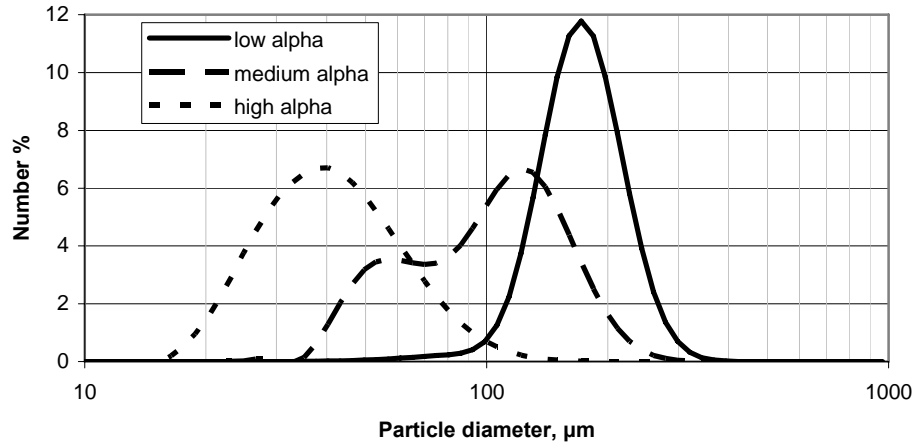
Figure 6-1: Effect of secondary nucleation parameter on hypothetical particle size distributions

At moderate values of α'' the distribution obtained is bimodal, giving some

credibility to the ability of using secondary nucleation to describe the bimodal particle

size distributions obtained experimentally. This effect can be explained by noting the

order of magnitude of secondary nucleation (see Figure 6-2). When α'' is low, primary

nucleation dominates and when it is high, secondary nucleation dominates; in both of

these cases Figure 6-1 shows a unimodal distribution. However, when α'' is of an

intermediate value, primary and secondary nucleation are on the same order of

magnitude, and this is what produces the bimodal distribution. Therefore, by accounting

for secondary nucleation it is possible to get a bimodal distribution, so the proper

selection of kinetic constants should be able to represent the experimental data. It should

be noted that the poor resolution in Figure 6-2 is because FEMLAB stores calculated

variables at discrete time points. Therefore, when only a small interval of time is

monitored (as in Figure 6-2, which displays only 2 seconds of data), the result will look jagged.
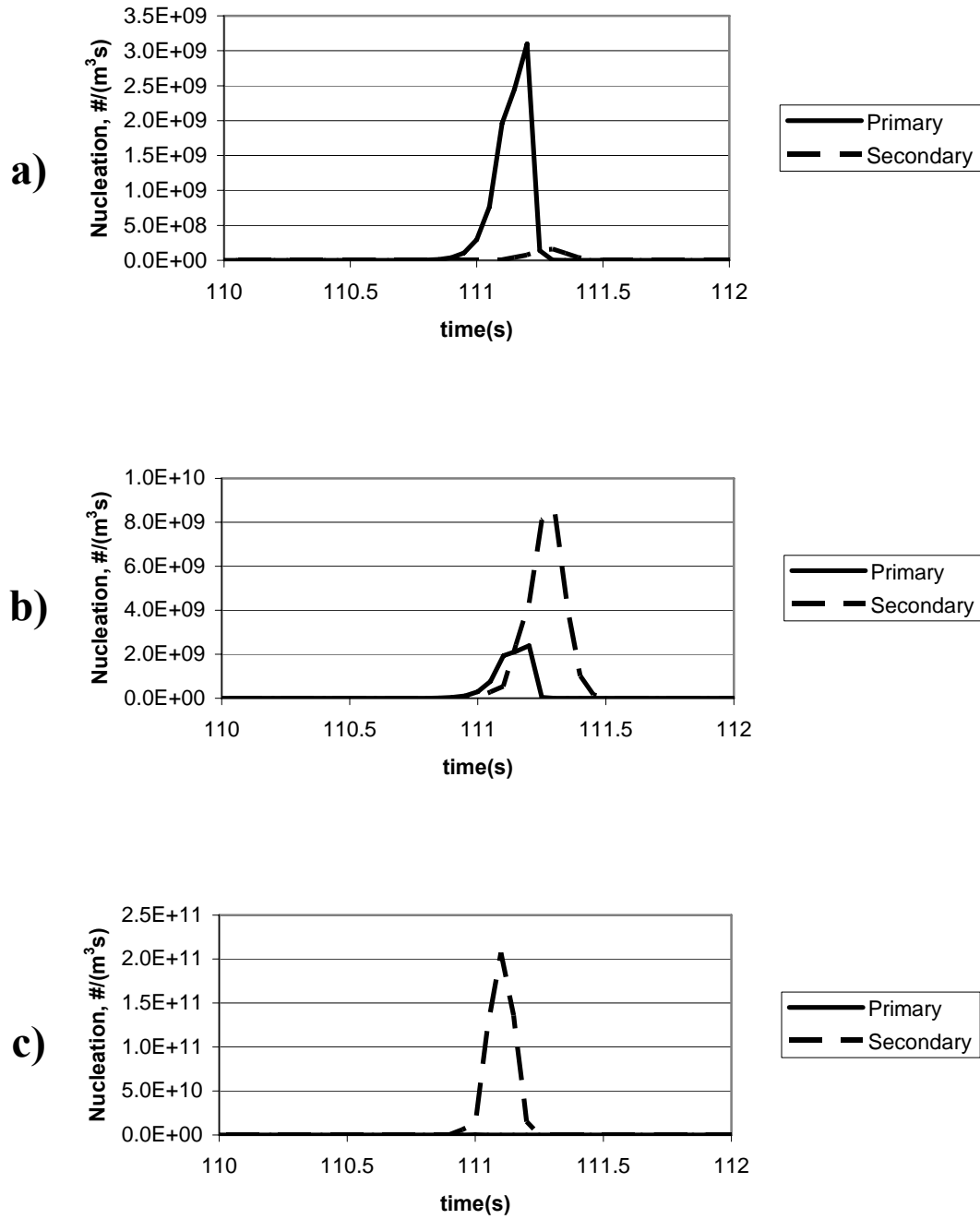
Figure 6-2: Effect of the secondary nucleation parameter on the magnitude of nucleation for: a) low (10^{-18}), b) moderate (5×10^{-17}) and c) high (10^{-15}) values

Equation (6.10) was used to model secondary nucleation, and the 3 constants (α'', k_g, g) were regressed from experimental data using Matlab. The constants are given in Table 6-1, along with the associated experimental run number (see Table 4-3). The average absolute deviation (AAD[20]) was used instead of the AARD because the model was not accurate at predicting the volume % when it approached zero, which inflated the AARD despite the reasonable fit. Therefore, the AAD was given because the error on small volume fractions would not affect the final result significantly. Also, it should be noted that the average was taken with respect to only the data points which had a moderate volume %, i.e. greater than 0.01%. This method provided a more accurate representation of the error.

For simplicity, the effect of agitation rate and temperature were ignored in the crystallization model. Therefore, only the effect of flowrate was considered. However, it is important to account for these parameters, as they can have an effect on the final particle size (see Section 4.2). Therefore, it is recommended that future work delves into this area.

When Equation (6.10) was employed (see Figure 6-3 and Table 6-2), the kinetic model was able to describe the location of the curve and the size of the large particles reasonably well. However, it overestimated the height of the primary mode by over 2 volume percent in each case, which amounts to a relative error of approximately 20%. Also, the model was unable to account for the secondary mode observed in Figure 6-3. Therefore, this model is not considered acceptable, and another equation for secondary

[20] The average absolute deviation is defined here as $AAD = \dfrac{1}{N}\sum\limits_{}^{N}| y_{calc} - y_{exp} |$

nucleation was implemented. It should be noted that the constants at 75 mL/min were not regressed. Given that the model had already proven unsuccessful, and the regression required several days, it was left out in the interests of time.
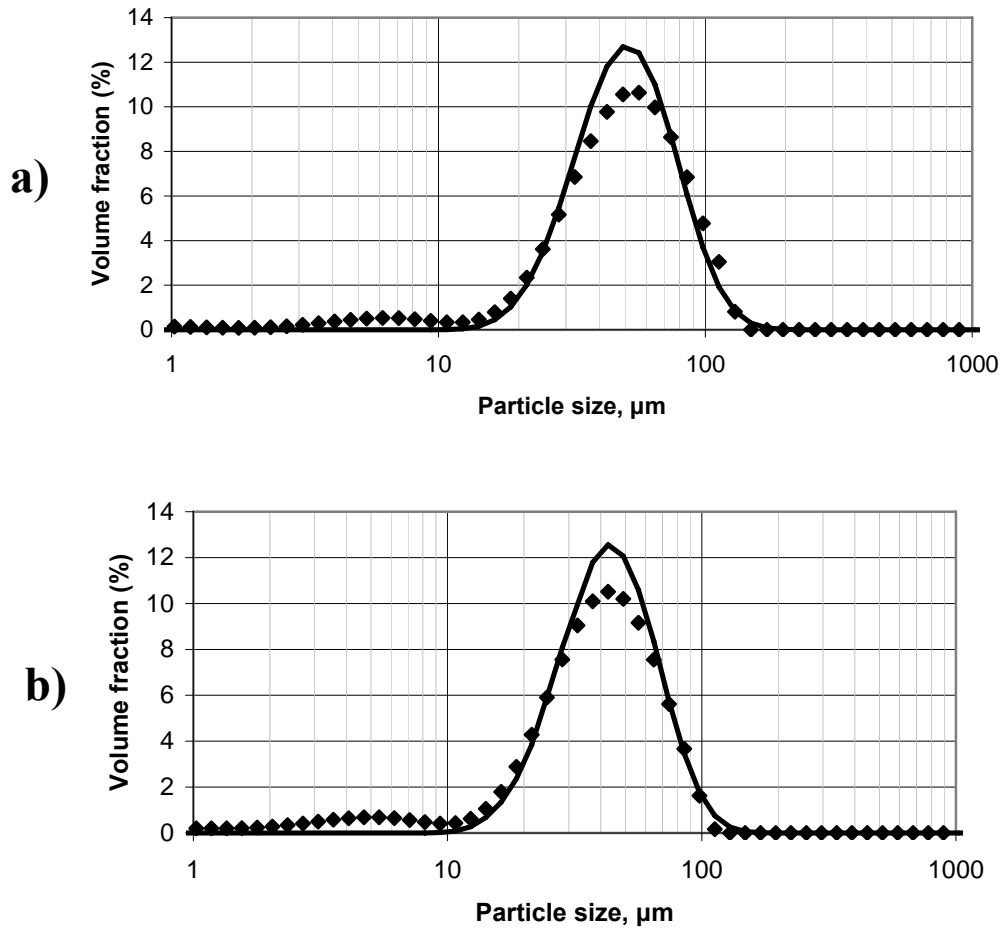
Figure 6-3: Experimental vs. model results for the crystallization kinetics using Equation for: a) 25mL/min, b) 50mL/min

Table 6-1: Regressed parameters for growth and secondary nucleation using Equation (6.10)

Run	$ln(\alpha'')$	k_g	g	AAD
F1	-33.79	$2.645x10^{-6}$	2.184	0.476
F2	-33.70	$2.574x10^{-6}$	2.170	0.500

Table 6-2: Summary of model results using Equation (6.10)

		$d_p(10\%)$ (µm)	$d_p(50\%)$ (µm)	$d_p(90\%)$ (µm)
	Data	18.97	47.28	86.64
F1	Model	26.47	46.63	79.64
	% difference	**39.54%**	**1.37%**	**8.09%**
	Data	17.22	36.51	68.14
F2	Model	22.18	39.72	68.18
	% difference	**28.76%**	**8.77%**	**0.05%**

Equation (6.11) was also used to model secondary nucleation, and the 5 constants (k_s, i, j, k_g, g) were regressed from experimental data using Matlab. The constants are given in Table 6-3, along with the associated experimental run number (see Table 4-3). The average absolute deviation (AAD) was given instead of the AARD, as described above.

The developed kinetic model was able to represent the primary mode quite well at all three flowrates, as seen in Figure 6-4, though the fraction of larger particles (>100µm) predicted was always slightly overestimated. However, as with Equation (6.10), the model was unable to account for the secondary mode in volume percent.
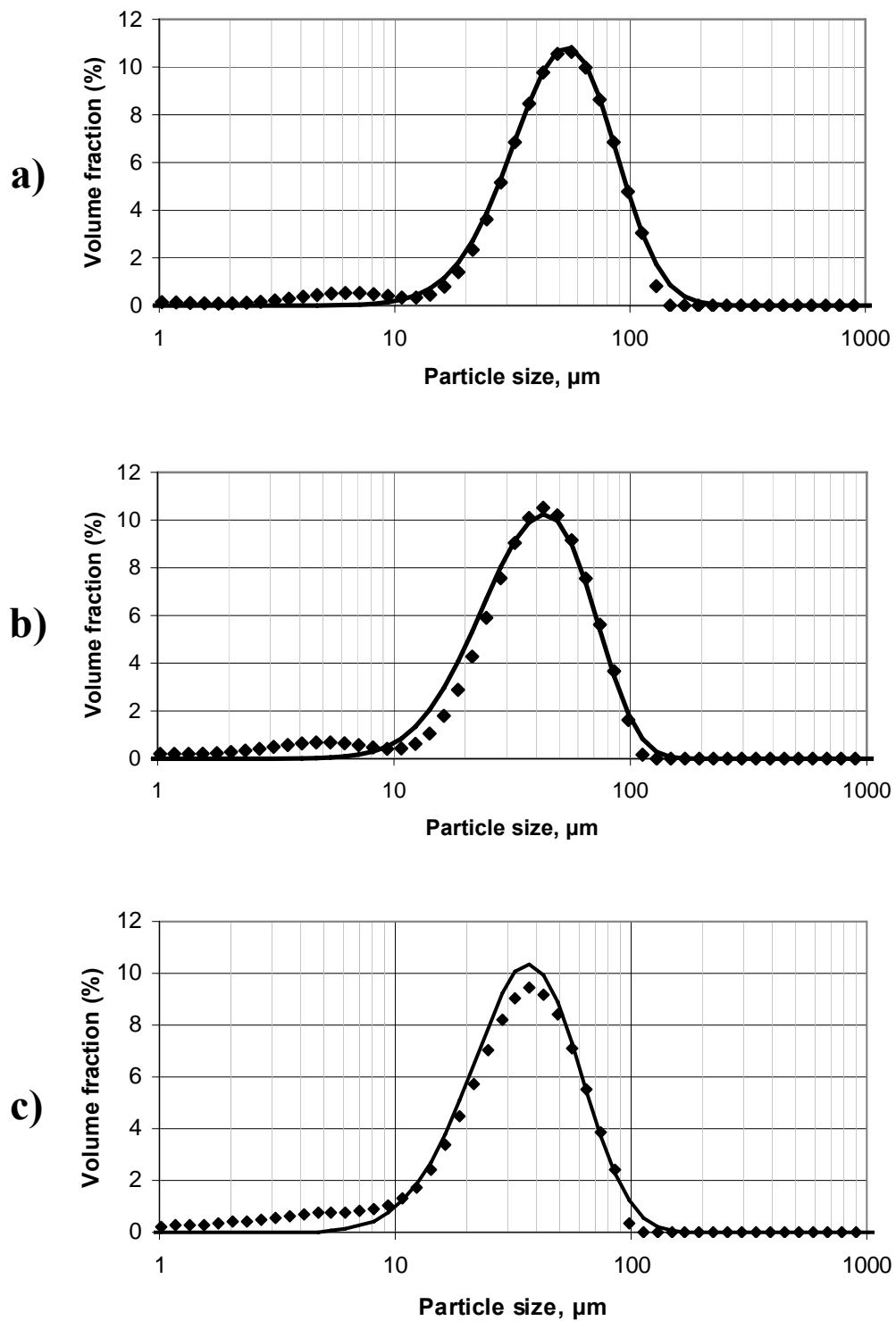
Figure 6-4: Comparison of experimental and predicted particle size distributions at 25°C, 1000RPM and a) 25 mL/min, b) 50 mL/min, c) 75 mL/min

Table 6-3: Regressed parameters for growth and secondary nucleation using Equation (6.11)

Run	$ln(k_s)$	i	j	k_g	g	AAD
F1	21.32	3.552	1.157	$5.651x10^{-6}$	1.910	0.224
F2	21.99	3.370	1.201	$3.836x10^{-6}$	1.855	0.402
F3	24.13	3.713	1.199	$1.5734x10^{-5}$	1.594	0.374

Table 6-4: Summary of model results using Equation (6.11)

		$d_p(10\%)$ (μm)	$d_p(50\%)$ (μm)	$d_p(90\%)$ (μm)
	Data	18.97	47.28	86.64
F1	Model	23.56	47.62	88.16
	% difference	**24.19%**	**0.72%**	**1.76%**
	Data	17.22	36.51	68.14
F2	Model	17.20	40.59	73.05
	% difference	**0.12%**	**11.17%**	**7.19%**
	Data	9.76	32.84	63.35
F3	Model	15.05	33.14	63.82
	% difference	**54.24%**	**0.93%**	**0.75%**

While accounting for secondary nucleation allows for an accurate description of the primary mode of the particle size distributions, and also performs reasonably well at calculating the $d_p(50\%)$, and $d_p(90\%)$, it cannot account for the second mode in the volume fraction regardless of whether Equation (6.10) or (6.11) is used. Therefore, under the conditions studied, secondary nucleation alone cannot describe the experimental particle size distributions.

There are several explanations for why secondary nucleation was unable to describe the bimodal nature of the particle size distributions obtained after GAS processing. The first problem relates to the sphericity of the particles. Laser diffraction calculates the spherical volume equivalent diameter[21], and thus is able to construct a volume weighted distribution. However, this can be problematic when the particles are not spherical, as was the case with BDP (see Section 4.2). Therefore, because the kinetic

---

[21] i.e. it computes the diameter of a sphere with equal volume to the particle analysed.

model calculates the number weighted density of a set of spherical particles, it is possible that problems could arise when the model results are compared to the experimental results.

Second, the bimodal distributions predicted by secondary nucleation often have both peaks rather close together (see Figure 6-1). Therefore, when the distribution is converted to a volume weighted diameter, the mode with a larger diameter will nearly always outweigh the one with a smaller diameter. However, the secondary peak GAS produced powders often results from a "tail" in the number weighted diameter (see Figure 6-5). However, secondary nucleation was found to be unable to mimic this behaviour, regardless of the kinetic constants chosen.
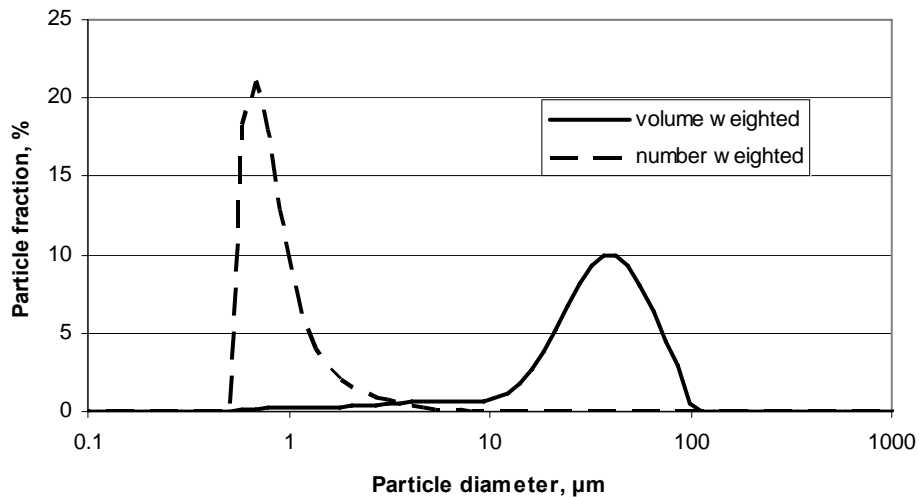
Figure 6-5: Comparison of volume and number weighted size distributions for GAS run F5

Finally, as was shown in Section 4.2, agglomeration plays a rather significant effect. While the model was compared to the sonicated samples, it is still possible that the particles were agglomerated. In fact, there is some evidence of this in many of the SEM's in Section 4.2, where several particles appear to be fused together. Therefore, an

accurate model of the GAS crystallization in the BDP-acetone-CO_2 will likely need to incorporate agglomeration effects.

7. Conclusions and Recommendations

In this work, both experimental and theoretical studies of the GAS process were studied with respect to the beclomethasone-acetone-CO_2 system. Beclomethasone powders were successfully produced using the GAS technique, and the effect of agitation rate, CO_2 addition rate, and temperature were studied. Also, the particle sizes were determined with and without sonication, so that the degree of agglomeration could be studied.

At 25°C an increase in agitation was found to decrease the particle size without sonication, but was found to have no effect on the size when sonication was used. This implies that the effect of agitation was to decrease the level of agglomeration without affecting the actual particles. However, at 20°C an increase in agitation led to a decrease in the particle size of both sonicated and unsonicated samples. Therefore, the agitation served to decrease both the level of agglomeration and the individual particle sizes. As the effect of agitation is primarily to increase CO_2 mass transfer into the liquid phase, these results show that at 20°C the system was mass transfer limited, while at 25°C it was not. Generally, the particles obtained at 20°C were smaller than those at 25°C.

The effect of flowrate was also studied, and an increase in flowrate was found to decrease the particle size of both the sonicated and unsonicated particles. When the powders were not sonicated, the sizes obtained for processing at 20°C were smaller than those at 25°C. However, there was little difference observed between the two temperatures when sonication was employed. This leads to the conclusion that a greater level of agglomeration occured at 25°C vs. 20°C, which is logical given that the energy of collisions would be higher at a higher temperature and therefore the particles would be

more likely to stick together. Also, this implies that mass transfer is not particularly affected by a change in flowrate, which agrees with theoretical work in the literature (Lin et al. 2003). Therefore, an increase in the flowrate decreased the particle size due to the shorter precipitation time, and not due to the increased mass transfer.

The temperature was also studied at 30°C to observe any difference between the runs at 1000RPM, 50mL/min and 20 or 25°C. At these conditions, a slight increase in particle size was observed with an increase in temperature for the unsonicated samples, but no change was observed for the sonicated powders. Therefore, the temperature at these conditions serves only to increase the level of agglomeration, and not actually affect the individual particles. The slight changes in the density of sub-critical CO_2 when the temperature was increased would have had little effect on the ability of CO_2 to dissolve into the liquid phase. Therefore, no effect of temperature would be expected.

To describe pressurization during the GAS process, a mass balance and a phase equilibrium model were required. Two phase equilibrium models were evaluated, the first being a classical phase equilibrium approach which models the complete three phase ternary GAS system using traditional methods (the ELPM), and the second being a semi-empirical approach which models the binary two phase solvent/CO_2 phase equilibrium, and then relates it to the solid concentration afterwards (the RPMVF). Both models were tested successfully against the phenanthrene-toluene-CO_2 and naphthalene-toluene-CO_2 model systems.

When the models were applied to a more complex system, the cholesterol-acetone-CO_2 system, only the RPMVF model was able to accurately represent the data. The ELPM failed because the treatment of large solids in solution can often not be

accomplished using traditional thermodynamic methods. As an example, the mixing rules most often employed in supercritical fluid phase modelling are quadratic. However, quadratic mixing rules do not often perform well for large molecules or polar/non-polar interactions (Poling et al. 2001), both of which are present in the beclomethasone/acetone system. The ELPM is the more theoretically sound model, and therefore should be used when possible, however the RPMVF model can substitute when the ELPM model does not give satisfactory results.

A population balance was used to model the experimentally determined particle size distributions. Secondary nucleation was used in an attempt to capture the bimodal nature of the distributions. Two models were used independently, an empirical equation which is commonly used to model secondary nucleation, and a theory based equation. While a good fit was achieved on the primary mode of the particle size distribution (in volume %), the secondary mode could not be modelled. While secondary nucleation can account for bimodal curves on a number weighted basis, when the distribution is converted to a volume basis, the mode with the larger particles outweigh the other mode.

The inability of secondary nucleation to account for the bimodal nature of GAS processed powders, regardless of the form employed for secondary nucleation, leads to the conclusion that this is not a predominant factor, at least in the beclomethasone-acetone-CO_2 system. Given the results obtained through SEM, which show what appears to be rather significant agglomeration, accounting for agglomeration/breakage kinetics might be a more accurate representation of what is physically occurring in the system, and thus would provide a better fit for the particle size distributions. However, secondary

nucleation was still able to give reasonable estimates of the $d_p(10\%)$, $d_p(10\%)$ and $d_p(10\%)$, and therefore is still useful as an approximation.

Some recommendations for future work are:

1. While the control systems developed were suitable for this work, there is room for improvement. In particular, there are two areas which would greatly increase the capabilities of the controller. First, the temperature in the vessel increases by a few degrees during pressurization, presumably due to kinetic effects, and then decreases immediately. However, this kind of behaviour is difficult for a standard PID controller to handle, and therefore the controller tries to correct the temperature change immediately, which often leads to the controller overshooting its setpoint. Therefore, a more sophisticated controller could be used (such as fuzzy logic) to better handle the pressurization stage. Second, as was discussed in Section 4.1 the control valve encounters some difficulty controlling the flowrate when the pump reaches its pressure set point of 2000psig. Therefore, a muti-input controller which monitors the pump pressure as well as flowrate would be beneficial.

2. Beclomethasone is used primarily as an asthma drug, and therefore it is normally administered through the lungs. However, in this study the GAS process was unable to produce particles within the inhalable range (2-5μm particle diameter), though it is possible that under different conditions than those studied (i.e. a high agitation combined with a high flowrate) particles within this range could be obtained. Therefore, alternative methods of crystallization should be examined. The SAS

process provides an alternative method which is quite similar to the GAS process, and thus would require little system modification. In terms of processing, the primary difference is that the solvent/solid solution is added directly to the pressurized CO_2. Therefore, the precipitation is much faster, as the CO_2 does not need to be pressurized, and so smaller particles are generally obtained.

3. To better study the nucleation process, it would be useful to have a monitoring system built into the precipitation vessel. One particular example of this is an online particle size analyzer, which would allow the user to monitor the particle size during precipitation and the rinse phase. This could give insight into how the particles precipitate and grow.

4. The experimental results detail the importance of mass transfer in GAS systems. Therefore, a more complete crystallization model should incorporate these effects, instead of assuming an instantaneous equilibrium in the system.

5. An alternative to secondary nucleation should be considered to accurately describe the particle size distribution. Two possibilities are agglomeration/breakage effects and size dependant growth terms. The development of an accurate predictive model for the GAS process would help to give a better understanding of the fundamentals underlying the system, which could be used to control the PSD for a specific application, such as inhalation therapy.

References

Allesi, P., A. Cortesi, I. Kikic, N. Foster, S. Macnaughton and I. Colombo (1996). "Particle Production of Steroid Drugs Using Supercritical Fluid Processing." Industrial and Engineering Chemistry Research **35**: 4718 - 4726.

Bakhbakhi, Y. (2004). Supercritical Crystallization of Pharmaceuticals: the Gas Antisolvent Process. Chemical and Biochemical Engineering. London, University of Western Ontario. **PhD**.

Bandi, N., W. Wei, C. Roberts, L. Kotra and U. Kompella (2004). "Preparation of budesonide– and indomethacin–hydroxypropyl-β-cyclodextrin (HPBCD) complexes using a single-step, organic-solvent-free supercritical fluid process." European Journal of Pharmaceutical Sciences **23**: 159 - 168.

Barnes, P. and I. Adcock (2003). "How do Corticosteroids Work in Asthma?" Annals of Internal Medicine **139**: 359 - 370.

Barnes, P., S. Pedersen and W. Busse (1998). "Efficacy and Safety of Inhaled Corticosteroids." American Journal of Respiratory and Critical Care Medicine (Supplement) **157**(3): S1 - S53.

Bertoldo, F., M. Olivieri, G. Franchina, F. De Blasio and V. Lo Cascio (2005). "Inhaled Beclomethasone Dipropionate Acutely Stimulates Dose-Dependent Growth Hormone Secretion in Healthy Subjects." Chest **128**: 902 - 905.

Bertucco, A., M. Lora and I. Kikic (1998). "Fractional Crystallization by Gas Antisolvent Technique: Theory and Experiments." AIChE Journal **44**: 2149 - 2158.

Bustami, R., H.-K. Chan, F. Dehghani and N. Foster (2000). "Generation of Micro-Particles of Proteins for Aerosol Delivery Using High Pressure Modified Carbon Dioxide." Pharmaceutical Research **17**: 1360 - 1366.

Campbell, N. and J. Reece (2002). Biology, Benjamin Cummings.

Cansell, F., B. Chevalier, A. Demourgues, J. Etourneau, C. Even, Y. Garrabos, V. Pessey, S. Petit, A. Tressaud and F. Weill (1999). "Supercritical fluid processing: a new route for material synthesis." Journal of Materials Chemistry **9**: 67-75.

Charoenchaitrakool, M., F. Dehghani and N. Foster (2000). "Micronization by Rapid Expansion of Supercritical Solutions to Enhance the Dissolution Rates of Poorly Water-Soluble Pharmaceuticals." Industrial and Engineering Chemistry Research **39**: 4794 - 4802.

Chattopadhyay, P. and R. Gupta (2002). "Protein Nanoparticles Formation by Supercritical Antisolvent with Enhanced Mass Transfer." AIChE Journal **48**: 235 - 244.

Clark, T. J. H. (1983). Steroids in Asthma: A Reappraisal in the Light of Inhalation Therapy, Adis Press.

Clifford, A. (1999). Fundamentals of Supercritical Fluids. New York, Oxford University Press Inc.

Coimbra, P., C. Duarte and H. de Sousa (2006). "Cubic Equation-of-State Correlation of the Solubility of Some Anti-Inflammatory Drugs in Supercritical Carbon Dioxide." Fluid Phase Equilibria **239**: 188 - 199.

Constantinou, L. and R. Gani (1994). "New Group Contribution Method for Estimating Properties of Pure Compounds." AIChE Journal **40**: 1697 - 1710.

Constantinou, L., R. Gani and J. O'Connell (1995). "Estimation of the Acentric Factor and the Liquid Molar Volume at 298K Using a New Group Contribution Method." Fluid Phase Equilibria **103**: 11-22.

Day, C.-Y., C. Chang and C.-Y. Chen (1996). "Phase Equilibrium of Ethanol and Acetone + CO_2 at Elevated Pressures." Journal of Chemical and Engineering Data **41**: 839 - 843.

de la Fuente, J., C. Peters and J. de Swaan Arons (2000). "Volume Expansion in Relation to the Gas-Antisolvent Process." Journal of Supercritical Fluids **17**: 13-23.

Dean, J., M. Kane, S. Khundker, C. Dowle, R. Tranter and P. Jones (1995). "Estimation and Determination of Steroid Solubility in Supercritical Carbon Dioxide." Analyst **120**: 2153 - 2157.

Dixon, D. and K. Johnston (1991). "Molecular Thermodynamics of Solubilities in Gas Antisolvent Crystallization." AIChE Journal **37**: 1441 - 1449.

Domingo, C., E. Berends and G. van Rosmalen (1997). "Precipitation of Ultrafine Organic Crystals from the Rapid Expansion of Supercritical Solutions over a Capillary and a Frit Nozzle." Journal of Supercritical Fluids **10**: 39 - 55.

Dykstra, M. (1992). Biological Electron Microscopy. New York, Plenum Press.

Edwards, D. and C. Dunbar (2002). "Bioengineering of Therapeutic Aerosols." Annual Reviews of Biomedical Engineering **4**: 93 - 107.

Ehrenstein, G., G. Riedel and P. Trawiel (2004). Thermal Analysis of Plastics: Theory and Practice. Cincinnati, Hanser Gardner Publications.

Elliott, J. R. and C. T. Lira (1999). Introductory Chemical Engineering Thermodynamics. Upper Saddle River, NJ, Prentice Hall PTR.

Elvassore, N., A. Bertucco and P. Caliceti (2001). "Production of Insulin-Loaded Poly(Ethylene Glycol)/Poly(l-Lactide) (PEG/PLA) Nanoparticles by Gas Antisolvent Techniques." Journal of Pharmaceutical Sciences **90**: 1628 - 1636.

Elvassore, N., A. Bertucco and P. Caliceti (2001). "Production of Protein-Loaded Polymeric Microcapsules by Compressed CO_2 in a Mixed Solvent." Industrial and Engineering Chemistry Research **40**: 795 - 800.

Elvassore, N., T. Parton, A. Bertucco and V. Di Noto (2003). "Kinetics of Particle Formation in the Gas Antisolvent Precipitation Process." AIChE Journal **49**: 859 - 868.

Foster, N., R. Mammucari, F. Dehghani, A. Barrett, K. Bezanehtak, E. Coen, G. Combes, L. Meure, A. Ng, H. L. Regtop and A. Tandya (2003). "Processing Pharmaceutical Compounds Using Dense Gas Technology." Industrial and Engineering Chemistry Research **42**: 6476 - 6493.

Fusaro, F. and M. Mazzotti (2004). "Gas Antisolvent Recrystallization of Paracetamol from Acetone Using Compressed Carbon Dioxide as Antisolvent." Crystal Growth & Design **4**: 881 - 889.

Gallagher, P., M. Coffey, V. Krukonis and N. Klasutis (1989). Gas Antisolvent Recrystallization: New Process to Recrystallize Compounds Insoluble in Supercritical fluids. Supercritical Fluid Science and Technology. K. Johnston and J. Penninger, American Chemical Society. **406:** 334 - 354.

Gordillo, M., C. Sanchez-Oneto and E. de la Ossa (2005). "Review of the Main Methods of Critical Parameter Estimation: Application to the Correlation of Palmitic Acid/Supercritical Carbon Dioxide Phase Equilibrium Data." Reviews in Chemical Engineering **21**: 71 - 94.

Grosch, R. and H. Briesen (2004). Getting Started with Parsival, RWTH -Aachen University.

Health Canada. (2001). "How to Breath Easier: Dealing with Allergies and Asthma." Retrieved January 20th, 2005, from http://www.hc-sc.gc.ca/english/feature/magazine/2001_04/allergies.htm.

Huang, Z., G.-B. Sun, Y. Chiew and S. Kawi (2005). "Formation of ultrafine aspirin particles through rapid expansion of supercritical solutions (RESS)." Powder Technology **160**: 127 - 134.

Jutan, A. (2004). recipe.m**:** Code to calculate PID control parameters.

Kilpio, K. and M. Hannuksela (2003). "Corticosteroid Allergy in Asthma." Allergy **58**: 1131 - 1135.

Kordikowski, A., A. P. Schenk, R. M. Van Nielen and C. Peters (1995). "Volume Expansions and Vapor-Liquid Equilibria of Binary Mixtures of a Variety of Polar Solvents and Certain Near-Critical Solvents." Journal of Supercritical Fluids **8**: 205 - 216.

Kosal, E., C. Lee and G. Holder (1992). "Solubility of Progesterone, Testosterone, and Cholesterol in Supercritical Fluids." Journal of Supercritical Fluids **5**: 169 - 179.

Koushik, K. and U. Kompella (2004). "Preparation of Large Porous Deslorelin–PLGA Microparticles with Reduced Residual Solvent and Cellular Uptake Using a Supercritical Carbon Dioxide Process." Pharmaceutical Research **21**: 524 - 535.

Kurnik, R., S. Holla and R. Reid (1981). "Solubility of Solids in Supercritical Carbon Dioxide and Ethylene." Journal of Chemical and Engineering Data **26**: 47 - 51.

Lin, C., G. Muhrer, M. Mazzotti and B. Subramaniam (2003). "Vapor-Liquid Mass Transfer During Gas Antisolvent Recrystallization: Modeling and Experiments." Industrial and Engineering Chemistry Research **42**: 2171 - 2182.

Lipworth, B. J. (1993). "Clinical Pharmacology of Corticosteroids in Bronchial Asthma." Pharmacology and Therapeutics **58**: 173 - 209.

Liu, Z., J. Wang, L. Song, G. Yang and B. Han (2002). "Study on the Phase Behavior of Cholesterol-Aceton-CO_2 System and Recrystallization of Cholesterol by Antisolvent CO_2." Journal of Supercritical Fluids **24**: 1 - 6.

Malvern (1999). Mastersizer 2000 Operating Guide. Worcestershire, UK, Malvern Instruments Ltd.

Marrero, J. and R. Gani (2001). "Group-Contribution Based Estimation of Pure Component Properties." Fluid Phase Equilibria **183-184**: 183 - 208.

Martin, T., N. Bandi, R. Shulz, C. Roberts and U. Kompella (2002). "Preparation of Budesonide and Budesonide-PLA Microparticles Using Supercritical Fluid Precipitation Technology." AAPS PharmSciTech **3**: article 18.

Mersmann, A. (1990). "Calculation of Interfacial Tensions." Journal of Crystal Growth **102**: 841 - 847.

Mishima, K., K. Matsuyama, D. Tanabe, S. Yamauchi, T. Young and K. Johnston (2000). "Microencapsulation of Proteins by Rapid Expansion of Supercritical Solution with a Nonsolvent." AIChE Journal **46**: 857 - 865.

Mortimer, K. J., T. W. Harrison and A. Tattersfield (2005). "Effects of Inhaled Corticosteroids on Bone." Annals of Allergy, Asthma & Immunology **94**: 15 - 22.

Muhrer, G., C. Lin and M. Mazzotti (2002). "Modeling the Gas Antisolvent Recrystallization Process." Industrial and Engineering Chemistry Research **41**: 3566 - 3579.

Muhrer, G. and M. Mazzotti (2003). "Precipitation of Lysozyme Nanoparticles from Dimethyl Sulfoxide Using Carbon Dioxide as Antisolvent." Biotechnology Progress **19**: 549 - 556.

Mukhopadhyay, M. (2003). "Partial Molar Volume Reduction of Solvent for Solute Crystallization Using Carbon Dioxide as Antisolvent." Journal of Supercritical Fluids **25**(213 - 223).

Mukhopadhyay, M. and S. Dalvi (2004). "Partial Molar Volume Fraction of Solvent in Binary (CO_2-Solvent) Solution for Solid Solubility Predictions." Journal of Supercritical Fluids **29**: 221 - 230.

Myerson, A. (1993). Handbook of Industrial Crystallization, Butterworth-Heinemann.

Ng, H.-J. and D. Robinson (1978). "Equilibrium Phase Properties of the Toluene-Carbon Dioxide System." Journal of Chemical and Engineering Data **23**: 325 - 327.

NIST (2003). NIST Chemistry WebBook, National Institute of Standards and Technology.

Poliakoff, M. and P. King (2001). "Phenomenal Fluids." Nature **412**: 125.

Poling, B., J. Prausnitz and J. O'Connell (2001). The Properties of Gases and Liquids. New York, McGraw-Hill.

Prausnitz, J., R. Lichtenthaler and E. G. de Azevedo (1986). Molecular Thermodynamics of Fluid-Phase Equilibria, Prentice-Hall.

Randolph, A. and M. Larson (1988). Theory of Particulate Processes. San Diego, Academic Press, Inc.

Randolph, T., A. Randolph, M. Mebes and S. Yeung (1993). "Sub-Micrometer-Sized Biodegradable Particles of Poly(L-Lactic Acid) *via* the Gas Antisolvent Spray Precipitation Process." Biotechnology Progress **9**(429 - 435).

Rees, J. and J. Price (1995). ABC of Asthma, BMJ Publishing Group.

Reverchon, E., G. Della Porta and A. Spada (2003). "Ampicillin Micronization by Supercritical Assisted Atomization." Journal of Pharmacy and Pharmacology **55**: 1465 - 1471.

Rogers, T., J. Hu, Z. Yu, K. Johnston and R. Williams (2002). "A novel particle engineering technology: spray-freezing into liquid." International Journal of Pharmaceutics **242**: 93 - 100.

Sarkari, M., I. Darrat and B. Knutson (2003). "CO_2 and Fluorinated Solvent-Based Technologies for Protein Microparticle Precipitation from Aqueous Solutions." Biotechnology Progress **19**: 448 - 454.

Seborg, D., T. Edgar and D. Mellichamp (2004). Process Dynamics and Control, 2nd Edition. Hoboken, NJ, John Wiley & Sons.

Sellers, S., G. Clark, R. Sievers and J. Carpenter (2001). "Dry Powders of Stable Protein Formulations From Aqueous Solutions Prepared Using Supercritical CO_2-Assisted Aerosolization." Journal of Pharmaceutical Sciences **90**: 785 - 797.

Sepassi, K. and S. Yalkowsky (2006). "Solubility Prediction in Octanol: A Technical Note." AAPS PharmSciTech **7**(1): Article 26.

Shekunov, B., M. Hanna and P. York (1999). "Crystallization Process in Turbulent Supercritical Flows." Journal of Crystal Growth **198/199**: 1345 - 1351.

Smith, J. M., H. Van Ness and M. Abbott (2004). Introduction to Chemical Engineering Thermodynamics, McGraw-Hill.

Statistics Canada (2005). Persons with Asthma by Age and Sex. **2005**.

Steckel, H. and B. Muller (1998). "Metered-dose inhaler formulation of fluticasone-17-propionate micronized with supercritical carbon dioxide using the alternative propellant HFA-227." International Journal of Pharmaceutics **173**: 25 - 33.

Steckel, H., J. Thies and B. Muller (1997). "Micronizing of Steroids for Pulmonary Delivery by Supercritical Carbon Dioxide." International Journal of Pharmaceutics **152**: 99 - 110.

Stefanis, E., L. Constantinou and C. Panayiotou (2004). "A Group-Contribution Method for Predicting Pure Component Properties of Biochemical and Safety Interest." Industrial and Engineering Chemistry Research **43**: 6253 - 6261.

Stock, P., O. Akbari, R. DeKruyff and D. Umetsu (2005). "Respiratory Tolerance is Inhibited by the Administration of Corticosteroids." The Journal of Immunology **175**: 7380 - 7387.

Tattersfield, A., A. Knox, J. Britton and I. Hall (2002). "Asthma." The Lancet **360**: 1313 - 1330.

Tom, J. and P. Debenedetti (1991). "Formation of Bioerodible Polymeric Microspheres and Microparticles by Rapid Expansion of Supercritical Solutions." Biotechnology Progress **7**: 403 - 411.

Turk, M., B. Helfgen, P. Hils, R. Lietzow and K. Schaber (2002). "Micronization of Pharmaceutical Substances by Rapid Expansion of Supercritical Solutions (RESS): Experiments and Modeling." Particle & Particle Systems Characterization **19**: 327 - 335.

Vatanara, A., A. Najafabadi, M. Khajeh and Y. Yamini (2005). "Solubility of some Inhaled Glucocorticoids in Supercritical Carbon Dioxide." Journal of Supercritical Fluids **33**: 21-25.

Velaga, S., R. Berger and J. Carlfors (2002). "Supercritical Fluids Crystallization of Budesonide and Flunisolide." Pharmaceutical Research **19**: 1564 - 1571.

Velaga, S. and J. Carlfors (2005). "Supercritical Fluids Processing of Recombinant Human Growth Hormone." Drug Development and Industrial Pharmacy **31**: 135-149.

Walsh, G. (2003). Biopharmaceuticals: Biochemistry and Biotechnology. Hoboken, NJ, John Wiley.

Winters, M., P. Debenedetti, J. Carey, H. Sparks, S. Sane and T. Przybycien (1997). "Long-Term and High-Temperature Storage of Supercritically-Processed Microparticulate Protein Powders." Pharmaceutical Research **14**: 1370 - 1378.

Winters, M., D. Frankel, P. Debenedetti, J. Carey, M. Devanney and T. Przybycien (1999). "Protein Purification with Vapour-Phase Carbon Dioxide." Biotechnology and Bioengineering **62**: 247 - 258.

Winters, M., B. Knutson, P. Debenedetti, H. Gerald Sparks, T. Przybycien, C. Stevenson and S. Prestrelski (1996). "Precipitation of Proteins in Supercritical Carbon Dioxide." Journal of Pharmaceutical Sciences **85**: 586 - 594.

Worlitschek, J. and M. Mazzotti (2004). "Model-Based Optimization of Particle Size Distribution in Batch-Cooling Crystallization of Paracetamol." Crystal Growth & Design **4**: 891 - 903.

Yeo, S.-D., P. Debenedetti, S. Patro and T. Przybycien (1994). "Secondary Structure Characterization of Microparticulate Insulin Powders." Journal of Pharmaceutical Sciences **83**: 1651 - 1656.

Yeo, S.-D., G.-B. Lim, P. Debenedetti and H. Bernstein (1993). "Formation of Microparticulate Protein Powders using a Supercritical Fluid Antisolvent." Biotechnology and Bioengineering **41**: 341 - 346.

Young, T., K. Johnston, K. Mishima and H. Tanaka (1999). "Encapsulation of Lysozyme in a Biodegradable Polymer by Precipitation with a Vapor-over-Liquid Antisolvent." Journal of Pharmaceutical Sciences **88**: 640 - 650.

Young, T., S. Mawson, K. Johnston, I. Henriksen, G. Pace and A. Mishra (2000). "Rapid Expansion from Supercritical to Aqueous Solution to Produce Submicron Suspensions of Water-Insoluble Drugs." Biotechnology Progress **16**: 402 - 407.

Yu, Z., T. Rogers, J. Hu, K. Johnston and R. Williams (2002). "Preparation and characterization of microparticles containing peptide produced by a novel process: spray freezing into liquid." European Journal of Pharmaceutics and Biopharmaceutics **54**: 221 - 228.

Appendices

Appendix A: Computer Programs
   Appendix A-1: Expanded Liquid Phase Model
   Appendix A-2: RPMVF model
   Appendix A-3: Crystallization Kinetics
   Appendix A-4: Liquid-Gas Solubility Modelling
   Appendix A-5: Solid-Gas Solubility Modelling

This appendix provides the basic algorithm and a flowchart to describe how each section was implemented. All code can be found on the accompanying CD.

Appendix B: Table of particle sizes
   Appendix B-1: Effect of Agitation
   Appendix B-2: Effect of CO2 addition rate
   Appendix B-3: Effect of Temperature

This appendix provides the raw data from the experiments. The particle sizes are listed in micrometers, based on volume weighted diameters, with the relative standard deviation given in brackets next to the particle size.

Appendix A-1: Expanded liquid phase model

The volume expansion simulation consisted of four separate files. The main file, volumeExpansionModel.m, is the one that actually solves the volume expansion. It calls volSolv.m through a solver to compute the equilibrium mole fractions, and also solidFugacity.m which calculates the molar volumes of both phases, and the fugacities of each component in each phase. Finally, volSolv.m must also call activityCalc.m to determine the activity coefficient of the solid phase at the initial conditions, as outlined in Section 5.1.

```
        ┌──────────────┐
        │    Start     │
        └──────┬───────┘
               │
               ▼
   ┌───────────────────────┐
   │ Load CO2, solvent, and │
   │    solid physical      │
   │      properties        │
   └──────────┬─────────────┘
              │
              ▼
   ┌───────────────────────┐
   │  Set run conditions    │
   │ (temperature, flowrate,│
   │        etc.)           │
   └──────────┬─────────────┘
              │
              ▼
   ┌───────────────────────┐
   │   Choose a pressure P  │
   └──────────┬─────────────┘
              │
              ▼
   ┌───────────────────────┐
   │ Use EOS and isofugacity│
   │  to solve for equilibrium│
   │   mole fractions at P  │
   └──────────┬─────────────┘
              │
              ▼
   ┌───────────────────────┐
   │  Use EOS to get molar  │
   │        volumes         │
   └──────────┬─────────────┘
              │
              ▼
   ┌───────────────────────┐
   │  Solve mass balance for│
   │  molar holdups and time│
   └──────────┬─────────────┘
              │
              ▼
        ┌──────────────┐
        │     End      │
        └──────────────┘
```
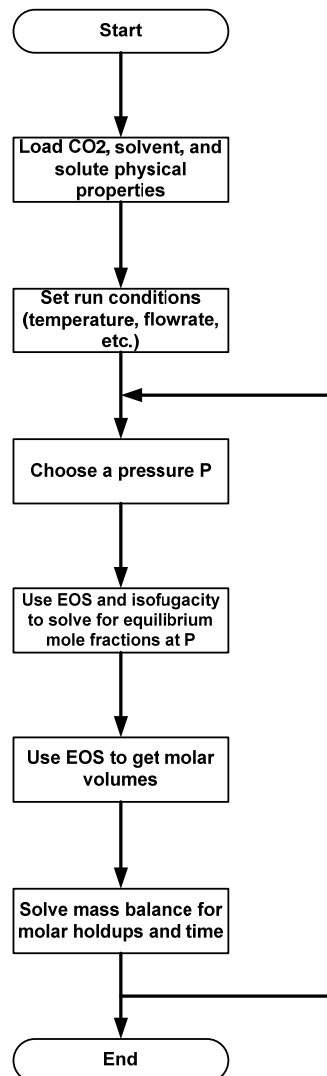
Appendix A-2: RPMVF model

The implementation of this model is quite similar to that of the expanded liquid phase model. The primary difference is that the solid is left out of the phase equilibrium calculation, and is instead calculated using the partial molar volume fraction. The same m-files are used, with slight modifications to each.

```
                    ┌──────────────┐
                    │    Start     │
                    └──────┬───────┘
                           │
                           ▼
                ┌────────────────────┐
                │ Load CO₂ and solvent│
                │ physical properties │
                └──────────┬─────────┘
                           │
                           ▼
                ┌────────────────────┐
                │  Set run conditions │
                │(temperature, flowrate,│
                │        etc.)        │
                └──────────┬─────────┘
                           │
                           ▼
                ┌────────────────────┐
                │  Choose a pressure P│
                └──────────┬─────────┘
                           │
                           ▼
                ┌────────────────────┐
                │ Use EOS and isofugacity│
                │ to get equilibrium CO₂/│
                │ solvent mole fractions │
                └──────────┬─────────┘
                           │
                           ▼
                ┌────────────────────┐
                │   Calculate PMV and │
                │        PMVF         │
                └──────────┬─────────┘
                           │
                           ▼
                ┌────────────────────┐
                │ Calculate solute mole│
                │ fraction with RPMVF │
                └──────────┬─────────┘
                           │
                           ▼
                ┌────────────────────┐
                │ Solve mass balance for│
                │ molar holdups and time│
                └──────────┬─────────┘
                           │
                           ▼
                    ┌──────────────┐
                    │     End      │
                    └──────────────┘
```
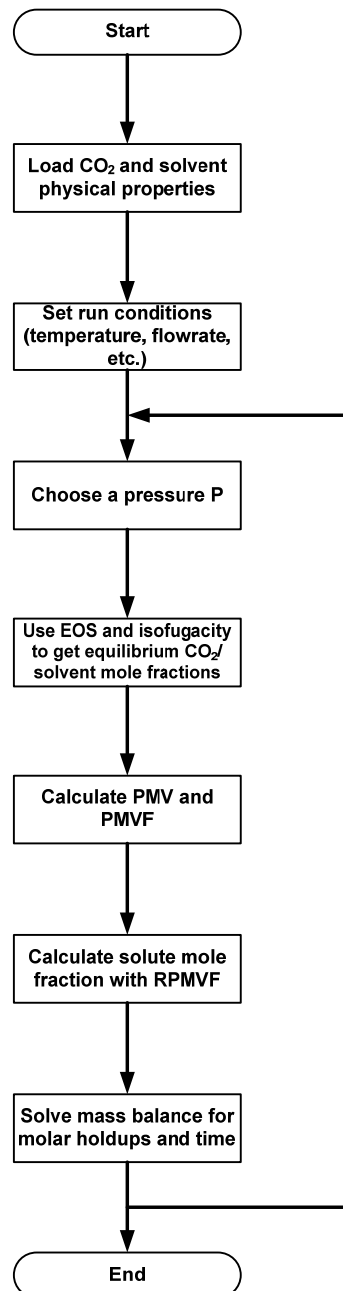
Appendix A-3: Crystallization kinetics

The crystallization model was implemented in Femlab using the following procedure:

1. Selection of PDE mode
   a. 1D coefficient mode was selected from "general PDE modes" option
   b. Time dependant analysis was chosen
2. Specification of subdomain space
   a. The object was specified by drawing a line from 1e-9 to 1e-3
3. Constants and functions
   a. All variables which do not change during precipitation (i.e. temperature, etc.) were entered in as constants
   b. All variables which can change during precipitation (i.e. Supersaturation) are entered in as scalar functions
   c. All variables which are calculated using the results from the Matlab phase model are entered in as functions of time. These functions call Matlab .m files of the same name (i.e. vLinterp(t) calls the file vLinterp.m, which loads the results from the phase equilibrium and outputs the liquid phase molar volume at time t)
   d. The moments were inplememnted as subdomain integration coupling variables
4. The boundary condition was implemented as a Neumann condition
5. The PDE was defined by setting the coefficients for the population balance in subdomain mode
6. The solution form was switched to weak in the solution manager

Appendix A-4: Liquid-gas solubility modelling

The liquid gas solubility modelling consisted of 5 separate files. interactionRegresser.m is the main file which calls regresser.m through a solver. regresser.m then guesses a value of k_{12} and calls fugacitySolver.m to calculate the pressure given the experimental values for the composition and the guessed value of k_{12}. fugacitySolver.m uses phiCalc.m to get the fugacity coefficients at the experimental composition and estimated pressure. The calculated pressures are then compared to the experimental values, and the difference between the two is optimized by selecting a different value of k_{12}.

```
                    ┌──────────────┐
                    │    Start     │
                    └──────┬───────┘
                           │
                           ▼
                  ┌──────────────────┐
                  │ Load CO₂ and solvent │
                  │ physical properties │
                  └────────┬─────────┘
                           │
                           ▼
                  ┌──────────────────┐
                  │ Guess a value for k₁₂ │
                  └────────┬─────────┘
                           │
                           ▼
                  ┌──────────────────┐
                  │ Calculate the pressure │
                  │   for this k₁₂   │
                  └────────┬─────────┘
                           │
                           ▼
                  ┌──────────────────┐
                  │ Compare calculated and │
                  │ experimental pressure │
                  │      vectors     │
                  └────────┬─────────┘
                           │
                           ▼
                       ◇ Is difference a      No
                         minimum? ────────────►
                           │
                          Yes
                           ▼
                  ┌──────────────────┐
                  │ Use k12 to calculate │
                  │ new set of mole  │
                  │    fractions     │
                  └────────┬─────────┘
                           │
                           ▼
                  ┌──────────────────┐
                  │ Plot calculated vs. │
                  │  experimental    │
                  │  compositions    │
                  └────────┬─────────┘
                           │
                           ▼
                    ┌──────────────┐
                    │     End      │
                    └──────────────┘
```
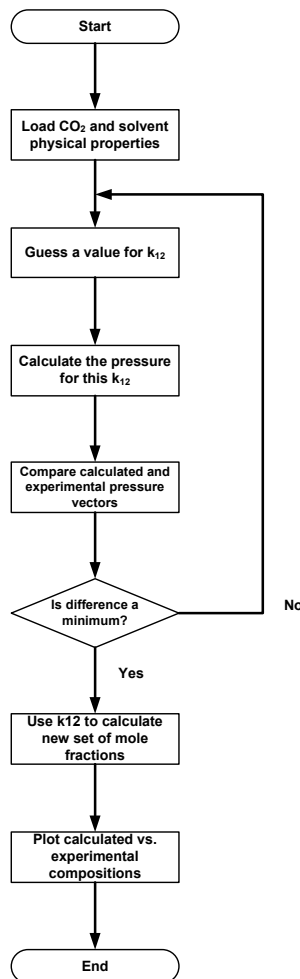
Appendix A-5: Solid-gas solubility modelling

The procedure for regression is quite similar to that used in liquid/gas solubility modelling. interactionRegresser.m is the main file which calls regresser.m through a solver to calculate k_{13}. regresser.m guesses a value for k_{13} and then calls phiCalc using the experimental CO_2 mole fraction and pressure to get the solid fugacity coefficient. It is then able to calculate a new solute mole fraction, which is compared to the experimental value. The difference between the calculated and experimental solute mole fractions is minimized by selecting different values of k_{13}.

```
                    ╭─────────────╮
                    │    Start     │
                    ╰─────────────╯
                           │
                           ▼
                  ┌─────────────────┐
                  │ Load CO₂ and solute │
                  │ physical properties │
                  └─────────────────┘
                           │
                           ▼◄───────────────┐
                  ┌─────────────────┐        │
                  │ Guess a value for k₁₃ │   │
                  └─────────────────┘        │
                           │                 │
                           ▼                 │
                  ┌─────────────────┐        │
                  │ Calculate the solute │    │
                  │ mole fraction for this │  │
                  │       k₁₂        │        │
                  └─────────────────┘        │
                           │                 │
                           ▼                 │
                  ┌─────────────────┐        │
                  │ Compare calculated and │ │
                  │ experimental mole │      │
                  │ fraction vectors │       │
                  └─────────────────┘        │
                           │                 │
                           ▼                 │
                       ◇◇◇◇◇◇◇◇              │
                      ◇ Is difference a ◇─────┘    No
                      ◇   minimum?   ◇
                       ◇◇◇◇◇◇◇◇
                           │  Yes
                           ▼
                  ┌─────────────────┐
                  │ Use k12 to calculate │
                  │ new set of mole │
                  │   fractions     │
                  └─────────────────┘
                           │
                           ▼
                  ┌─────────────────┐
                  │ Plot calculated vs. │
                  │ experimental │
                  │ compositions │
                  └─────────────────┘
                           │
                           ▼
                    ╭─────────────╮
                    │     End      │
                    ╰─────────────╯
```
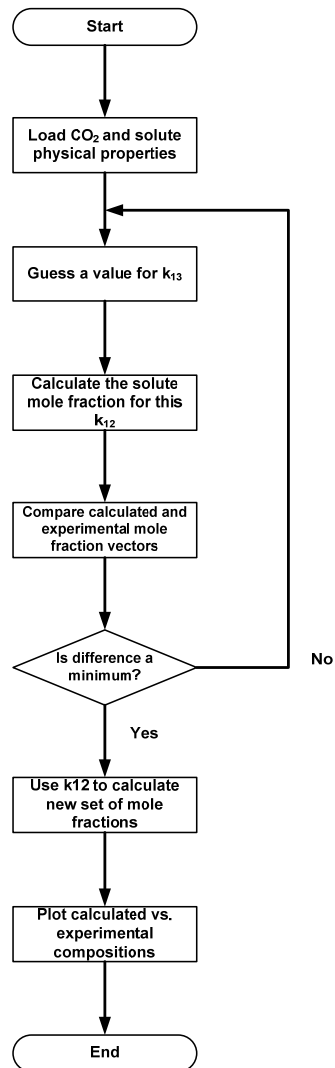
Appendix B-1: Effect of Agitation

Table B1-1: Experimental results for different agitation rates without sonication

run	T (°C)	Agitation Rate (RPM)	$d_p(10\%)$ (μm)	$d_p(50\%)$ (μm)	$d_p(90\%)$ (μm)	$d_p(4,3)$ (μm)
A1	25	200	58.3 (4.0%)	120 (6.8%)	228 (9.0%)	132 (7.3%)
F2	25	1000	49.9 (5.3%)	101 (4.6%)	182 (4.9%)	109 (4.4%)
A2	25	1800	39.7 (7.7%)	93.9 (5.6%)	183 (3.9%)	103 (4.3%)
A3	20	200	49.0 (2.6%)	102 (6.2%)	202 (11%)	115 (8.4%)
A4	20	1000	39.9 (10%)	85.9 (5.3%)	156 (4.6%)	92.3 (5.5%)
A5	20	1800	16.2 (4.2%)	53.9 (1.3%)	152 (0.3%)	74.6 (0.3%)

Table B1-2: Experimental results for different agitation rates with sonication

run	T (°C)	Agitation Rate (RPM)	$d_p(10\%)$ (μm)	$d_p(50\%)$ (μm)	$d_p(90\%)$ (μm)	$d_p(4,3)$ (μm)
A1	25	200	13.4 (9.8%)	34.2 (1.0%)	63.6 (1.6%)	36.5 (1.0%)
F2	25	1000	17.2(22.6%)	40.6 (8.1%)	73.0 (7.0%)	43.0 (8.6%)
A2	25	1800	19.5 (0.3%)	41.2 (2.8%)	73.0 (3.6%)	43.7 (2.8%)
A3	20	200	17.3 (15%)	41.3 (4.6%)	75.4 (3.8%)	43.9 (4.6%)
A4	20	1000	15.2 (16%)	39.0 (7.1%)	71.8 (4.2%)	41.5 (7.0%)
A5	20	1800	5.28 (4.3%)	26.6 (11%)	58.4 (5.0%)	29.7 (7.2%)

Appendix B-2: Effect of CO$_2$ addition rate

Table B2-1: Experimental results for different CO$_2$ addition rates without sonication

run	T (°C)	Flowrate (mL/min)	$d_p(10\%)$ (µm)	$d_p(50\%)$ (µm)	$d_p(90\%)$ (µm)	$d_p(4,3)$ (µm)
F1	25	25	57.0 (2.3%)	113 (2.0%)	200 (4.2%)	121 (2.6%)
F2	25	50	49.9 (5.3%)	101 (4.6%)	182 (4.9%)	109 (4.4%)
F3	25	75	36.1 (0.8%)	83.7 (1.2%)	157 (1.2%)	90.7 (1.1%)
F4	20	25	55.1 (2.1%)	115.2 (0.8%)	208 (1.4%)	123 (0.8%)
A4	20	50	39.9 (10%)	85.9 (5.3%)	156 (4.6%)	92.3 (5.5%)
F5	20	75	33.0 (1.3%)	78.3 (0.8%)	147 (1.2%)	84.5 (1.0%)

Table B2-2: Experimental results for different CO$_2$ addition rates with sonication

run	T (°C)	Flowrate (mL/min)	$d_p(10\%)$ (µm)	$d_p(50\%)$ (µm)	$d_p(90\%)$ (µm)	$d_p(4,3)$ (µm)
F1	25	25	19.0 (19%)	47.3 (4.6%)	86.6 (2.8%)	50.2 (4.6%)
F2	25	50	17.2 (23%)	40.6 (8.1%)	73.0 (7.0%)	43.0 (8.6%)
F3	25	75	9.21 (9.3%)	31.3 (5.8%)	62.3 (2.9%)	35.0 (5.3%)
F4	20	25	12.3 (13%)	44.4 (5.2%)	86.1 (2.5%)	47.0 (4.8%)
A4	20	50	15.2 (16%)	39.0 (7.1%)	71.8 (5.8%)	41.5 (7.0%)
F5	20	75	11.6 (11%)	35.3 (0.7%)	66.2 (1.0%)	37.5 (0.9%)

Appendix B-3: Effect of Temperature

Table B3-1: Experimental results for different process temperatures without sonication

run	T (^{o}C)	$d_p(10\%)$ (μm)	$d_p(50\%)$ (μm)	$d_p(90\%)$ (μm)	$d_p(4,3)$ (μm)
F2	20	39.9 (10%)	85.9 (5.3%)	157 (4.6%)	92.3 (5.5%)
A4	25	49.9 (5.3%)	101 (4.6%)	181 (4.9%)	108 (4.4%)
T1	30	45.9 (2.8%)	98.4 (1.0%)	181 (0.9%)	106 (0.9%)

Table B3-2: Experimental results for different process temperatures with sonication

run	T (^{o}C)	$d_p(10\%)$ (μm)	$d_p(50\%)$ (μm)	$d_p(90\%)$ (μm)	$d_p(4,3)$ (μm)
F2	20	15.2 (16%)	39.0 (7.1%)	71.8 (5.8%)	41.5 (7.0%)
A4	25	17.2 (23%)	40.6 (8.1%)	73.0 (7.0%)	43.0 (8.6%)
T1	30	15.6 (3.4%)	42.7 (2.6%)	79.0 (2.2%)	45.3 (2.5%)

Curriculum Vitae

Name: Shawn Dodds

Education: M.E.Sc.
Chemical Engineering
University of Western Ontario
London, Ontario, Canada
2005 - 2006

B.E.Sc
Chemical Engineering
University of Western Ontario
London, Ontario, Canada
2001 - 2005

Awards: NSERC CGS Scholarship, 2005 - 2006
NSERC USRA Scholarship, 2002, 2003, 2004

Experience: Teaching Assistant
University of Western Ontario
2005 - 2006

Research Assistant
University of Western Ontario
2002, 2003, 2004

Conferences: Bakhbakhi, Y; Dodds, S; Rohani, S; Charpentier, P; "Recrystallization of Beclomethasone Dipropionate Using Compressed CO_2 as an Antisolvent". Poster presentation, 7th International Symposium on Supercritical Fluids, May 1-4 2005, Orlando, Florida.

Publications: Dodds, S.; Wood, J. A.; Charpentier, P; "Micronization of Beclomethasone Using Near Critical CO_2 Part I: Theoretical Study". In preparation.

Dodds, S; Wood, J.A.; Charpentier, P; "Micronization of Beclomethasone Using Near Critical CO_2 Part II: Experimental Study". In preparation